Engineering Cell-Based Selections for Translatable Ligand Discovery

A DISSERTATION
SUBMITTED TO THE FACULTY OF THE
UNIVERSITY OF MINNESOTA
BY

Patrick Samuel Lown

IN PARTIAL FULFILLMENT OF THE REQUIREMENTS
FOR THE DEGREE OF
DOCTOR OF PHILOSOPHY

Benjamin J. Hackel

December 2021

© Patrick Samuel Lown 2021

Acknowledgements

While compiling the last five years of my work into a single document has proven a daunting task, it has allowed me to recollect all the amazing people I have had the pleasure of meeting and interacting with during my time at the University of Minnesota, for which I feel truly blessed.

For his guidance in shaping me into the scientist I am today, my sincerest and most heartfelt thanks to my advisor and mentor, Benjamin Hackel. His vast patience with me as a novice first-year student allowed me to find my footing and his confidence in my abilities allowed me to thrive. Ben has been with me for every step of my journey, supporting me through failure and pushing me to expand my knowledge. His voracious inquisitiveness, unwavering optimism, and true moral bearing are all traits that I aspire to emulate and hope that I can impart upon my colleagues going forward.

I also owe a huge debt of gratitude to the rest of the Hackel lab for their indispensable help, friendship, and positive impact upon my life. Lawrence Stern was my predecessor in this space and the person that first convinced me to embark upon this journey with a PowerPoint presentation in the back of a long-since defunct coffee shop. His help extended long beyond his tenure in the lab, for which I will always be thankful. Daniel Woldring, Sadie Johnson, Max Kruziki, Brett Case, Andrew Lewis, and Omkar Zore, my senior lab mates, helped me troubleshoot more experiments than I care to admit, engaged me in great discussions, both scientific and not, and generously welcomed me into the lab. Justin Klesmith, in particular, is responsible for my proficiency in molecular biology and deep sequencing, a skill that was non-existent upon

my start in the lab. Seth Ritter deserves a great deal of thanks, both for his great insight and ingenious technique for linker creation, which is featured in this work. Alexander Golinski was essential for both his knowledge and his help convincing more Michiganders to join the lab. Daniel Tresnak, Suvam Das, Abbigael Harthorn, Jonathan Collins, Adelyn Crabtree, Joseph Hassler, Paul Blanchard, Adam McConnell, Greg Nielsen, Sarah Whillock, Zach Schmitz, and Tse-Han Kuo have all taught me at least as much as I have taught them; they are the future of the lab, and that future seems very bright. Last, but most certainly not least, Ryan Wong, Jessy Cai, and Jacob Otolski, my undergraduate students, are my pride and joy as a mentor. Watching their development, both as scientists and as people, has been awe-inspiring and I can't wait to see what the future holds for them.

Many thanks also to my close friends, without which graduate school would have been a great deal harder. Chance Parrish was always quick with a joke (even if they were objectively terrible), ran and participated in my favorite D&D campaigns so far, and uplifted me with his infectious enthusiasm. Seongjun Kim, who coincidentally also came from Michigan to the University of Minnesota for graduate school, was instrumental in starting my hobby of building computers. Elisah Vanden Bussche, McKenzie Coughlin, Ellie Raethke, Vincent Pang, and Daniel Du were always up for new experiences, whether it be TV-binging or berry-picking. Many thanks to Chelsea Delaney, Austin Yantes, Heidi Marie, Allison Serakos, Mike Kubisiak, and Seongjun Kim for their love of bar trivia. Michael Tsuei, Angelica Smith-Evans, Haihan Lin, Seonjgun Kim, Leon Wang, and Michael Norton comprise the best gaming group and text chat of all time. A special thanks to Michael Tsuei, who helped me survive undergraduate chemical

engineering at the University of Michigan, had a parallel career at Cornell University, and has constantly supported me throughout our shared experiences.

Lastly, I wish to thank my family. The love and support of my mother, father, and sister has meant the world to me. My aunt, uncles, cousins, and grandparents were formative in my pursuit of knowledge and continue to inspire me as an adult. And Grace, my partner, who has been my rock on this adventure. Without them, this work would not have been possible.

Dedication

For my parents, Deborah and Kenneth Lown, who fostered scientific curiosity in me from a young age; my sister, Katherine Lown, whose late-night conversations and cat pictures have kept me sane(ish); and Grace Kroeger, whose love and unwavering support brightens my life each day.

Abstract

Engineered protein ligands with specific, high-affinity binding to a biomarker that are differentially expressed in a disease state have been applied in a variety of therapeutic and diagnostic applications. Yeast surface display libraries coupled with high-throughput selection strategies have shown effectiveness in discovering and maturing ligands towards a variety of target molecules. These high-throughput selection strategies often require soluble protein as a target molecule. This requires that cell surface biomarkers with transmembrane domains, constituting a large class of interesting targets, be produced as recombinant extracellular domains due to the hydrophobic nature of the transmembrane domain. However, a variety of factors including poor stability, improper folding, incorrect post-translational modifications, the addition of chemical purification tags, and the lack of plasma membrane may result in additional non-natural epitopes or the masking of native epitopes. Thus, ligand discovery campaigns performed using recombinantly-produced extracellular domains may result in ligands that bind to the recombinant target but fail to recapitulate that binding towards full-length target on target-expressing cells or tissues. The use of either whole cells or detergent-solubilized cell lysate expressing full-length target has been successfully applied as an alternative to recombinant target in discovering ligands that translate binding to target-expressing cells and tissues in the context of cancer and blood-brain barrier targets. However, these selections lack the throughput to effectively screen full-sized yeast surface display libraries and are limited in their ability to select ligands from naïve libraries with limited affinity if overexpressing cell lines are not available. Finally, the heterogeneous nature of

the mammalian cell surface often results in non target-specific ligands dominating the campaign, making the isolation of target-specific ligands difficult. All these factors limit the wide-spread use of cell-based selections. The work presented below aims to tackle each of these issues, as well as to elucidate the factors that affect successful cell-based selections and isolate panels of ligands with specific, high-affinity binding to biomarkers overexpressed in cancer. Naïve affibody and fibronectin libraries were sorted against cluster of differentiation 276 (CD276 or B7-H3) and cluster of differentiation 90 (CD90 or Thy1) by five selection strategies using recombinant extracellular domains and target-expressing cells. Cellular selection strategies provided a higher frequency of ligands that translate to binding on target-expressing cell monolayers, albeit with a relatively high degree of non target-specific binding. Sequential depletion on target-negative cell monolayers was insufficient to deplete these non target-specific binders, but pre-blocking yeast populations with disadhered target-negative cells provided significant depletion. Directed evolution through helix walking of a preliminary affibody molecule with modest but specific binding to CD276 (AC2, K_d = 310 ± 100 nM) resulted in a panel of CD276-specific ligands, including a sub-nanomolar binder (AC12, K_d = 0.9 ± 0.6 nM). Next, the use of mammalian cell-magnetic bead conjugates was investigated for use as effective cell-based pulldown agents to provide a new method of cell-based selection. This method displayed an order of magnitude higher throughput than traditional adherent cell panning, putting it on par with recombinant target magnetic-activated cell sorting (MACS), and was effective in enriching ligands under the same conditions as adherent cell panning in an EGFR model system, but failed to provide sufficient enrichment in a CD276 model system. Additionally, the use of an extended 641-amino acid linker was investigated to

provide more consistent yeast-mammalian cell engagement and enhanced avidity. This extended linker provided enhanced enrichment in a >600-nM affinity ligand, 10^6 EGFR per cell system where the original 80-amino acid linker failed to provide effective enrichment (23 ± 7 vs. 0.8 ± 0.2, $p = 0.004$). This enrichment benefit was generalizable to a CD276 model system and mathematical modelling of the linkers as random chain polymers confirmed that this enhanced enrichment was likely due to the ability of an increased number of ligands to access the extracellular environment. Lastly, a method of high-throughput clonal specificity screening was developed using deep sequencing to observe clonal frequency in populations differentially panned on target-expressing and target-negative populations in the context of insulin-like growth factor receptor (IGF1R) and insulin receptor isoforms A (InsRA) and B (InsRB). Adherent cell panning yielded affibodies that were preferentially enriched on IGF1R-expressing cells relative to IGF1R-negative cells and affibodies and fibronectins that were preferentially enriched on InsR-expressing cells relative to parental HEK293T cells, but with limited isoform specificity. Deep sequencing of the IGF1R populations revealed several affibody sequences with specificity towards IGF1R-expressing cells. In total, the results contained in this thesis elucidate the factors that dictate successful cell-based panning and provide new methods to increase the throughput, enrichment, and specificity of cell-based panning to motivate wider adoption, as well as panels of compelling molecules with high-affinity, specific binding to cancer-relevant biomarkers for therapeutic and diagnostic applications.

Table of Contents

List of Tables

List of Figures

Chapter 1 – Introduction

1.1 Engineered Protein Ligand Applications and Discovery

Engineered protein ligands, proteins that are designed to possess high affinity and specific binding activity towards a biomolecule, have been utilized extensively in numerous applications including immune system recognition, specific activation and inhibition of cell signaling pathways, and targeted delivery of molecular agents[1], as well as *in vitro* diagnostics, such as the detection of endogenous[2] or synthetic[3] biomarkers in blood and urine. The broad functionality and high specificity of protein ligands make them compelling molecules for disease treatment and diagnosis and has resulted in a substantial increase in demand as new ligands continue to be approved. This demand is expected to continue to drastically increase in the coming years as discovery and approval rates increase. Therapeutic monoclonal antibodies, the predominant form of clinically available protein ligand therapeutics, generated an approximate 115 billion USD in sales in 2018, and is expected to reach as high as 300 billion USD by 2025[4]. In keeping with this demand, the rate of antibody discovery and approval has also drastically increased. Of the 100 current FDA-approved monoclonal antibodies, the first half took 29 years to be approved, while the latter half took just 6 years[5].

Despite the dramatic increase in clinical antibody approval, the discovery pipeline for protein ligands is far from optimal, with all approved antibodies only targeting 60 unique biomolecules[6], a high degree of redundancy and only a small fraction of the over 4,000 estimated druggable proteins in the human proteome[7]. Part of this difficulty in discovery is due to the vastness of protein sequence space, combined with the sparseness

of functional sequences and potential ruggedness of functional sequence landscape caused by protein epistasis[8]. These factors necessitate either the use of *de novo* protein design, which requires target crystal structures that are not available for all druggable proteins, or combinatorial ligand libraries that require the use of high-throughput screening strategies to assay binding activity.

Traditional high-throughput methods for antibody discovery involve the immunization of animals, effectively utilizing the host's natural immune system as a naïve combinatorial library, followed by B-cell or hybridoma screening to isolate lead candidates. However, this method is costly, time-intensive, has limited affinity selection pressure, and is intractable for the discovery of non-antibody ligands[9], which have been shown to have superior tissue penetration, stability, and producibility[10]. As an alternative, *in vitro* high-throughput selection methods for binding activity have been developed. The core concept of these technologies is the genotype-phenotype linkage, by which the expressed protein ligand and encoding DNA are physically tethered. This allows for the screening of up to 10^{13} protein ligand variants with effective downstream identification and propagation of selected ligands. Common genotype-phenotype linkage strategies include *in vitro* (DNA, RNA, and ribosome), virus (bacteriophage and eukaryotic virus), and cell (bacterial, mammalian, and yeast) display technologies[11] (Figure 1-1).

DNA Display

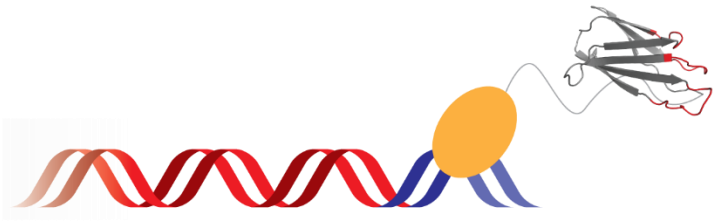

10 nm

mRNA Display

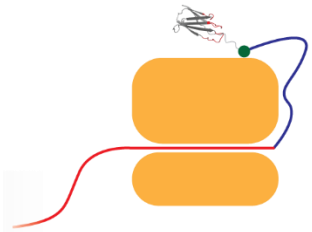

Ribosome Display

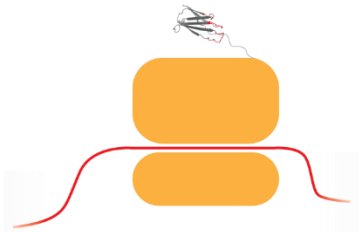

Eukaryotic Viral Display

Phage Display

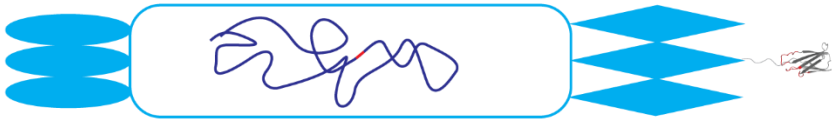

100 nm

Yeast Surface Display

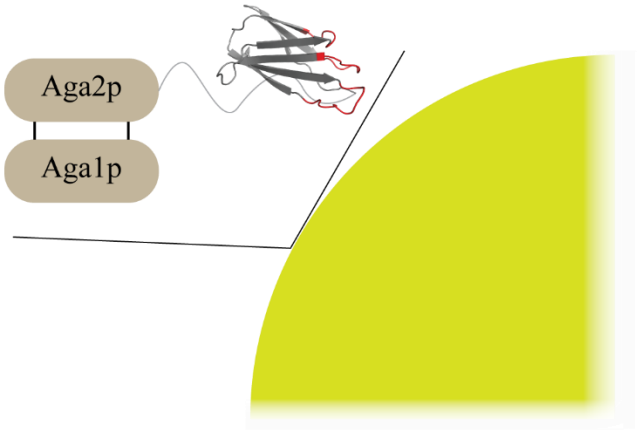

1 µm

Figure 1-1. Genotype-phenotype linkage display formats. Several different types of genotype-phenotype linkage strategies are shown here, with a scale bar below. In DNA display, DNA encoding for the ligand is tethered to the ligand by a DNA binding protein. Ribosome and mRNA display tether the RNA encoding for the ligand to the ligand either by the ribosome or a noncoding DNA linker conjugated to puromycin, respectively. Viral and phage display contain the genetic information encoding for the ligand within their capsid and display the ligand as a fusion of a capsid or coat protein. Yeast surface display contains plasmid encoding for the ligand within the yeast cell and displays the ligand as a fusion protein of Aga2p, which is immobilized to the yeast cell by a pair of disulfide bonds between Aga1p and Aga2p. Encoding genetic material is shown in red and the ligand is shown as fibronectin[12].

1.2 Protein Display Formats

In vitro display methods involve the direct attachment of the genetic material to the encoded protein ligand. In DNA display[13–15], the linkage of the display construct to the encoding DNA occurs by exploiting specific proteins that bind to their own gene sequence, while RNA display[16–18] links encoding mRNA to the expressed ligand through a covalent linkage with single-stranded DNA modified with a puromycin molecule on the 3' end. Ribosome display[19–21] utilizes mRNA lacking stop codons to stall translation, resulting in mRNA-ribosome-ligand complexes that can be stabilized by altering solution conditions. These display technologies are not limited by cellular transformation efficiencies and thus are capable of library sizes on the order of 10^{12}-10^{15} ligands[14,17,22], but suffer from difficulties expressing larger proteins, multichain proteins with disulfide bonds, and proteins with post-translational modification – such as antibodies – due to the lack cellular protein folding and modification pathways[23]. Despite this, *in vitro* display methods have been used to successfully screen libraries of peptides[14,24,25], antibody fragments[13,26,27], and non-immune scaffolds[28] including affibodies[29], and fibronectin domains[30].

Viral display methods generally involve the expression of encoded protein ligand as a fusion with a constituent coat or envelope protein, with the genetic material contained within the viral particle. Eukaryotic virus display technologies (including baculoviruses[31,32], retroviruses[33–35], and adeno-associated viruses[36,37]) were originally generated for targeted delivery of viral vehicles[38] and modulation of immunogenicity[39], but have limitedly expanded into peptide[36,40] and antibody fragment[41] libraries with sizes on the order of 10^6-10^8 ligands[36,41], constrained by the growth and transfection efficiency of eukaryotic cells. However, the use of the eukaryotic host's native folding and modification pathways allows for the proper expression of more complex proteins. In contrast, bacteriophage display[42–44], commonly referred to as phage display, has been extensively used for a variety of libraries including peptides[45], antibody fragments[46], and a wide variety of non-immune scaffolds[28], with a phage-displayed Kunitz domain being the only FDA-approved non-immune scaffold identified by display technologies to date[47]. Phage display also exhibits larger library sizes, up to 10^{12} ligands[44], due to the higher cell densities and enhanced transformation efficiency of bacterial cells, as well as several molecular biology enhancements, but is limited to displaying proteins that can fold with prokaryotic machinery. One major advantage of viral display technologies is the ability to encode for multiple copies of an individual ligand on the capsid surface, termed multivalent display. Multivalent display can provide avidity[48], the observed affinity of multiple ligand-antigen binding interactions, to lower selection stringency and aid in the recovery of lower affinity ligands that can be further evolved through directed mutagenesis. Viral display can also be monovalent, providing for finer affinity discrimination in selection campaigns.

Cell display functions by expressing the encoded protein on the cell plasma membrane and/or the cell wall through fusion with integral membrane, outer membrane, or cell-wall binding proteins[49] while the genetic material is either incorporated into a plasmid located in the cytoplasm or nucleus or directly integrated into the host cell's genome. Bacterial cell display[50,51] has seen limited use to screen peptide[52,53] and antibody fragment[54] libraries with limited sizes on the order of 10^6-10^8 ligands[52–54]. However, since bacterial transformation is the limiting step, the upper bound of bacteria display library sizes could theoretically approach that of phage display. Mammalian cell display[55,56] provides an alternative to bacterial cell display with eukaryotic protein folding and has been used to screen antibody fragment libraries[57–59] with limited sizes on the order of 10^6-10^8 ligands that could theoretically scale up to 10^9 ligands[57].

Yeast surface display[60–62] combines many of the benefits of existing display technologies. In yeast surface display, plasmids are used that encode for the ligand of interest as a fusion protein with yeast mating protein agglutinin 2 (Aga2p) or another cell-wall anchoring protein[63]. Aga2p is secreted and immobilized on the yeast cell surface through conjugation of a pair of disulfide bonds with the GPI-anchored protein agglutinin 1 (Aga1p)[64]. The high expression of Aga1p on the yeast cell surface allows for the immobilization and display of tens of thousands of ligands[65], which provides high avidity for the selection of weak binding ligands in manner similar to phage display. Additionally, while yeast surface display has not been designed for monovalent display, the use of dithiothreitol to reduce the effective valency of yeast displayed ligand[66] or modification of local antigen concentrations[48] has been used to modulate the affinity of binders that are enriched. Yeast surface display also possesses similar eukaryotic folding,

modification, and secretion pathways to eukaryotic virus and mammalian cell display techniques, which may aid in the proper expression of complex proteins[56]. In one study, phage and yeast were transformed with identical antibody fragment libraries for display and selected against soluble HIV-1 glycoprotein gp120, with yeast surface display discovering several unique ligands that could not be effectively expressed by phage display[67]. Yeast surface display has also been used to screen a wide variety of ligand libraries, including antibody fragments[60] and a variety of non-immune scaffolds[28], such as affibodies[68], fibronectin domains[69,70], and Gp2 domains[71]. While yeast surface display libraries are smaller than their *in vitro* and phage display counterparts due to limits on yeast transformation efficiency, advancements in yeast transformation allows the construction of libraries with as many as 10^{10} ligands[72], allowing substantially larger libraries than other cell-based display platforms. Combined, this makes yeast surface display a highly modular and robust display platform.

1.3 Common Recombinant-Target Based Protein Selection Methods

Most *in vitro* modes of screening display libraries for binding ligands require soluble protein; however, membrane proteins, which have hydrophobic transmembrane domains, thus making them insoluble in an aqueous system, constitute a substantial portion of compelling targets. While progress has been made in the stabilization of membrane proteins in phospholipid bilayer nanodiscs[73,74], relatively few targets have been successfully prepared in this manner. Thus, the most common method of soluble membrane protein preparation is to recombinantly produce the extracellular domain.

Once produced, the soluble target protein can be used in a variety of different techniques for ligand selection. Target-coated microtiter plates are commonly used to

screen *in vitro*[13,19,20] and viral[35,44] display libraries due to the ease of preparation and high throughput, but are not compatible with yeast surface display libraries[48] (Figure 1-2A). Target proteins are attached to the microwell surface either through direct immobilization, which involves adsorption of the protein to the plate's polymer surface, or indirect immobilization, which involves the binding of an affinity tag on the target protein to a directly immobilized molecular binding partner or capture antibody. The display library can then be introduced to the immobilized target and allowed to incubate for a sufficient time to induce binding. The plate surface is then washed, removing unbound ligands. The remaining binding ligands can then be recovered and propagated for future rounds of selection, sequencing, or characterization.

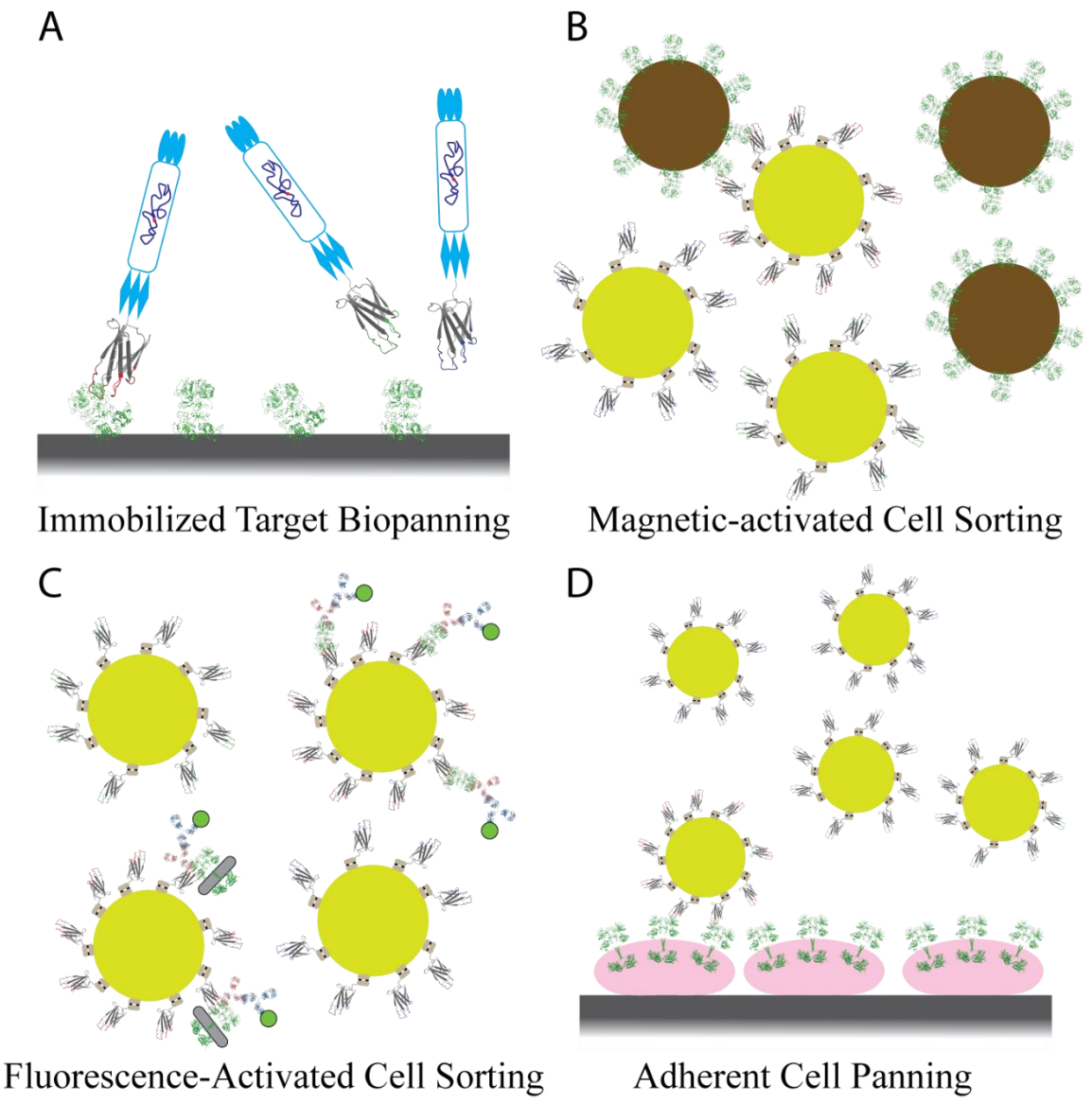

Figure 1-2. Common high-throughput ligand selection techniques. (A) Soluble target immobilized to well plates are commonly used to screen small surface display construct (*in vitro*, viral, or phage) libraries for target binding (phage display shown). (B) Magnetic-activated cell sorting (MACS) screens libraries for target binding by magnetic pulldown and allows for avid interactions (yeast display shown). (C) Fluorescence-activated cell sorting (FACS) uses fluorescently tagged target, either recombinant (upper right) or detergent-solubilized cell lysate (lower left) to label yeast for sorting by flow cytometry. (D) Cell panning utilizes target-expressing cell monolayers as a source of native target. Ligand (fibronectin shown[12]) and target (EGFR[75–77]) are enlarged to show binding.

As an alternative high-throughput selection assay, magnetic-activated cell sorting (MACS), which uses functionalized magnetic beads as substrate for both direct and indirect immobilization has been successfully applied to select ligands from ribosome[18], phage[78], and yeast surface[48,79] display libraries (Figure 1-2B). Magnetic bead selections can be run in either a multivalent or monovalent format. In multivalent format, beads are coated with immobilized target and washed prior to the introduction of the display library. After sufficient incubation time, a magnet is applied, and the beads are washed. In the case that the display library is also multivalent, the combined avidity and high local surface concentration allows the capture of even weak binding interactions. By contrast, monovalent selection involves mixing the display library with a specified concentration of soluble target before adding magnetic beads. Eliminating avidity in this manner allows for more stringent selection, but avidity can still occur to a lesser degree in multivalent display systems, allowing the capture of moderate affinity binders.

Fluorescence-activated cell sorting (FACS) using soluble target is another monovalent selection technique used to screen cell-based display platforms[55,80] (Figure 1-2C). Displayed ligands are labelled with a fluorescent antibody to quantitate expression and incubated with fluorescent-tagged target protein prior to screening by a cell sorting flow cytometer. The control over target protein concentration and ability to collect cells by their ligand-to-target fluorescence ratio allows for fine tuning of sorting stringency, as well as high single-round enrichment. While useful for selections from focused display libraries, the current throughput of FACS (10^7-10^8 per hour) is lacking to effectively screen full-size yeast surface display libraries.

1.4 Drawbacks of Recombinant Extracellular Domains

While campaigns using recombinantly-produced extracellular domains have been previously successful in selecting ligands whose binding translates to full-length target on expressing mammalian cells[81–86], many other campaigns conducted in such a manner fail to produce ligands with translatable binding, discussed more in depth in Chapter 2 of this dissertation. This failure is likely caused by differences in the epitopes present on the soluble extracellular domain relative to the full-length protein on the cell surface.

Improper folding of the extracellular domain may result in different tertiary and/or quaternary structure of the soluble protein as compared to its cellular equivalent, resulting in differing conformational epitopes. Misfolding can be caused by instability related to the absence of accompanying transmembrane domain or plasma membrane, as well as association with other misfolded proteins. Additionally, the choice of production host may result in misfolding. As previously discussed, protein production in prokaryotic cells may induce misfolding due to differing conditions between the bacterial cytoplasm and mammalian cell endoplasmic reticulum, limited molecular chaperones to assist partially folded proteins, difficulties forming proper disulfide bonding pairs, and propensity for misfolded protein to induce aggregation in newly synthesized protein molecules[87,88]. Even non-mammalian eukaryotic cells, such as yeast, fungi, and insect cells, may cause misfolding due to differential environmental factors such as temperature, pH, and oxidative stress[89].

Even in the event of properly folded protein, other modifications can result in non-native epitopes absent from cell-bound protein or the masking of native epitopes. Affinity tags may be added to recombinantly-produced protein to aid in purification or

immobilization, but such tags may generate additional non-native epitopes while masking native neighboring epitopes[71]. As well, the lack of transmembrane domain, plasma membrane, or molecular crowding of additional membrane proteins may expose additional epitopes that are not sterically accessible on the cell surface. In addition, improper glycosylation and lack of co-receptors can both introduce improper epitopes or mask native epitopes[88,90,91]. Combined, these factors reduce the number of natural epitopes available for selection while increasing the number of non-native epitopes that may result in ligands that bind to soluble extracellular domains but not to full-length target on expressing cells.

1.5 Protein Selections Against Mammalian Cells

Mammalian cells have been used as an alternative selection agent to recombinant soluble extracellular domains to avoid many of the issues mentioned above. Both phage and yeast surface display libraries have been screened against mammalian cells in a variety of selection formats to generate ligands that bind to specific biomarkers or cell types.

In vivo panning of phage display libraries[92–94], a method that flips the paradigm of animal immunization strategies by injecting the library and using the host's cells as a source of target, has been used to isolate peptides and antibody fragments targeting healthy and diseased organs in humans and mice[95,96], as well as tumor xenografts in mouse models. This technique allows for binding of ligands in the native context of tissue but suffers from the limited biodistribution of the phage particles and potential high nonspecific uptake of phage by the liver, spleen, and kidney[97].

In vitro selection methods utilizing mammalian cells have also been applied to isolate binding ligands to cell lines and specific biomarkers. Selection methods with adherent cell monolayers function similarly to methods with surface immobilized recombinant protein and have effectively screened yeast[98,99] and phage[100,101] display libraries for cancer[100,102–105] and blood-brain barrier targets[106–109] (Figure 1-2D). Suspended whole mammalian cells or detergent solubilized cell lysates have been used as antigen sources for FACS to sort yeast[99,110,111] and phage[112,113] display libraries for cancer targets[111,114–116]. Two phage display selection campaigns conducted with differential centrifugation to separate phage-mammalian cell complexes were able to isolate binding ligands where adherent mode selections failed, indicating that suspension mode panning may provide some advantages over adherent mode panning[117,118]. However, differential centrifugation of yeast-mammalian cell complexes requires density gradient centrifugation, which has only been applied to screening millions of yeast[119]. Selection strategies with whole mammalian cells immobilized to magnetic beads, a cell-based analog of soluble protein MACS, have been successfully applied to phage display libraries[120,121].

Despite the variety of selection methods using mammalian cells, selecting binding ligands yeast surface display libraries using mammalian cells has not been optimized. All existing methods lack the throughput necessary to effectively screen full size yeast surface display libraries. In addition, a study using yeast surface displayed fibronectins with specific binding to epidermal growth factor receptor (EGFR) found that selections on adherent cell monolayers have limited enrichment when using cells with fewer than 10^5 receptors per cell or when using micromolar or weaker affinity ligands[65], which

indicates that the use of adherent cell panning to select ligands from naïve libraries of small, nonimmune scaffolds may be hindered if highly overexpressing cell lines are not available. Finally, the heterogenous nature of the mammalian cell surface allows the enrichment of off-target or nonspecific binding ligands that may quickly dominate the population in cell-based selections, hindering the ability to select target-specific ligands by clonal screening[109]. While methods have been developed to deplete off-target and nonspecific interactions in phage display libraries, including panning against target-negative cells[122–124] or masking with polyclonal mixture enriched for binding to a target-negative cell line[125], depletion against target-negative cell monolayers in the yeast surface display context has shown limited efficacy in depleting nonspecific ligands[109].

1.6 Thesis Overview

This thesis discusses methods to improve the throughput, enrichment, and specificity of existing mammalian-cell based selections in the context of yeast surface display and applies these new methods to the discovery of binding affibody and fibronectin molecules to cancer-relevant biomarkers including cluster of differentiation 276 (CD276 or B7-H3), cluster of differentiation 90 (CD90 or Thy1), insulin-like growth factor 1 receptor (IGF1R), and insulin receptor (IR).

To determine the optimal sorting method to generate ligands with specific cellular binding, naïve fibronectin and affibody ligand libraries were sorted using recombinant extracellular domain and mammalian cell-based methods to select binding ligands to CD276 and Thy1. Cell-based selections alone or a combination of recombinant protein and cell-based selections were able to generate ligands with binding to full-length target on expressing mammalian cells in a higher frequency of campaigns (9/16 campaigns)

than recombinant protein-based selections alone (1/4 campaigns). However, all campaigns using adherent cell panning coenriched ligands that bound to both target-expressing and target-negative cells, with depletion against adherent target-negative cell monolayers failing to effectively eliminate non target-specific ligands. Pre-blocking yeast populations with disadhered target-negative mammalian cells prior to panning on adherent target-expressing mammalian cells conferred a significant specificity advantage to a panel of CD276-specific clones relative to a panel of non CD276-specific clones, motivating the use of this technique in future adherent cell panning selections. A lead CD276-specific binding affibody, AC2 (K_d = 310 ± 100 nM), was used to generate focused, rationally-designed libraries that were aggressively sorted with a combination of soluble CD276 ectodomain and CD276-expressing cell lysate FACS, which generated a panel of high affinity CD276-specific binding affibodies. Together, this study motivated the use of adherent cell panning, either in tandem with pre-blocking with target-negative mammalian cells or recombinant MACS to deplete non target-specific ligands and created a panel of affibodies with high-affinity, specific cellular binding that were successfully applied to *in vivo* targeted imaging studies.

While the adherent cell panning selections were functional in yielding binding ligands to CD276 and Thy1, the number of screened ligands was limited by the method's throughput. Guided by the success in selecting phage display libraries on whole mammalian cells immobilized to magnetic beads, as well as the high throughput of traditional recombinant protein MACS, a yeast sorting method utilizing both direct and indirect immobilization of target-expressing mammalian cells was compared to adherent cell panning in model EGFR and CD276 systems consisting of binding ligands of known

affinities diluted in plasmidless EBY100 panned against immobilized cells of known target expression. This system exhibited a 25-fold greater throughput than adherent cell panning, on par with recombinant protein MACS, while effectively enriching binding ligands in the same EGFR systems as adherent panning, albeit with a moderate reduction in enrichment. However, suspension cell panning was unsuccessful in enriching binding yeast in the CD276 system, indicating that some cell types may not be appropriate for this technique.

As previously noted, selections with libraries containing micromolar or lower affinity ligands or cells expression fewer than 10^5 targets per cell result in poor enrichment and difficulty isolating binding yeast from background nonbinding yeast. Motivated by prior work in extending the yeast surface display linker and research indicating stearic hinderance by the yeast cell wall limits ligand-target engagement with shorter linkers, an efficient molecular biology technique to exponentially lengthen repetitive DNA segments was adapted to construct a 641-amino acid linker. Adherent cell panning of binding yeast expressing this new construct in comparison to binding yeast expressing a construct containing the existing 80-amino acid linker in the above EGFR and CD276 systems showed an enrichment advantage for yeast expressing the 641 amino acid linker, with the longer linker successfully enriching binding yeast in a low affinity (> 600 nM), high expression (4×10^6 EGFR/cell) EGFR system where the 80-amino acid linker could not, despite fewer of the 641-amino acid construct being expressed on the yeast cell surface. This, combined with mathematical modeling of the linkers as random coils, suggests that the observed enrichment advantage is due to improved ligand access to the extracellular space, increasing the effective avidity of the system.

While the physical depletions developed above showed promise, the expanding bandwidth and reduction in cost of next-generation sequencing techniques prompted investigation into the generation of clonal ligand specificity information through sequencing differentially sorted yeast populations. Affibody and fibronectin yeast libraries were initially enriched on adherent cell monolayers overexpressing IGF1R or insulin receptor isoform A (InsRA). The IGF1R-enriched population was split and panned in parallel on either IGF1R-expressing or IGF1R-negative cell monolayers in triplicate, while the InsRA-enriched population was split and panned in parallel on InsRA-expressing, InsRB-expressing, or parental HEK293T cell monolayers in triplicate. The IGF1R populations were deep sequenced and the observed frequencies of ligands in the target-positive populations relative to the target-negative populations used to infer specificity.

Altogether, this thesis expands the practical application of cell-based selections by improving throughput to be on par with existing yeast surface display library sizes, increasing enrichment to provide efficient selection of naïve non-immune scaffold libraries on cells expressing moderate levels of target, and providing an informatic-based method of determining ligand specificity. This thesis also expands upon the fundamental knowledge of the factors that dictate successful yeast displayed ligand-mammalian cell interactions in cell-based panning. Combined, this information motivates the application of these techniques to ligand selection campaigns against targets that cannot be currently produced in a soluble format, are not highly overexpressed on the cell surface, and have high sequence homology among protein family members such as G-coupled protein receptors or ion channels.

Chapter 2 – Cellular-Based Selections Aid Yeast-Display Discovery of Genuine Cell-Binding Ligands: Targeting Oncology Vascular Biomarker CD276

Adapted with permission from "Stern, L.A.; Lown, P.S.; Kobe, A.C., Abou-Elkacem, L.; Willmann, J.K.; Hackel, B.J. "Cellular-Based Selections Aid Yeast-Display Discovery of Genuine Cell-Binding Ligands: Targeting Oncology Vascular Biomarker CD276" *ACS Comb. Sci.* **2019**, 21 (3), 207-222" Copyright 2019 American Chemical Society. Initial ligand discovery campaigns, clonal specificity characterizations, clonal Sanger sequencing, cell panning incubation optimization, error-prone PCR, and depletion studies with clones HS, LS, HN, LN, and A were conducted by Professor Lawrence A. Stern.

2.1 Summary

Yeast surface display is a proven tool for the selection and evolution of ligands with novel binding activity. Selections from yeast surface display libraries against transmembrane targets are generally carried out using recombinant soluble extracellular domains. Unfortunately, these molecules may not be good models of their true, membrane-bound form for a variety of reasons. Such selection campaigns often yield ligands that bind a recombinant target but not target-expressing cells or tissues. Advances in cell-based selections with yeast surface display may aid the frequency of evolving ligands that do bind true, membrane-bound antigens. This study aims to evaluate ligand selection strategies using both soluble target-driven and cellular selection techniques to determine which methods yield translatable ligands most efficiently and generate novel

binders against CD276 (B7−H3) and Thy1, two promising tumor vasculature targets. Out of four ligand selection campaigns carried out using only soluble extracellular domains, only an affibody library sorted against CD276 yielded translatable binders. In contrast, fibronectin domains against CD276 and affibodies against CD276 were discovered in campaigns that either combined soluble target and cellular selection methods or used cellular selection methods alone. A high frequency of non target-specific ligands discovered from the use of cellular selection methods alone motivated the development of a depletion scheme using disadhered, antigen-negative mammalian cells as a blocking agent. Affinity maturation of CD276 binding affibodies by error-prone PCR and helix walking resulted in strong, specific cellular CD276 affinity (K_d = 0.9 ± 0.6 nM). Collectively, these results motivate the use of cellular selections in tandem with recombinant selections and introduce promising affibody molecules specific to CD276 for further applications.

2.2 Introduction

Advances in genomic and proteomic methods[126] have increased knowledge of disease biomarkers at a rate that has outpaced the development of new molecularly targeted agents for diagnosis and therapy. Several classes of molecules can be applied to bridge this gap including engineered proteins[10,28,127]. A variety of scaffolds have shown therapeutic effectiveness as inhibitors, targeting agents for drug delivery, radioisotope carriers, and immune system engagers[1] as well as diagnostic success for early disease detection, patient stratification, and treatment monitoring[128].

Numerous high-throughput screening methods for selection of engineered proteins with novel specific binding activity have been applied. Most often, the discovery

of ligands targeting cell surface receptors is directed using recombinantly produced soluble extracellular domains. The use of these molecules as selection targets allows for efficient screening via immobilization on solid supports[48,129] or fluorescent tagging[60]. However, these targets are unlikely to be perfect models of full length targets expressed on intact cells due to several factors including (a) improper folding of the soluble domains[87,89,130,131], (b) differential post-translational modification due to the production host[88,91], (c) the presence of non-natural epitopes resulting from the biological or chemical addition of tags for purification and/or selection[71], and (d) possible exposure of epitopes that would not be accessible to ligands in the presence of the transmembrane domain or cell membrane. Despite selection against these molecules yielding successful, translatable engineered ligands in numerous cases[81–83], many ligand engineering campaigns end in failure due to the inability of isolated soluble domain binding ligands to bind full length targets expressed on intact cells. As there is no good outlet, these results are seldom reported, skewing perception of the difficulties of ligand discovery. Herein, we will use the term "translatable" to refer to ligands that bind a molecular target in the genuine cellular form.

This study aims to evaluate different ligand selection methods to advance our understanding and technical ability to robustly generate ligands that bind intact, extracellularly expressed target molecules. We compare the following selection methods: (1) magnetic bead sorting[48,132] and fluorescence activated cell sorting (FACS)[60,132] using biotinylated soluble extracellular domains, (2) magnetic bead sorting using biotinylated soluble extracellular domains followed by FACS with detergent-solubilized cell lysate[99,110], (3) magnetic bead sorting using biotinylated soluble extracellular domains

followed by direct yeast panning on adherent cell monolayers[65,98,99], (4) direct yeast panning on adherent cell monolayers, and (5) direct yeast panning on adherent cell monolayers preceded by magnetic bead depletion using biotinylated soluble proteins. Magnetic bead sorting enables very high valency (up to five million targets per 3 μm magnetic bead[48]) and efficiently scalable volumes. Fluorescence-activated cell sorting enables stringent quantitative analysis for fine affinity and selectivity discrimination[80]. Detergent-solubilized cell lysate provides complete membrane-spanning protein albeit in a modified detergent context. Direct yeast panning on adherent cell monolayers provides a complete target in the full cellular context, though the nature of cell–cell (yeast–human) interactions is fundamentally different than cell–protein interactions in the other modes of selection.

The comparative analysis of selection methods is performed toward the discovery of ligands for tumor vasculature biomarkers CD276 (also known as B7–H3) and thymocyte differentiation antigen 1 (Thy1). CD276 is an immune checkpoint molecule that has both costimulatory and coinhibitory roles in T cell regulation[133]. It is overexpressed in a variety of cancers, including clear cell renal cell carcinoma[134], cutaneous melanoma[135], diffuse intrinsic pontine glioma[136], hypopharyngeal squamous cell carcinoma[137], prostate cancer[138], ovarian cancer[139], and pancreatic cancer[140]. Its expression is associated with progression and metastasis in several of these diseases[135,137,141]. Thy1 overexpression in the neovasculature of pancreatic ductal adenocarcinoma differentiates the diseased tissue from normal pancreas or chronic pancreatitis, allowing for detection of disease with superior sensitivity and specificity relative to the current standard of care[142]. These characteristics make both molecules

attractive targets for molecular ultrasound imaging as well as other diagnostic and therapeutic applications.

This study uses two alternative ligand scaffolds, the beta-sandwich fibronectin domain[69,143] and the three-helix bundle affibody[144,145], whose small, single-domain architectures provide for efficient chemical conjugation and rapid physiological distribution[10,146–148]. Selections from both libraries efficiently yielded subpopulations with measurable binding activity.

Clonal characterization shows that campaigns utilizing cellular-based enrichment in part or entirely (9/16 campaigns) have a higher success rate for yielding at least one target-specific cellular binder relative to campaigns relying on completely soluble extracellular domains for enrichment (1/4 campaigns). The ability of selections using soluble extracellular domains to yield target-specific cellular binders appears to be dependent on both the target molecule and ligand library used. Selections using direct yeast panning against mammalian cell monolayers yielded a high frequency of non target-specific binders, motivating the development of a depletion scheme using disadhered antigen-negative mammalian cells as a blocking agent. This method confers a 14 ± 6-fold selectivity advantage to recovery of a dilute high-yield antigen-specific ligand from a pool containing a high-yield non target-specific ligand and a nonbinding ligand.

While affinity maturation of Thy1-binding affibodies by error-prone PCR yielded a prevalently non target-specific population, maturing CD276-binding affibodies pooled from all five campaigns resulted in the isolation of a specific ligand of modest affinity (AC2, K_d = 310 ± 100 nM). Further maturation by helix-walking resulted in the

successful discovery of a panel of strong, specific binding ligands to cellular CD276 (K_d = 0.9–20 nM).

2.3 Results

Twenty ligand selection campaigns were carried out using two naïve ligand scaffold libraries—fibronectin domain and affibody—to discover binders to two vascular biomarkers—CD276 and Thy1—via five selection approaches. Three approaches used soluble extracellular domains immobilized on magnetic beads for initial sorting followed by recombinant extracellular domain FACS selections, detergent-solubilized lysate FACS, or yeast cell panning selections added as translatable sorts after sufficient monovalent affinity for soluble domains was established (Figure 2-1). Two approaches used panning on adherent mammalian cells with or without depletion of nonspecific binders with streptavidin-coated magnetic beads. Iterative selections and affinity maturation were performed until monovalent binding detectable by flow cytometry was observed in the FACS-based schemes or strong yield enrichment were observed in the adherent cell panning schemes.

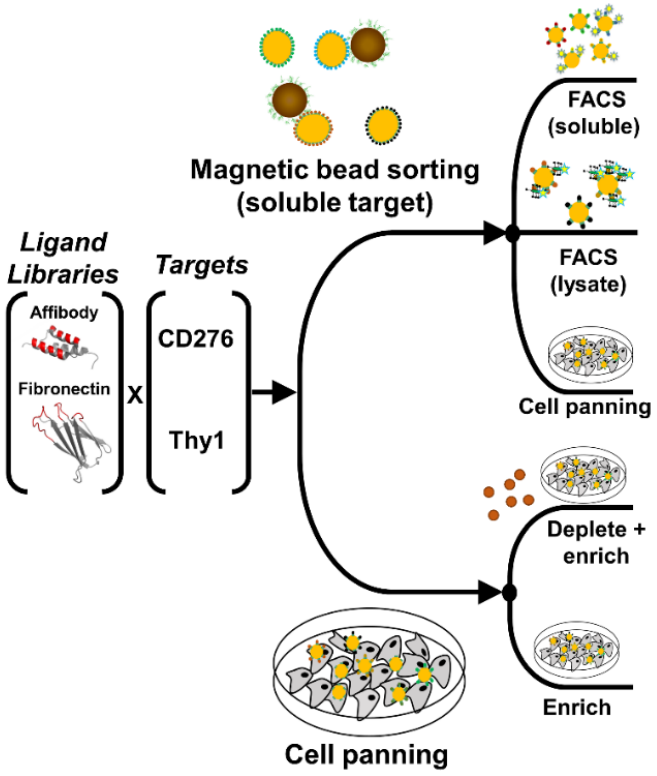

Figure 2-1. Ligand discovery methods. An affibody library and a fibronectin domain library were sorted for ligands that bound CD276 or Thy1 specifically. Libraries were sorted by five different schemes: (1) magnetic bead selection with recombinant extracellular domains followed by FACS with recombinant extracellular domains, (2) magnetic bead selection followed by FACS with detergent solubilized cell lysate, (3) magnetic bead selection followed by cell panning selection, (4) cell panning selection with magnetic bead depletion, and (5) cell panning selection.

2.3.1 Ligand Selections Using Soluble Extracellular Domain Driven Methods

Ligand selections using magnetic bead sorting and FACS with only soluble extracellular domains successfully generated ligands that exhibit binding at 100 nM target concentrations (Figure 2-2A–D). Ligands from both campaigns isolated against CD276 appear to have high specificity for their targets, showing no cross-reactivity with streptavidin, the reagent used for both immobilization and fluorescent labeling in all sorts. Ligands evolved against Thy1-Fc, despite depletion during magnetic bead selection

with biotinylated human IgG exclusively, do still show a significant amount of cross-reactivity for human IgG, suggesting that depletion was not complete enough. This phenomenon is similarly prevalent in the fibronectin and affibody populations. Through stringent gating, ligands that appear to bind Thy1-Fc differentially were isolated but were not further validated prior to clonal screening.

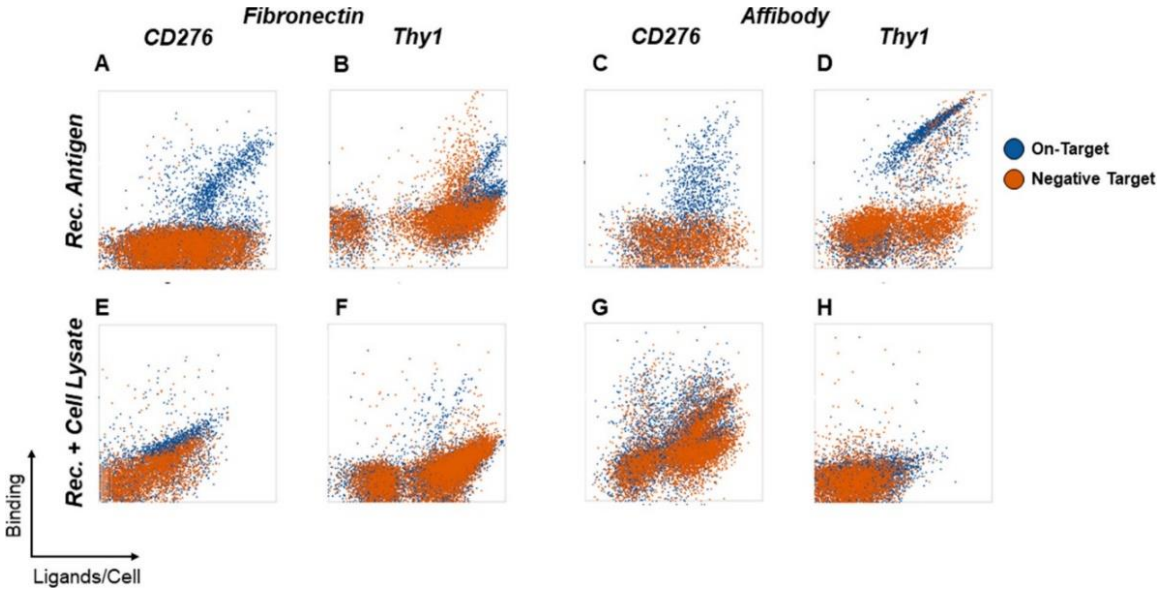

Figure 2-2. Enriched ligands evaluated for soluble extracellular domain and detergent-solubilized cell lysate binding. Yeast-displayed ligand populations were enriched for binders against CD276 and Thy1 using soluble extracellular domains immobilized on magnetic beads followed by FACS with either soluble extracellular domains or detergent-solubilized cell lysates. Binding specificity for each enriched population was assessed by comparison to negative controls. For FACS with soluble extracellular domains, yeast was labeled with 100 nM soluble CD276 or Thy1-Fc extracellular domains (blue) or irrelevant negative control proteins (300 nM streptavidin for CD276 or 100 nM human IgG for Thy1-Fc; orange; A–D). For selection of ligands with detergent-solubilized cell lysates against CD276, yeast was labeled with lysate from Mile Sven 1 cells stably transfected to express human CD276 (MS1-CD276) (blue) or human Thy1 (MS1-Thy1) (orange). For selection of ligands with detergent-solubilized cell lysates against Thy1, yeast was labeled with MS1-Thy1 lysate (blue) or MS1-CD276 lysate (orange; E–H).

The use of detergent-solubilized cell lysate FACS as a translatable sort was largely not beneficial to isolation of target-specific binders (Figure 2-2E–H). The Thy1-targeted affibody campaign did not yield substantial binding while the Thy1-targeted

fibronectin campaign yielded minimal Thy1 binding and comparable cross-reactivity. Enrichment of affibodies to CD276 yielded frequent binders but prevalent cross-reactivity. The CD276-targeted fibronectin population was likewise cross-reactive albeit with some preferential CD276 binding.

The introduction of cellular panning selections after enrichment on target-conjugated magnetic beads allowed for isolation of cellular target specific binding in several cases (Figure 2-3A–D). Single-trial ligand selections against CD276, initially via recombinant CD276-coated magnetic beads and then via adherent MS1-CD276 cell panning, showed a strong yield preference for MS1-CD276 cells relative to MS1-Thy1 cells (3% vs 0.3% for fibronectin after three rounds and 7% vs 0.1% for affibody after a single round of panning). Nominal yield preference was observed for both ligand campaigns selected against Thy1-Fc, with reasonable yield for fibronectins and negligible yield of affibodies.

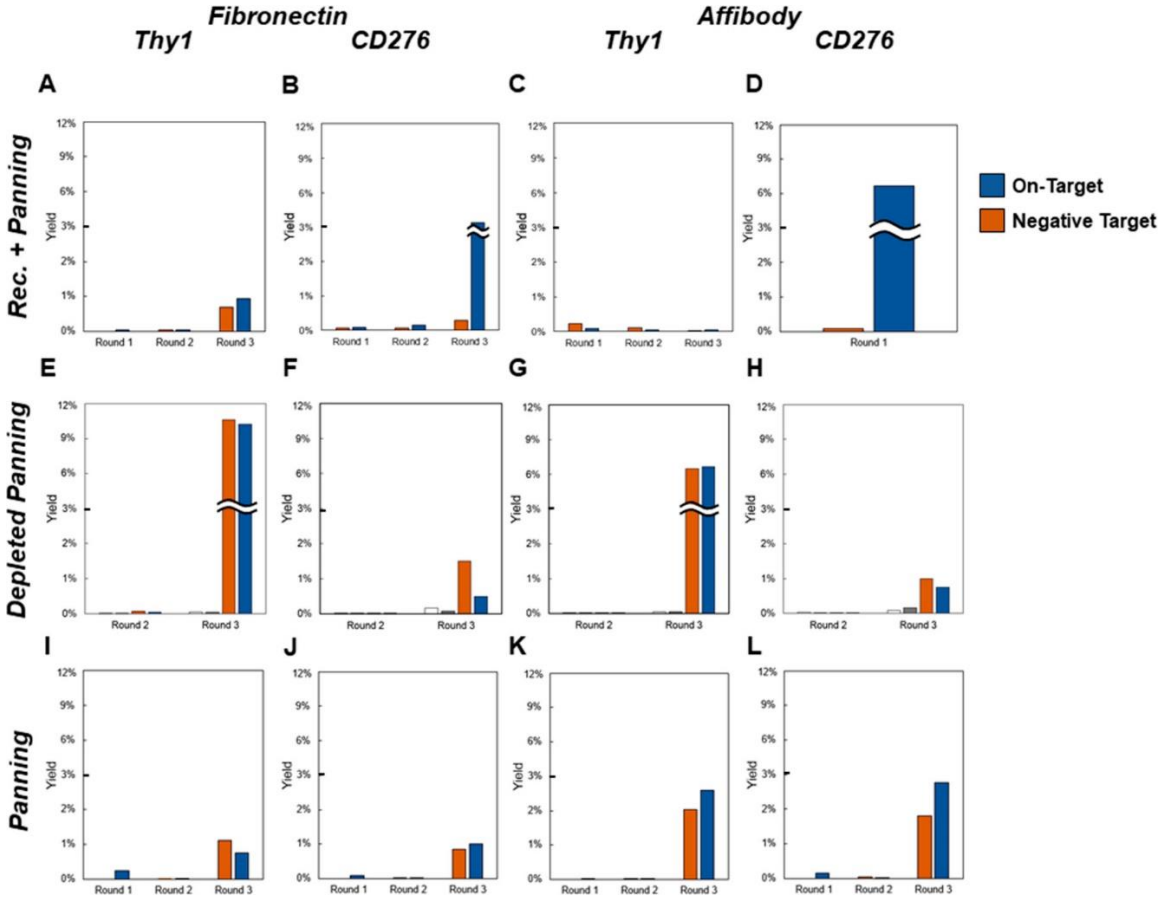

Figure 2-3. Enriched ligands evaluated for cellular binding. Yeast-displayed ligand populations were enriched through sequential rounds of selection for binding against CD276 and Thy1 using cell panning methods. *Rec. + Panning* indicates recombinant target-coated magnetic bead selections followed by cellular panning. *Depleted Panning* and *Panning* indicate cellular panning with or without, respectively, depletion of nonspecific binders via streptavidin-coated magnetic beads. Binding specificity for each enriched population was assessed by cell panning. Yeast were panned for binders on monolayers of target-positive MS1 cells (blue) or target-negative MS1 cells as a negative control (orange). In the depleted panning case, recovery of yeast from the first (white) and second (gray) magnetic beads was also quantified. Data represent single-run analyses during the course of each discovery campaign.

2.3.2 Ligand Selections Using Cell Panning Driven Methods

The enrichment-only selection strategy for adherent cellular panning yielded enrichment of ligands after three rounds of selection in all cases (Figure 2-3I–L). For fibronectin-based campaigns, yield preference was not observed for target-expressing

cells relative to target negative cells. Nominal yield preference was observed for both affibodies selected against MS1-Thy1 (2.6% vs 2.0%) and MS1-CD276 (2.8% vs 1.8%). These outcomes are reasonable given the use of a naïve library, which likely contains binders to a variety of common cellular epitopes.

Depletion selections using streptavidin-coated magnetic beads were employed as a facile way to attempt to remove nonspecific ligands. Unfortunately, the recovery of yeast during magnetic bead depletions was minimal across all campaigns and did not result in yield preference for target-expressing cells relative to target-negative cells after three rounds of selection (Figure 2-3E–H). Notably, the populations exhibit substantially higher yields on mammalian cell panning (both target-positive and target-negative) than on streptavidin-coated magnetic bead selections.

2.3.3 Cellular Target Specificity and Relative Binding Strength Characterization

While the previous analyses provide valuable binding characterization of the enriched populations, ligand discovery relies on the identification of individual clones with the desired function. Thus, characterizations of cellular target specificity and relative binding strength of isolated clones were carried out using a clonal cell panning microscopy assay (Figure 2-4). Forty-eight clones from each enriched population were grown, induced for yeast display, and evaluated for binding to target-expressing and target-negative cells via yeast display/adherent mammalian cell panning. Binding strength was characterized by a relative count of yeast present in a microscope field (Figure 2-4B). Clones were characterized as “hits” if ligand-displaying yeast substantively bound target-expressing cells and did not appreciably bind target-negative cells. Ligands characterized in this way have previously translated to binding cellular

targets as soluble ligands[106]. Unsuccessful clones, or "misses," have multiple phenotypes: binding to both target-expressing and target-negative cells (not specific for target of interest), binding only to target-negative cells (counterspecific), and nonbinding to target-expressing and target-negative cells (nonbinding). Clones that specifically bound to target-expressing cells were sequenced to assess the diversity of the selected populations.

A

	Cellular Binding								Hit Binding Strength						Sequences	
	Hit		Miss													
Target+ Cells	Yes		Yes		No		No								Uniques from Hits	
Selection Method *Target- Cells*	No		Yes		Yes		No		+++		++		+			
Soluble Target	0	0	0	0	0	0	48	48	0	0	0	0	0	0	N.D.	N.D.
	47	0	0	0	1	0	0	48	18	0	26	0	3	0	3/5	N.D.
Soluble Target + Cell Lysate	0	0	0	0	0	0	48	48	0	0	0	0	0	0	N.D.	N.D.
	15	0	0	0	2	0	31	48	0	0	3	0	12	0	4/5	N.D.
Soluble Target + Cell Panning	28	0	1	0	1	0	18	48	0	0	0	0	28	0	1/9	N.D.
	41	0	4	0	0	0	3	48	15	0	17	0	10	0	4/5	N.D.
Deplete + Cell Panning	3	1	42	41	0	2	3	4	0	0	0	0	3	1	3/3	1/1
	4	0	20	21	3	2	21	25	0	0	2	0	2	0	3/4	N.D.
Cell Panning	0	1	47	40	1	1	0	6	0	0	0	0	0	1	N.D.	1/1
	5	10	18	30	0	0	25	4	0	0	1	3	4	7	4/5	5/5

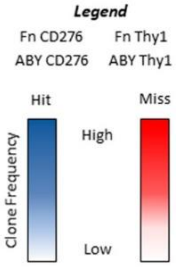

B

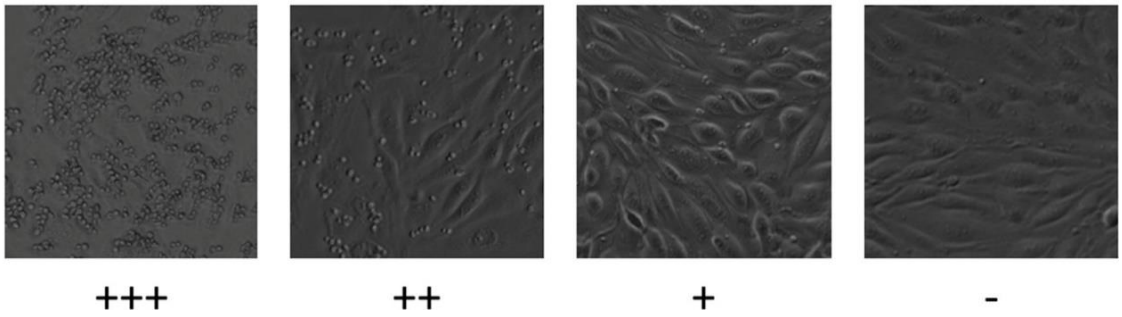

Figure 2-4. Clonal assessment of specificity for cellular target by yeast-displayed cell panning. Clonal assessment of specificity for cellular target by yeast-displayed cell panning. (A) Forty-eight individual clones from each sorted population were panned for binding to target-expressing and target-negative MS1 cells and characterized by phase microscopy. Binding specificity was characterized as described in the text. Relative binding strength was classified by yeast density observed in a random microscopy field. Sequence diversity of specific binders was determined by Sanger sequencing random hits. Each box contains results for four scaffold/target pairs as detailed in the legend at the right. (B) Representative images of yeast displaying "+++," "++," "+," and "–" clones are shown.

Fibronectins selected against both soluble Thy1-Fc and CD276 ectodomains, as well as affibodies selected against Thy1-Fc, failed to yield any cell-binding ligands, with all attempts falling into the nonbinding category. In contrast, affibodies selected against soluble CD276 showed a hit rate of 47/48 with various binding strengths. This population also retained ample diversity with three unique sequences out of five analyzed (Table 2-1). Similarly, when selections with detergent-solubilized cell lysates were added to soluble target magnetic selections, only affibodies selected against CD276 yielded hits, albeit with weaker relative binding strength than the analogous population selected with soluble target methods only. This result is contrary to expectations as the concentration of soluble CD276 used for FACS (100 nM) is less stringent than the estimated CD276 concentration in the detergent-solubilized cell lysate (~33 nM). It is possible that the avidity afforded by multiple proteins present in individual detergent micelles encouraged the recovery of ligands with lower binding affinity, yielding this observation. These same clones would not be recovered using soluble CD276 for FACS, as the target would be monovalent. This hypothesis is supported by the lack of overlap in sequences recovered from both campaigns, albeit with a small sample size (Table 2-1).

The addition of cellular selections to soluble target methods yielded hits from both the fibronectin and affibody populations selected against CD276. The fibronectin domains bound weakly and have converged on a single sequence, whereas the affibodies exhibit diversity of both binding strength and sequence (Table 2-1 and Table 2-2). Cellular selections were not able to salvage cell-binding activity from either the fibronectin or affibody populations selected against soluble Thy1-Fc.

Isolated Affibody Sequences

	CD276-Targeted	Frequency
Soluble Target	AEAKYAKEKIFAVGEIYWLPNLTHGQIMAFIAALNDDPSQSSELLSEAKKLNDSQAPK	3/5
	AEAKYYKELHNAIVSIRVLPNLTVDQITAFIRALVNDPSQSSELLSEAKKLNDSQAPK	1/5
	AEAKYSKEWFNAYVSIWGLPNLTVDQKSAFSYALDDDPSQSSELLSEAKKLNDSQAPK	1/5
Soluble Target + Lysate	AEAKYNKEWKYAYFSIVALPNLTGTQVHAFIQALHNDPSQSSELLSEAKKLNDSQAPK	1/5
	AEAKYSKEWFTAYYQIGYLPNLTEYQRYAFVKALYDDPSQSSELLSEAKKLNDSQAPK	2/5
	AEAKYYKELHNAIGVIRNLPNLTPIQKVAFAIALANDPSQSSELLSEAKKLNDSQAPK	1/5
	AEAKYAKEYANAMVEIVCLPNLTLSQSGAFIAALLDDPSQSSELLSEAKKLNDSQAPK	1/5
Soluble Target + Cell Panning	AEAKYTKEKANAIVQILVLPNLTVSQLHAFLSALHNDPSQSSELLSEAKKLNDSQAPK	1/5
	AEAKYSKEWFNAYVSIWGLPNLTVDQKSAFSYALDDDPSQSSELLSEAKKLNDSQAPK	1/5
	AEAKYAKERLKAWLEIVELPNLTYTQLHAFIRALSDDPSQSSELLSEAKKLNDSQAPK	2/5
	AEAKYNKEKFNAIASIFNLPNLTHTQKTAFIVALNDDPSQSSELLSEAKKLNDSQAPK	1/5
Depleted Cell Panning	AEAKYTKEMYTAFDEIAQLPNLTQVQKVAFIVALWNDPSQSSELLSEAKKLNDSQAPK	1/4
	AEAKYSKEKADAILSILLLPNLTRAQVVAFMHALHNDPSQSSELLSEAKKLNDSQAPK	1/4
	AEAKYAKEFSSALVEILTLPNLTVRQSSAFIRALHDDPSQSSELLSEAKKLNDSQAPK	2/4
Cell Panning	AEAKYAKESSDAWHEIVQLPNLTHGQIHAFIRALHDDPSQSSELLSEAKKLNDSQAPK	2/5
	AEAKYAKEFSSALVEILTLPNLTVRQSSAFIRALHDDPSQSSELLSEAKKLNDSQAPK	1/5
	AEAKYSKERLRAWMEITGLPNLTKPQRIAFILALRDDPSQSSELLSEAKKLNDSQAPK	1/5
	AEAKYYKELHNAIYSIRWLPNLTRVQKAAFLRALANDPSQSSELLSEAKKLNDSQAPK	1/5
	Thy1-Targeted	
Cell Panning	AEAKYSKELHDAVDSIIALPNLTGHQMDAFISALINDPSQSSELLSEAKKLNDSQAPK	1/5
	AEAKYAKEMDAAIIVILQLPNLTGYQMAAFIDALADDPSQSSELLSEAKKLNDSQAPK	1/5
	AEAKYNKEMPTADYVIRQLPNLTLSQKQAFIHALHDDPSQSSELLSEAKKLNDSQAPK	1/5
	AEAKYYKEQDDAIDEILSLPNLTGLQMRAFIVALYDDPSQSSELLSEAKKLNDSQAPK	1/5
	AEAKYNKEMDTAFDEILALPNLTGFQMDAFIYALSNDPSQSSELLSEAKKLNDSQAPK	1/5

Table 2-1. Isolated Affibody Sequences and Frequencies

Isolated Fibronectin Domain Sequences

	CD276-Targeted	**Frequency**
Soluble Target + Cell Panning	SSDSPRNLEVTNATPNSLTISWDAPCNTDTSGYRITYGETGGNSPSQESTVPGSNSATISGL KPGQDYTITGYAVSYGDYWWSNPISINYRTEIDKPSQ	4/9
	SSGSPRNLEVTNATPNSLTISWDAPCNTDTSGYRITYGETGGNSPSQESTVPGSNSATISGL KPGQDYTITGYAVSYGDYWWSNPISINYRTEIDKPSQ	3/9
	SSDSPRNLEVTNATPNSLTISWDAPCNTDASGYRITYGETGGNS PSQESTVPGSNSATISGLKPGQDYTITGYAVSYGDYWWSNPISINYRTEIDKPSQ	1/9
Depleted Cell Panning	SSDSPRNLEVTNATPNSLTISWDDSYDRAYYYRITYGETGGNSPSQEFTVPGTTNATISGL KPGQDYTITVYAVSYVNYAYYRSNPISINYRTEIDKPSQ	1/3
	SSDSPRNLEVTNATPNSLTISWDAPYYVYTYGYRITYGETGGNSPSQEFTVPGYNTATISG LKPGQDYTITVYAVSYHNTRYYSSNPISINYRTEIDKPSQ	1/3
	SSDSPRNLEVTNATPNSLTISWDAPCRYYAYGYRITYGETG GNSPSQEFTVPGNTNATISGLKPGQDYTITVYAVSNINYRYYASNPISINYRTEIDKPSQ	1/3
	Thy1-Targeted	
Depleted Cell Panning	SSDSPRNLEVTNATPNSLTISWDAPYVYTFGYRITYGETGGNSPSQEFTVPGTNSATISGL KPGQDYTITVYAVSYDNYKYAHSNPISINYRTEIDKPSQ	1/1
Cell Panning	SSDSPRNLEVTNATPNSLTISWDAPDDGYTNGYRITYGETGGNSPSQEFTVPGSNNTATIS GLKPGQDYTITVYAVSYTSYAYYLSNPISINYRTEIDKPSQ	1/1

Table 2-2. Isolated Fibronectin Domain Sequences and Frequencies

Selections for ligands using cell panning with magnetic bead depletion yielded hits for fibronectin against CD276 as well as affibody against CD276. These hits generally had weak to moderate binding strength with high sequence diversity (Table 2-1 and Table 2-2). Conversely to the methods that started with recombinant target-coated magnetic beads, the major source of misses was a lack of desired target specificity, with all populations having at least 20/48 within this category. Similarly, direct cell panning without depletion yielded hits for affibodies against both Thy1 and CD276. These populations generally showed weak to moderate binding, high sequence diversity, and a high frequency of undesired specificity (Table 2-1). In total, 8 of 12 campaigns that

involved adherent cell panning yielded specific hits, whereas 2 of 8 campaigns without adherent cell panning yielded specific hits.

2.3.4 Depletion of Nonspecific Binders Against Adhered Mammalian Cells

The ability to recover cellular binders via adherent mammalian cell panning that were not enriched via recombinant target approaches motivates further study. Yet, the abundance of enriched ligands that were not specific for the desired target warrants development of improved selection methods. One identified potential avenue for decreasing the prevalence of non target-specific ligands was sequential depletion against target-negative mammalian cell monolayers. Unfortunately, the previously demonstrated effective incubation time for cellular selections is 2 h[65,99], which limits the number of sequential depletion steps that can be completed in a day. However, optimization of incubation time has not been reported. To determine if a reduced incubation time can be comparably effective, two CD276-specific affibody clones (named HS and LS for high- and low-yielding in the clonal panning assay) were panned against MS1-CD276 with 15, 30, 45, 60, or 120 min incubation times. Both clones showed yields that were effectively invariant with time, with the slope of the recovery versus incubation time plot being essentially zero in both cases ($0.5 \times 10^{-4} \pm 2 \times 10^{-4}$ for LS and $0.45 \times 10^{-3} \pm 1 \times 10^{-3}$ for HS; Figure 2-5). Thus, 15 min was the chosen duration for depletion steps for the remainder of the study.

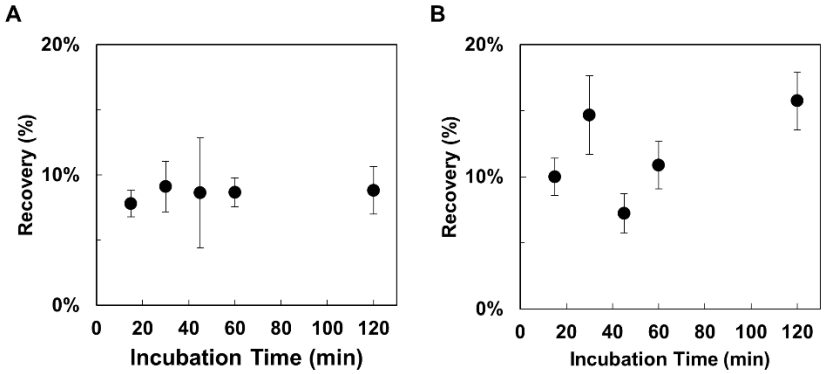

Figure 2-5. Optimization of incubation time for yeast-displayed ligand enrichment. Yeast displaying affibody clones LS (A) or HS (B) were panned for binding to adherent MS1-CD276 with varying incubation times. Recoveries are presented as the mean ± standard error of 7–12 trials.

2.3.5 Sequential Depletion of Nonspecific Binders Against Adhered Mammalian Cells

The ability to deplete nonspecific binders while retaining specific binders was then experimentally investigated. Mixtures of CD276-specific, nonspecific, and nonbinding ligands were sorted by depleting with 0, 2, 4, or 6 sequential exposures to MS1-Thy1 cells followed by an enrichment step against MS1-CD276 (Figure 2-6). For the mixture of high-yield binders (clones HS, HN (high-yield nonspecific), and A5 (nonbinder)), the 0-depletion case yielded similar enrichment ratios for clones HS (24 ± 20) and HN (29 ± 7). The use of sequential depletion steps, on average, conferred an enrichment advantage to the CD276-specific HS clone relative to the nonspecific HN (Figure 2-6A), but these differences largely lack statistical significance ($p = 0.08$ for two depletions, $p = 0.03$ for four depletions, and $p = 0.3$ for six depletions). As additional depletion steps were added, the enrichment ratio of both clones HS and HN remained essentially unchanged ($p > 0.05$ for all comparisons). However, it was difficult to draw conclusions from this data set because the enrichments after mammalian cell depletion

were moderately inconsistent. For example, the average enrichment ratio of clone HS with two depletion steps was 140 ± 130. The enrichment ratios that yield this average were 220, 260, 270, 24, 20, and 17. Importantly, the final three trials listed essentially matched the average enrichment ratio of clone HN under this condition (24 ± 2), which suggested that there was no advantage conferred to clone HS despite the two depletion steps in these instances. Yet, no depleted experiment was ever appreciably less enriched than the nondepleted samples, suggesting the potential for benefit over multiple iterations. Results using the low-yield binder mixture (LS (low-yield specific), LN (low-yield nonspecific), and A5) showed similar performance (Figure 2-6B). Thus, sequential depletions exhibited potential efficacy for high-yielding clones, although performance was variable.

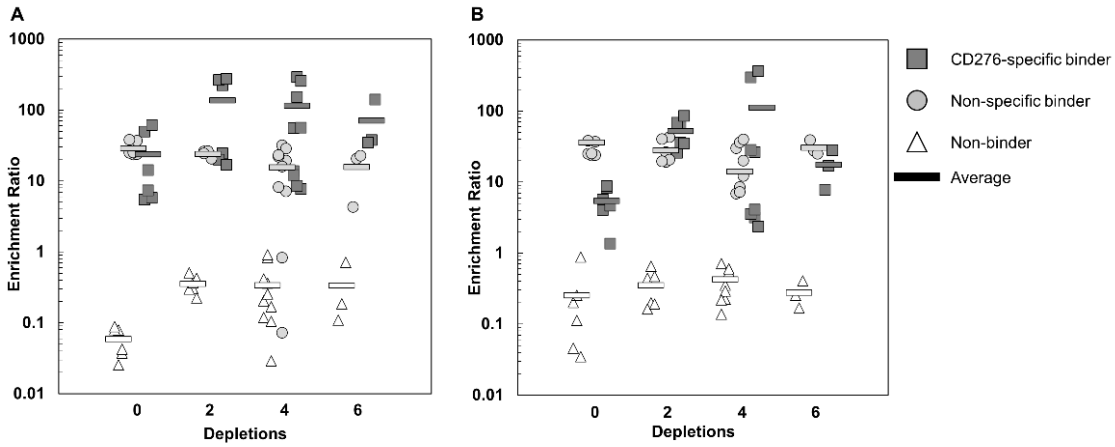

Figure 2-6. Sequential depletion of nonspecific binders with mammalian cell monolayers. Mixtures of high-yield (A) or low-yield (B) CD276-specific, nonspecific, and nonbinding yeast were subjected to selection with 0, 2, 4, or 6 depletion steps followed by a single enrichment step. All individual enrichment ratios are shown for 3–10 trials as well as the average.

2.3.6 Ligand Selections Using Cellular-Based Depletion

As an alternative to sequential depletion against mammalian cell monolayers, a preblocking strategy using disadhered mammalian cells was employed. In this approach, yeast mixtures are incubated with disadhered target-negative mammalian cells for 2 h prior to introduction of the whole mixture to a target-positive mammalian cell monolayer. Application of this scheme to a high-yield binder mixture conferred a considerable enrichment advantage to CD276-specific clone HS (120 ± 32) relative to nonspecific clone HN (12 ± 10), resulting in 14 ± 6-fold selectivity in favor of clone HS (Figure 2-7A). This was a significantly higher selectivity (p = 0.0002) than the nondepletion scheme (0.7 ± 0.6), the current standard in the field. However, application of the same strategy to the low-yield mixture resulted in a weaker selectivity advantage of 7 ± 10 for CD276-specific clone LS relative to nonspecific clone LN (Figure 2-7B). This selectivity was nominally improved over, but not definitively better than, the nondepletion case (0.2 ± 0.1, p = 0.07).

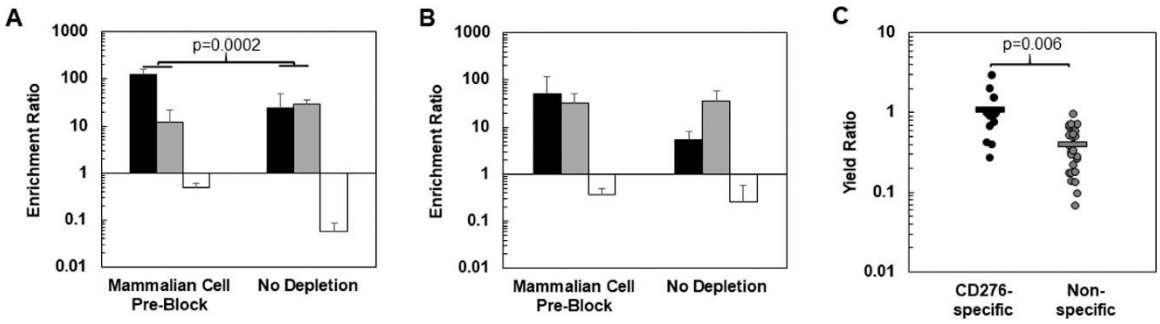

Figure 2-7. Depletion of nonspecific binders with mammalian cell preblocking. Mixtures of high-yield (A) or low-yield (B) CD276-specific, nonspecific, and nonbinding yeast were incubated with either CD276-negative disadhered MS1-Thy1 cells (mammalian cell preblock) or buffer only (no depletion) followed by incubation with MS1-CD276 cell monolayers. Enrichment ratios for CD276-specific (black), nonspecific (gray), or nonbinding (white) clones are shown as the mean ± standard deviation of 6–12 trials. (C). Specific (black) or non target-specific (gray) clones were subjected to selection with or without mammalian cell preblocking for a total of 13 clones. Each point represents the

yield of a single well of selection using preblocking normalized by a corresponding well selected without preblocking. Each clone was panned either in duplicate or triplicate.

To further investigate this trend, we panned 13 clones previously assayed for their cellular specificity (five CD276-selected specific clones, four non target-specific ligands isolated from selections against MS1-CD276, and four non target-specific ligands isolated from selections against MS1-Thy1) in parallel with and without preblocking. Nonspecific clones were effectively depleted relative to specific binders ($p = 0.006$; Figure 2-7C). For a majority of clones, preblocking by target-negative mammalian cells was able to deplete the nonspecific clones ($p < 0.05$ for 6 of 8 clones; median yield ratio = 0.33) without altering the recovery of specific ligands ($p > 0.05$ for 5 of 5 clones; median yield ratio = 0.93) compared to panning without preblocking (Figure 2-7C). Thus, preblocking nonspecific ligands with suspended target-negative mammalian cells provides a compelling approach to improving yeast cell panning on adherent mammalian cells.

2.3.7 Directed Evolution of CD276-Binding Affibodies

The preceding sections elucidate and enhance the ability to discover and select ligands against cellular targets using yeast surface display. To further exemplify this ability and to engineer synthetic ligands for targeting cancer vasculature, we also performed directed evolution of affibodies targeting CD276. Collectively across the selection campaigns, a diverse set of specific CD276-binding affibodies was identified. These clones were pooled for further directed evolution to select mutants with improved affinity amenable to preclinical development. DNA from this pooled population was mutated via error-prone PCR on the whole gene and on shuffled helices. The resulting

diversified population was subjected to one round of cell panning, one round of FACS with 5 nM recombinant CD276, and one round of FACS with cell lysate. DNA sequencing of the enriched affibodies revealed a dominant clone hereafter termed AC2. Notably, this clone was also identified in sequencing binders from the unmutated soluble, recombinant target selection (Table 2-1). AC2 was produced and purified from *E. coli* and evaluated for binding to MS1-CD276 cells. Despite isolation by binding to low concentrations of antigen in the yeast-displayed context, affinity titration experiments with soluble AC2 revealed a weak binding affinity (K_d = 310 ± 100 nM) to MS1-CD276 (Figure 2-11).

Prior work evolving antibodies, Gp2 domains, and fibronectin type III domains has shown success in isolating binders by loop-walking[84,149,150] in which each structural segment of the binding paratope is independently evolved and then improved segments are merged. To perform an analogous maturation of the AC2 affibody, combinatorial libraries were created by diversifying helix one while retaining parental helix two and vice versa. The genetic diversity was designed to include the parental amino acid and chemically homologous amino acids accessible with degenerate codons (Figure 2-8). The diversity of each library was limited to 5×10^7 to retain high confidence of sampling any sequence through yeast surface display by FACS. Each sublibrary was subjected to a single magnetic bead sort, with nontarget depletion, to eliminate nonbinders and non target-specific binders, followed by FACS with 5 nM soluble extracellular CD276 and then FACS with 150 nM solubilized MS1-CD276 cell lysate. Analysis showed an increase in the binding to CD276-positive lysate with minimal cross-reactivity toward target-negative lysate (Figure 2-9A). Deep sequencing of the resulting populations

showed a relatively diverse first helix with at least four mutations from parental AC2 in the top sequences (Figure 2-10). Sites K9 and W18 were conserved, while I10 was either conserved or mutated to homologous valine. F11 and G14 tolerated numerous options including the parental residue, while V13 and Y17 strongly favored two hydrophobic residues other than parental. Conversely, the second helix library retained less diversity, with parental being the dominant clone.

		Library	
		Helix 1	Helix 2
Site	K9	HIKLMNQRS	K
	I10	ADFHILNPSTVY	I
	F11	ADFHILNPSTVY	F
	V13	ADFHILNPSTVY	V
	G14	ACDFGINSTVY	G
	Y17	ADFHILNPSTVY	Y
	W18	AEGKLMRSTVW	W
	H24	H	ACDFGHILNPRSTVY
	G25	G	ACDFGHILNPRSTVY
	I27	I	ACDFGHILNPRSTVY
	N28	N	ACDFGHILNPRSTVY
	A32	A	ACDFGHILNPRSTVY
	N35	N	ACDFGHILNPRSTVY

Figure 2-8. Affibody helix walking library designs. Amino acid diversity for each site of the sublibrary.

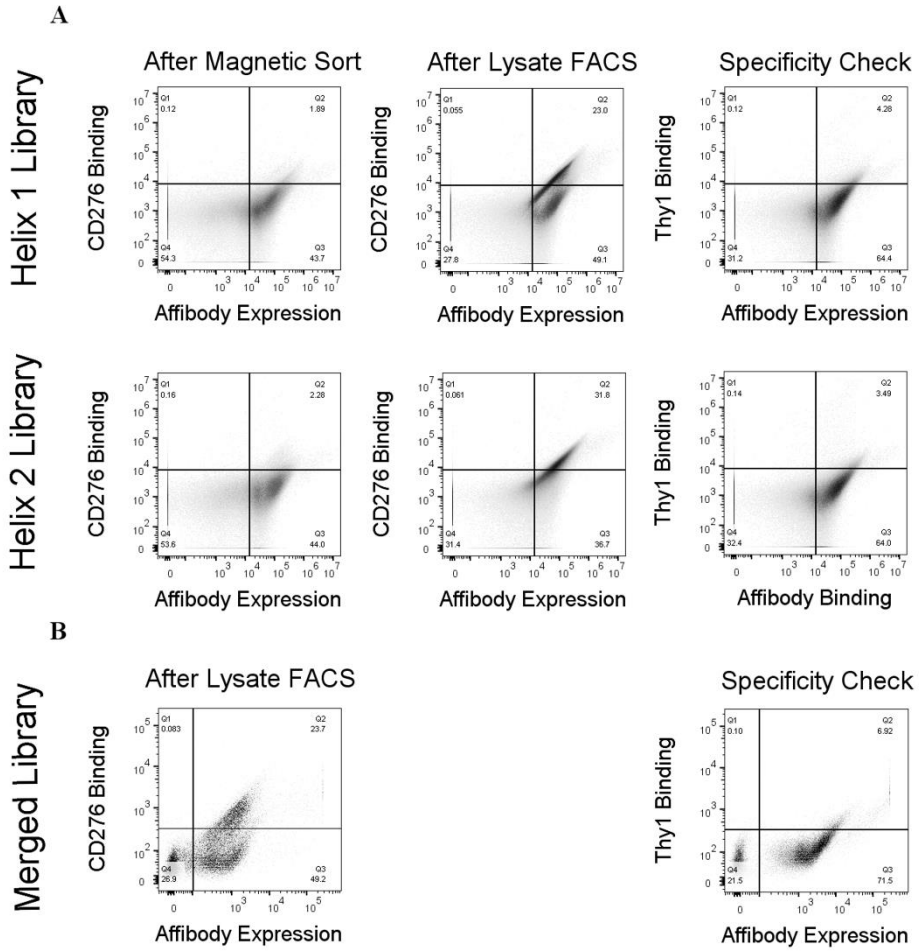

Figure 2-9. Evolved populations of yeast-displayed ligands show increasing binding to CD276 lysate while maintaining target specificity. (A) Yeast populations collected after preliminary sorting on recombinant target beads (first column) or final sorting on target-positive lysate (second column) were labeled with 150 nM target cell lysate and analyzed for binding by flow cytometry. Yeast collected after sorting on target-positive lysate (third column) was labeled with 150 nM target-negative cell lysate and analyzed for specificity by flow cytometry. Substantial binding improvement can be observed between preliminary sorting and the final population, with low cross-reactivity to target-negative lysate. (B) A mixture of the merged library and triple-sorted single-helix library was labeled with 0.5 nM target lysate (left) or 50 nM target-negative lysate (right) and analyzed for binding by flow cytometry. The population shows significant binding to target-positive lysate with minimal cross-reactivity to target-negative lysate.

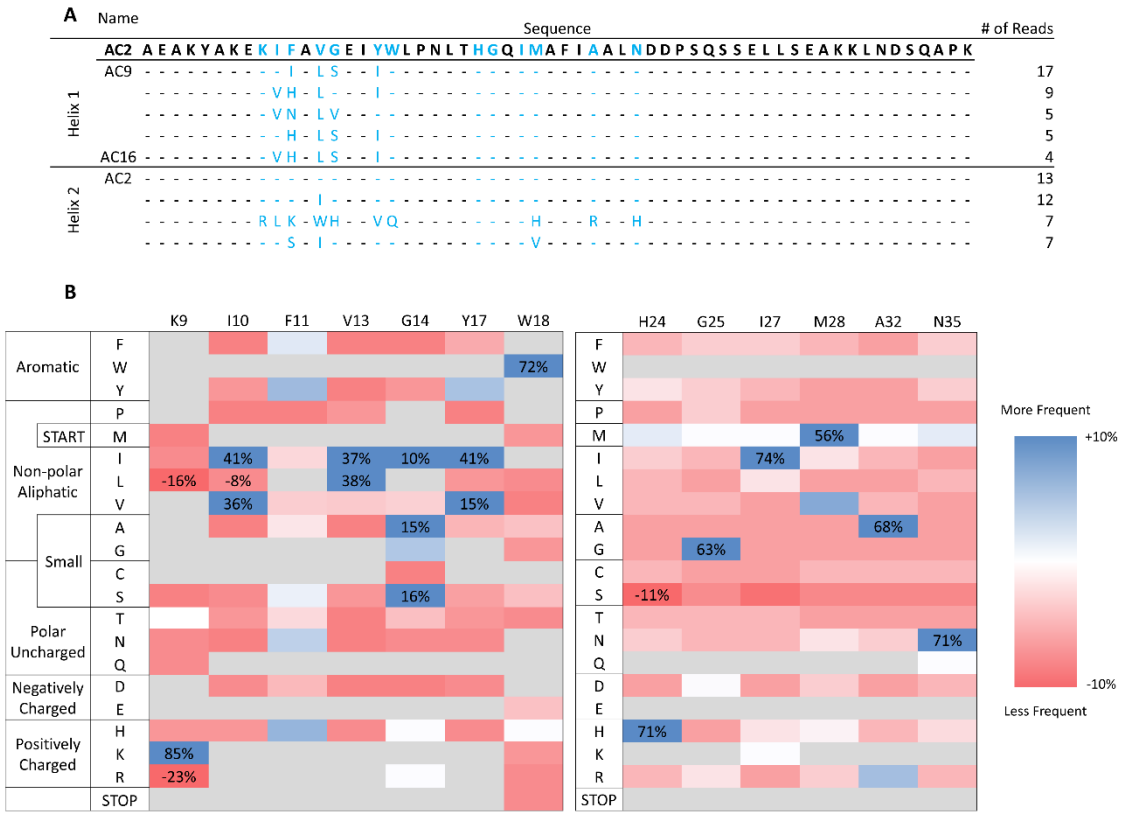

Figure 2-10. Deep sequencing of sorted single-helix libraries reveals substantially improved mutants. (A) Top unique sequences of each single-helix library listed by number of reads. Parental AC2 is supplied as a reference. Blue lettering indicates diversified residues in the helix-walking libraries and dashes indicate parental amino acids at the indicated position. Clone names are supplied for sequences that were pursued for characterization. (B) Sitewise amino acid enrichments for the helix one (left) and helix two (right) libraries. Amino acid frequencies were calculated by grouping, counting, and quad-root dampening identical sequences. Values shown are change in amino acid frequency in sorted populations compared to theoretical amino acid diversity of the naïve library. Amino acids not allowed by library design are shown in grey, except in cases where they are substantially enriched or depleted.

DNA from the diversified helix from both libraries was extracted and merged to create a library with both helices diversified. The merged library and final single-helix library populations were combined and sorted stringently on FACS with 0.5 nM target-positive cell lysate. Analysis of this final library showed significant binding to CD276 cell lysate relative to control Thy1 lysate (Figure 2-9B).

Clonal Sanger sequencing returned three unique sequences: AC9 (5 of 8 sequences), AC12 (2 of 8 sequences), and AC16 (1 of 8 sequences). Consistent with the single-helix enrichment data, while each clone possessed mutations in the first helix, all clones retained the parental genotype in the second helix (Figure 2-11). Affinity titration of each of these clones revealed strong specific binding (K_d =18 ± 4 nM for AC9, K_d = 0.9 ± 0.6 nM for AC12, and K_d = 20 ± 4 nM for AC16; Figure 2-11A and B), an increase of 15–300× compared to parental AC2. Notably, these clones did not strongly bind to MS1-Thy1 cells relative to MS1-CD276 cells (Figure 2-14). The thermal stability, secondary structure, and refoldability of all affibody variants was evaluated by circular dichroism spectroscopy. The thermal stability of all clones was substantially increased (T_m = 61.5 ± 0.1 °C for AC9, T_m = 62.4 ± 0.1 °C for AC12, and T_m = 58.5 ± 0.1 °C for AC16) relative to AC2 (48.6 ± 0.1 °C; Figure 2-11D and Figure 2-12). As expected, the secondary structure was shown to be predominately α-helical (Figure 2-11C and Figure 2-13). Additionally, both parental AC2 and AC12 were tested for refolding by cooling after thermal denaturation. Both AC2 and AC12 showed almost no change in their CD spectra after cooling, indicating that they were likely refoldable (Figure 2-11C and Figure 2-13).

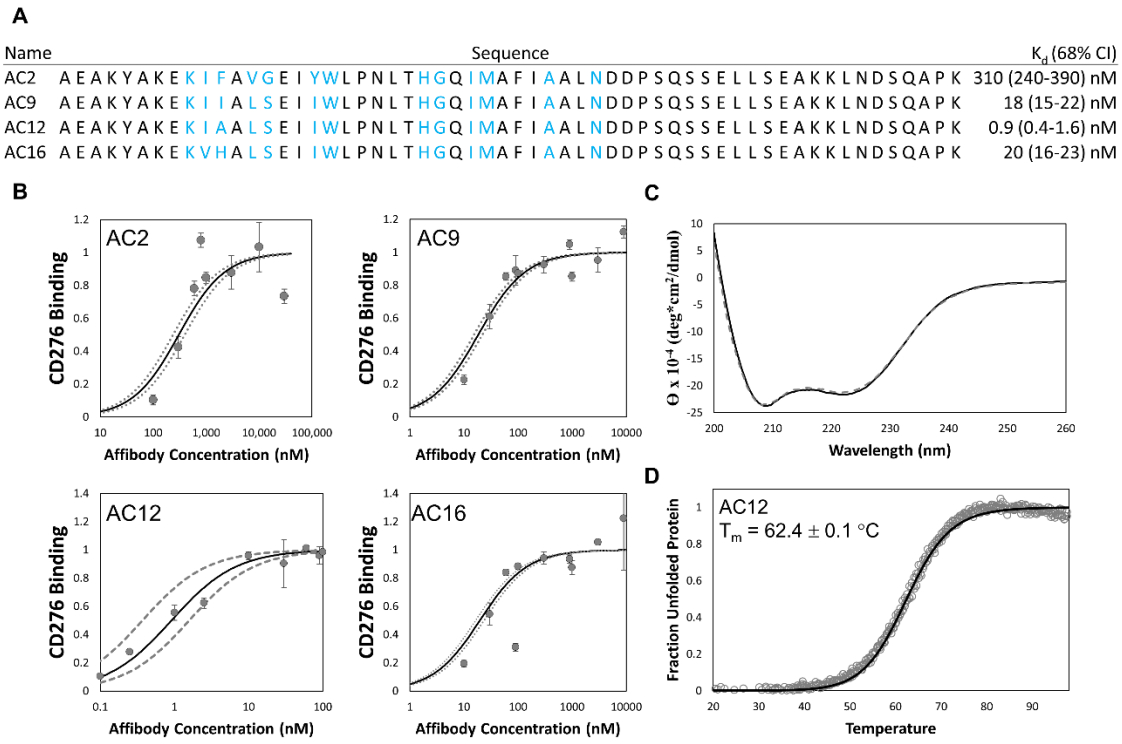

Figure 2-11. Characterization of parental and evolved CD276-binding affibodies. (A) Affibody variants AC2, AC9, AC12, and AC16 were characterized for their binding affinity (K_d). Blue lettering indicates diversified residues in the helix-walking libraries. (B) Purified affibody variants AC2 (upper-left), AC9 (upper-right), AC12 (lower-left), and AC16 (lower-right) were used to label MS1-CD276 cells at the indicated concentrations. Binding was quantified by flow cytometry. The best-fit estimate of K_d and 68% confidence interval are indicated by solid and dashed lines, respectively. (C) Purified affibody AC12 was analyzed by circular dichroism spectroscopy in triplicate between 200 and 260 nm wavelengths before (solid) and after (dashed) thermal denaturation and cooling. (D) Purified affibody AC12 was scanned at a wavelength of 220 nm during heating from 20 to 98 °C (1 °C/min). The midpoint of thermal denaturation (T_m) was calculated by linear least-squares regression using a two-state protein unfolding model.

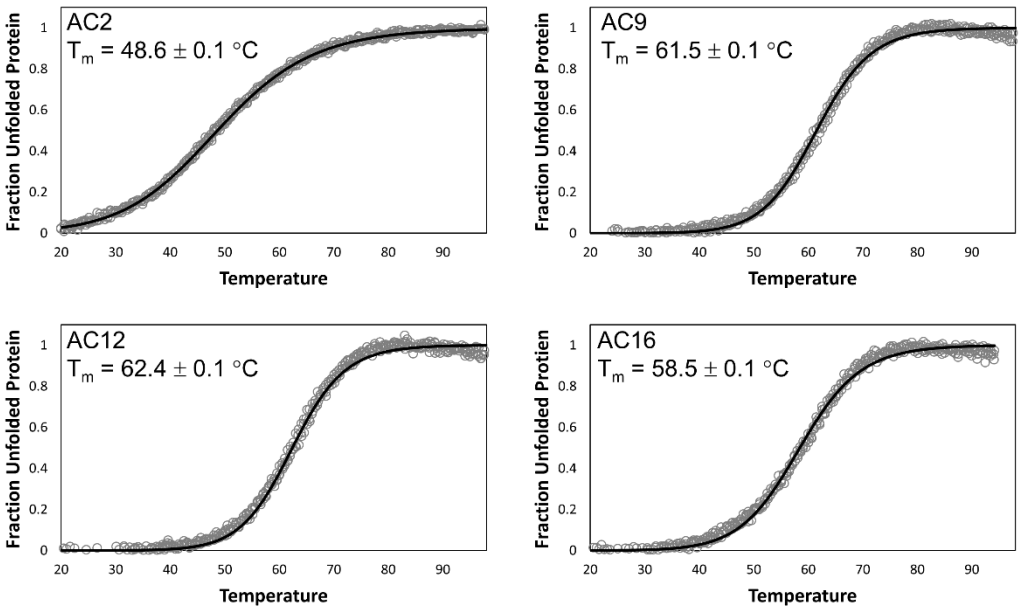

Figure 2-12. Thermal denaturation curves of affibody variants. Purified affibody variants were scanned at a wavelength of 220 nm during heating from 20 to 98 °C (1 °C/min). The midpoint of thermal denaturation (Tm) was calculated by linear least-squares regression using a two-state protein unfolding model.

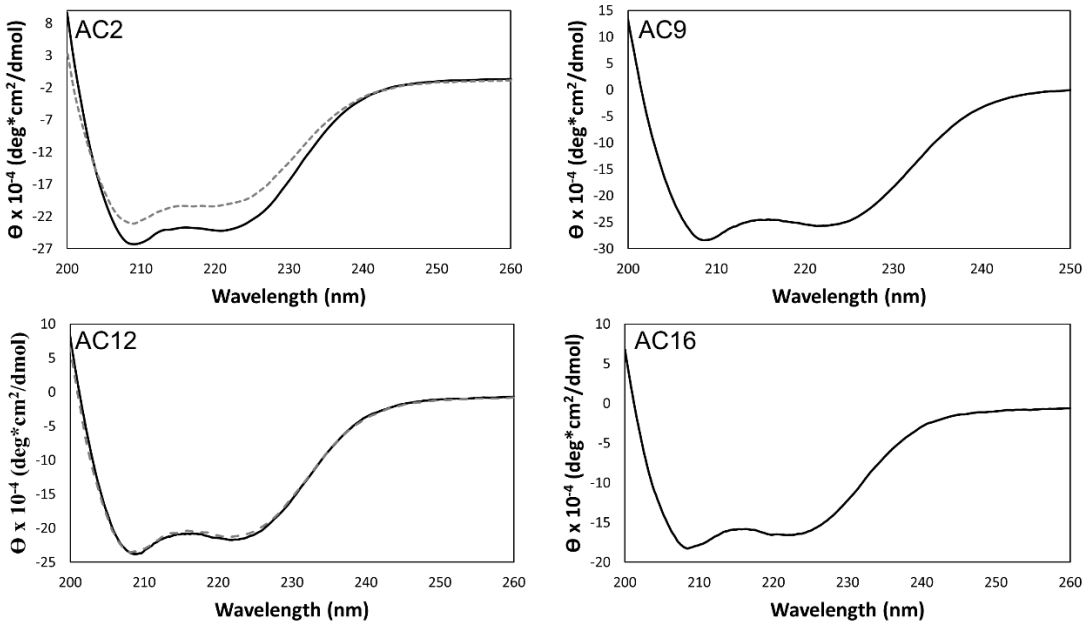

Figure 2-13. Circular dichroism spectra of affibody variants. Purified affibody variants were analyzed by circular dichroism spectroscopy in triplicate between 200 and 260 nm wavelengths before (solid) and after (dashed) thermal denaturation and cooling. No spectral data after cooling collected for AC9 or AC16.

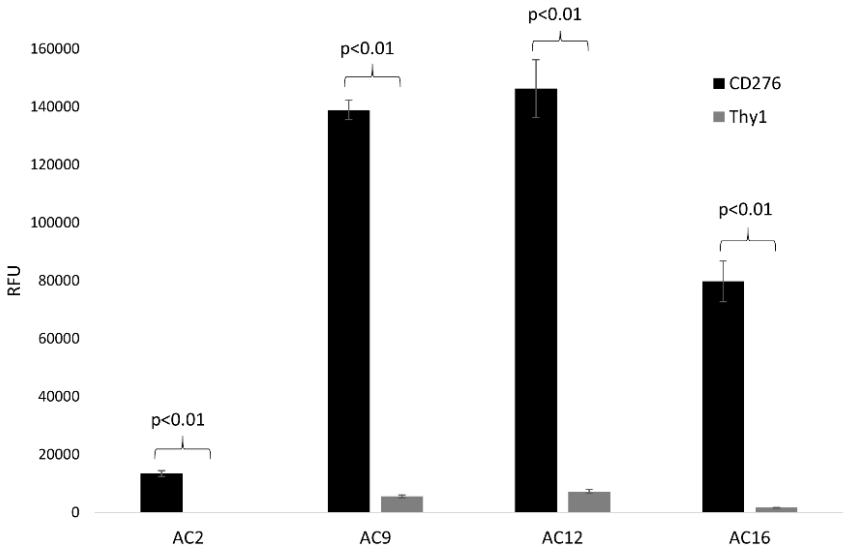

Figure 2-14. Specificity of affibody variants. Purified parental and evolved affibody variants were used to label either MS1-CD276 or MS1-Thy1 cells at saturating conditions (10 µM for AC2, 1 µM for all others). Binding was detected by fluorophore tagged anti-His6 antibody via flow cytometry. Fluorescence was quantified as the difference between affibody labelled cells and control cells labelled with secondary antibody with n = 3 trials (68% confidence interval indicated). AC2 showed no significant binding to MS1-Thy1 cells relative to control. All other variants, while showing significant binding to MS1-Thy1 cells, bound significantly less strongly to MS1-Thy1 cells relative to MS1-CD276 cells.

To expand upon Sanger sequencing, the final library was also deep sequenced (Figure 2-15). While the first helix of the merged library showed similar trends in enrichment to the single-helix version of the library, a dominant amino acid appeared to have emerged at each site with the exception of F11 and G14. Notably, while the preferred amino acids in the merged G14 were not drastically altered from the single-helix counterpart, isoleucine emerged as the predominant residue of F11, when it was previously less prevalent in the single-helix library. As well, the top sequences once again showed a lack of diversity in the second helix, with parental being the favored phenotype. However, an interesting exception to this trend existed in the second most

prevalent sequence, which possessed the parental first sequence and a number of mutations in the second helix not seen elsewhere.

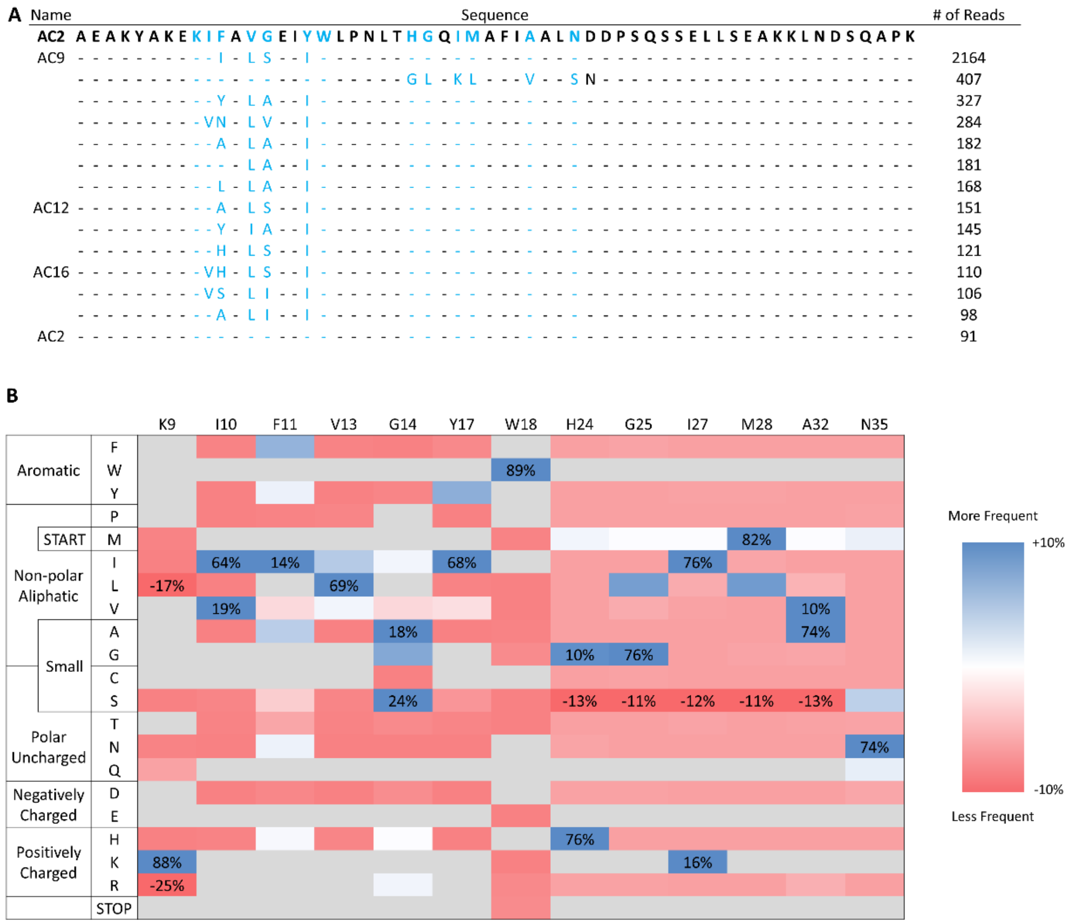

Figure 2-15. Deep sequencing of the merged library after enrichment reveals substantially improved mutants compared to parental.(A) Top unique sequences of the merged library listed by number of reads. Parental AC2 is supplied as a reference. Blue lettering indicates diversified residues in the helix-walking libraries, and dashes indicate parental amino acids at the indicated position. Clone names are supplied for sequences that were pursued for characterization. (B) Sitewise amino acid enrichments for the merged library. Amino acid frequencies were calculated by grouping, counting, and quad-root dampening identical sequences. Values shown are change in amino acid frequency in sorted populations compared to theoretical amino acid diversity of the naïve library. Amino acids not allowed by library design are shown in gray, except in cases where they are substantially enriched or depleted.

2.4 Discussion

High-throughput screening methods have facilitated the discovery of proteins with novel binding activity, but difficulties translating these interactions from the laboratory targets to cellular targets have hampered progress in meeting clinical demands. The majority of ligand selection campaigns for membrane-bound targets—which represent a broadly important class of molecules—are performed with purified soluble domains, which are not necessarily good models of their corresponding full length antigens and can thus yield pools of binders with high affinity and specificity for the soluble domain but no activity toward the cellular antigen. Yeast surface display methods for direct cellular selections[65,98,99] and fluorescence-activated cell sorting with detergent-solubilized cell lysates[99,110] have been developed to sort for ligands with activity toward full length, cellular antigens, but the efficacy of all of these methods for ligand development has yet to be directly compared. We compared combinations of five selection techniques using two different naïve ligand libraries and two clinically relevant targets to determine the most efficient method for selection of proteins with specific activity toward cellular antigens. Hybrid selection techniques proved to yield the highest frequency of successful campaigns.

Campaigns conducted against only purified extracellular domains of Thy1 and CD276 failed, at this point in the discovery process, to yield ligands that bound cellular antigens in three out of four cases. It remains possible that mutation and/or additional selections would have yielded functional ligands. In all three failed campaigns, some level of nonspecificity was observed at levels detectable with flow cytometry analysis. The Thy1 used in this study was an Fc fusion, and despite aggressive depletion with

human IgG during magnetic bead selections, the presence of this tag allowed for the enrichment of clones that bind human IgG instead of their intended target (Figure 2-2). Interestingly, although it did not bind other reagents, the fibronectin population selected against CD276 also bound the soluble extracellular domain of MET (Figure 2-16), a target it had never been exposed to during sorting. These case studies illustrate the importance of both careful consideration in reagent selection and sort design, as incomplete depletion or depletion with irrelevant antigens can allow specificity problems to persist. In contrast, the affibody population sorted against soluble CD276 returned a high frequency of diverse clones that specifically bound cellular CD276 with various binding strengths, suggesting that the CD276 used in this study contains some unknown number of translatable epitopes that could be accessed with the helical surface paratope library more efficiently than the loop paratope library.

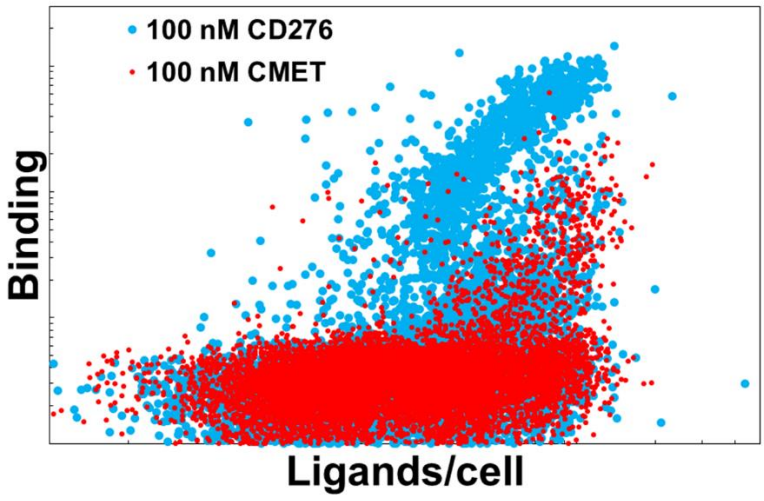

Figure 2-16. Assessment of specificity of fibronectin population against soluble CD276 extracellular domain.The population of fibronectin domains selected by magnetic bead sorting against soluble CD276 extracellular domain was assessed for target specificity. The population was labeled by either 100 nM soluble CD276 extracellular domain (blue) or 100 nM soluble CMET extracellular domain (red).

The addition of FACS with detergent-solubilized cell lysates after magnetic bead selections with soluble extracellular domains was not able to salvage translatable binding ligands from any of the three failed campaigns (Figure 2-2E–H and Figure 2-4A). It is unclear whether lysate quality or target affinity prevented the isolation of a minority population of translatable binders in these selections. However, affibodies sorted against soluble CD276 were able to be isolated from two rounds of FACS sorting, albeit with weaker binding strength than the corresponding population isolated by soluble target selection methods only.

Direct cellular selections conducted after soluble target-based enrichment were able to enrich a population of CD276-specific fibronectin domains that consisted of a single translatable clone family (Figure 2-3B and Figure 2-4A). This clone was likely a minority component in the bead sorted population as it was not isolated without cellular enrichment. However, its existence in the bead sorted population does confirm that at least one translatable epitope exists in the soluble CD276 extracellular domain that is accessible by a loop paratope. Cellular selections also isolated a wide variety of CD276-binding affibodies. Interestingly, none of the affibodies isolated from bead sorting followed by cellular selection showed sequence overlap with those isolated from soluble target methods alone. This likely has to do with the nature of the affinity-based FACS conducted prior to characterization of clones isolated with soluble target only. Unmodified cellular selections provide minimal affinity pressure[66], so affibodies isolated with this method likely fall in the population of clones with weaker affinity for both soluble and cellular CD276. Even cellular selections were not able to isolate cell-binding ligands from the fibronectin and affibody populations selected against soluble Thy1-Fc,

suggesting that any translatable epitopes in this protein were not accessible by either paratope type.

Collectively, the use of cellular selections yielded hits in three out of four campaigns attempted. In contrast with the soluble domain-driven selection methods, which predominantly suffered from nonbinders at the cellular level, the major source of "misses" for cellularly selected clones was nonspecificity in all cases. Because the cell surface contains a wide array of macromolecules, including proteins, lipids, and polysaccharides, nonspecific ligands have many options for binding partners. A subset of nonspecific ligands potentially bind a specific antigen that is expressed on both target-expressing and target-negative cell lines. Others could bind macromolecules nonselectively through hydrophobic interactions, allowing them high avidity for enrichment on any cell type. In an attempt to deplete these nonspecific binders, a set of campaigns utilized magnetic bead depletions prior to enrichment on mammalian cell monolayers. Population level quantification of recovery showed that this type of depletion was insufficient, recovering sub-1% quantities of yeast displaying nonspecific ligands in all attempts (Figure 2-3). Indeed, when individual clones were assessed, the nonspecificity problem persisted essentially identically to the case of cellular selection without depletion (Figure 2-4A). This result suggests that nonspecificity has different characteristics depending on which selection method is used. Importantly, not all clones determined as "hits" in the clonal cell panning assay showed antigen specificity. Three affibodies against Thy1 from the cellular selection only arm showed nonspecificity when produced as soluble proteins, suggesting some unquantified level of inconsistency between the yeast displayed and soluble versions of the proteins.

To decrease the prevalence of nonspecific clones in cellular selections, multiple potential depletion techniques were explored. Sequential depletion, which has previously shown selectivity enhancement in panning for antibody fragments that bind glioblastoma stem-like cells[109], resulted in inconsistent enrichment of target specific binders from these mixtures, which could be a result of nonspecific yeast–mammalian cell interactions that are not ligand mediated or sequestration of yeast in the corners of the plate wells (Figure 2-6). It is known from previous studies that there is a baseline level of background recovery of approximately 0.1% of the yeast input[65]. Loss of the rare CD276-specific yeast through this mechanism would be impactful on their ability to be recovered. This effect may be compounded through each additional depletion step, potentially explaining the generally decreasing trend in enrichment of CD276-specific binders as more depletion steps are added. It is unclear, however, why the enrichment ratio of the nonspecific binding yeast remains essentially unchanged with increasing depletion. It is possible that the yield of a nonspecific binder against target negative cells may have been lower than expected, disfavoring depletion. Overall, these results suggest that sequential depletion against target negative mammalian cell monolayers will not confer the enrichment advantage to target specific binders in a practical setting.

Initial studies using depletion with disadhered mammalian cells yielded encouraging results in the high-yield case (Figure 2-7). If continued through multiple rounds, the 14 ± 6-fold selectivity advantage for the CD276-specific binder relative to the nonspecific binder would propagate, accomplishing this study's goal of nonspecific binder depletion. The reduced ability to accomplish the same selectivity with the low-yield binder mixture was a surprising result. It appeared, based on the 0-depletion data,

that the low-yield nonspecific binder enriched more strongly against target positive cells than the low-yield CD276-specific binder. This could be the cause for the lack of selectivity, as any nonspecific binder that is not depleted by the preblocking strategy has a 6-fold higher enrichment ratio than the CD276-specific binder. When 13 additional clones were tested with and without preblocking, a selective advantage to antigen-specific binders was observed.

The ability to strongly deplete the high-yield nonspecific binders while being unable to deplete low-yield nonspecific binders can still yield a functional improvement in selections from naïve libraries. It has been shown that strong- and midaffinity binders can quickly out-enrich weaker binders in an EGFR-binding model system[66]. With the depletion of high-yield nonspecific binders, the high- and mid-yield specific binders will have the opportunity to similarly out-enrich the remaining low-yield nonspecific binders that could not be effectively depleted. Although the depletion of nonspecific binders will not be complete in this regime, it will confer an important incremental improvement for cellular selections using yeast surface display libraries.

Toward the preclinical development of a synthetic ligand for CD276, we aimed to further enhance the affinity of existing CD276 binders by evolving the hits from all affibody campaigns toward CD276 via error-prone PCR and aggressive sorting. Despite this, sequenced clones were revealed to be a single sequence, AC2, which was found when the unmutated recombinant-selected population was sequenced (Table 2-1). This indicates that random mutation was unsuccessful in producing a functional clone with higher binding affinity to CD276 cell lysate. Given the moderate affinity of AC2, it is

possible that the sparse sampling of sequence space created by error-prone PCR was insufficient to produce a substantially improved clone over AC2.

As an alternate approach, helix-walking, analogous to CDR-walking or loop-walking, was pursued as a mutagenesis strategy to create a more focused library with a higher proportion of functional clones. Two libraries were created in which a single helix was mutated while the other was constrained to parental AC2. Given the relative success of translating affibodies matured against recombinant CD276, a preliminary bead and FACS sort was conducted with recombinant target to deplete nonfunctional and nonspecific molecules under low affinity pressure. Further sorting with cell lysate FACS showed little cross-reactivity relative to previous sorts conducted on the naïve library and isolated a wide variety of CD276-binding affibodies in the helix one library (Figure 2-10). The helix two library returned parental as the most prevalent sequence, with very little sequence diversity observed, indicating that far fewer beneficial mutations in the second helix exist.

Once merged and more aggressively sorted, the final population yielded a variety of sequences more prevalent than parental (Figure2-11 and Figure 2-15). For the most part, all sequences more prevalent than parental contained no mutations in the second helix, with the notable exception of the second most prevalent sequence, which contained several second helix mutations. This sequence warrants further study as to whether combination with any of the observed first helix mutations would provide further affinity, but is outside the scope of this study.

To confirm the increased affinity of the population, several top sequences were chosen at random and tested for binding affinity and thermal stability, which displayed substantial improvement over the parental CD276-binding affibody.

2.5 Conclusion

In conclusion, the current study advances the understanding of the advantages and disadvantages of multiple yeast-displayed ligand selection techniques, which can lead to the identification of more robust ligand selection strategies. Ligands isolated from soluble extracellular domain-driven campaigns can yield surprising nonspecificity despite aggressive depletion and ultimately cannot translate to cellular binding. Cellular selections can be employed as a follow-up to the use of soluble targets to enrich clones that bind translatable domains, but these are not present and accessible in all target-ligand pairings. Cellular selections from naïve libraries often lead to nonspecificity, but depletion using disadhered mammalian cells—more so than soluble control proteins—shows promising results. A lead affibody against CD276 was isolated through these methods, which can be utilized for diagnostic and therapeutic benefit in future work.

2.6 Materials and Methods

2.6.1 Cells and Cell Culture

Mile Sven 1 cells stably transfected to express human CD276 (MS1-CD276)[139] or human Thy1 (MS1-Thy1)[142] were grown at 37 °C in a humidified atmosphere with 5% CO_2 in DMEM with 4.5 g/L glucose, sodium pyruvate, and glutamine supplemented with 10% (v/v) fetal bovine serum.

Yeast surface display was performed essentially as described[132]. EBY100 yeast harboring expression plasmids were grown in SD-CAA medium (16.8 g/L sodium citrate dihydrate, 3.9 g/L citric acid, 20.0 g/L dextrose, 6.7 g/L yeast nitrogen base, 5.0 g/L casamino acids) at 30 °C with shaking. Protein expression was induced by transferring yeast cells in logarithmic phase ($OD_{600\ nm} < 6$) into SG-CAA medium (10.2 g/L sodium phosphate dibasic heptahydrate, 8.6 g/L sodium phosphate monobasic monohydrate, 19.0 g/L galactose, 1.0 g/L dextrose, 6.7 g/L yeast nitrogen base, 5.0 g/L casamino acids) and growing at 30 °C with shaking for at least 8 h. EBY100 without plasmid were grown in YPD medium (10.0 g/L yeast extract, 20.0 g/L peptone, 20.0 g/L dextrose) at 30 °C with shaking.

2.6.2 Naïve Library Construction and Characterization

Oligonucleotides encoding for the second-generation sitewise gradient hydrophilic fibronectin domain library[70] and second-generation sitewise gradient affibody library[68] were synthesized by IDT DNA Technologies. Full length amplicons for each respective library were assembled by overlap extension PCR and homologously recombined into pCT-40 yeast surface display vector, with a linker extended by 40 additional amino acids[65], within yeast strain EBY100 by electroporation transformation as previously described[70]. Transformation efficiency was quantified by dilution plating on SD-CAA agar plates.

Full-length library construction was characterized by simultaneous labeling of the N-terminal hemagglutinin (HA) epitope and C-terminal c-Myc epitope by flow cytometry. Two million yeast were pelleted at 12 000*g* for 1 min, washed once with phosphate-buffered saline (PBS) with 1 g/L bovine serum albumin (PBSA), then labeled

with mouse anti-c-Myc antibody 9E10 (0.5 μg/mL, BioLegend, Cat: 626802) and biotinylated goat anti-HA polyclonal antibody (2 μg/mL, Genscript, Cat: A00203) for 30 min at room temperature. Cells were washed once with 1 mL of PBSA, labeled by goat antimouse Alexa Fluor 647 conjugate (10 μg/mL, Life Technologies, Cat: A-21235) and streptavidin Alexa Fluor 488 conjugate (2 μg/mL, Life Technologies, Cat: S11223) for 15 min at 4 °C, and washed once. Fluorescence was analyzed by flow cytometry (Accuri C6, BD Biosciences).

2.6.3 Magnetic Bead Selections with Soluble Extracellular Domains

Recombinant human Thy1 extracellular domain Fc fusion (Thy1-Fc; Abcam, Cat: ab157072) was biotinylated on free amines using EZ-Link NHS-PEG4-Biotin (Thermo Fisher Scientific, Cat: 21330) with a NHS-PEG4-biotin/protein ratio of 5:1. Biotinylation was verified using matrix-assisted laser desorption ionization mass spectrometry (Sciex 5800, Applied Biosystems). Recombinant human CD276 extracellular domain (Sino Biological, Cat: 11188-H08H-B) was obtained already biotinylated from the manufacturer.

Magnetic bead selections were carried out essentially as previously described[48] using 15-fold oversampling of ligand diversity at all stages. For the first round of selection, libraries were depleted of magnetic bead binders three times with streptavidin coated Dynabeads (Thermo Fisher Scientific, Cat: 11205D). Remaining yeast were incubated with CD276 or Thy1-Fc coated magnetic beads at 4 °C and washed twice with ice cold PBSA. Beads with attached cells were resuspended in SD-CAA for growth. Magnetic beads were removed using a Dynal magnet prior to the induction of protein expression for the next round of selection. For subsequent rounds, nonspecific binders

were depleted with streptavidin-coated magnetic beads and negative control protein-coated magnetic beads prior to enrichment with target-coated magnetic beads. Negative control targets included human IgG (Rockland Immunochemicals, biotinylated by manufacturer), glucose-6-phosphate dehydrogenase (Sigma, biotinylated by manufacturer), and a scrambled peptide of a loop from prostate stem cell antigen (United Peptide, biotinylated during peptide synthesis). Selections were carried out at room temperature, and target-coated beads were washed three times with PBSA before regrowth of the attached yeast. Dilution plating on YPD plates of all negative control and target-coated bead populations was completed to quantify yield for each round.

2.6.4 FACS with Soluble Extracellular Domains

Fluorescence-activated cell sorting (FACS) was carried out essentially as described[132]. Induced yeast were simultaneously labeled with mouse anti-c-Myc antibody (9E10, BioLegend, Cat: 626802, 2.5 μg/mL) and 10–100 nM biotinylated target protein or biotinylated negative control protein for at least 30 min at room temperature. Cells were washed once with PBSA, labeled with goat antimouse Alexa Fluor 647 conjugate (Thermo Fisher Scientific, Cat: A-21235, 10 μg/mL) and streptavidin Alexa Fluor 488 conjugate (Thermo Fisher Scientific, Cat: S-11223, 2 μg/mL) for 15 min at 4 °C, and washed with 1 mL of PBSA. Cells with the highest binding/ligand display ratio (AlexaFluor488/AlexaFluor647) were sorted using a FACS Aria II (BD Bioscience).

2.6.5 FACS Selections with Detergent Solubilized Cell Lysates

Detergent-solubilized cell lysates were prepared essentially as described[99]. MS1-Thy1 and MS1-CD276 cells were grown to 70–90% confluence in 75 cm^2 tissue culture-treated flasks. Culture medium was removed, and the cells were washed once with 5 mL

of PBS. Cells were detached by trypsin-EDTA treatment for 4–7 min, quenched with serum-containing culture medium, and centrifuged at 500*g* for 3 min. Pelleted cells were washed three times with ice cold PBS and pelleted at 300*g* for 3 min at 4 °C. Washed cells were resuspended in PBS with 0.5 mg/mL fresh sulfo-NHS-biotin (Thermo Fisher Scientific, Cat: 21217), rotated for 30 min at room temperature, and washed twice with ice cold PBSA to quench and remove excess biotin. Cells were resuspended in 100–200 μL of FACS lysis buffer (PBS with 1% (v/v) Triton X-100, 2 mM EDTA, and 1 × cOmplete protease inhibitor cocktail (Roche)) and incubated with rotation at 4 °C for 15 min. Cell debris was pelleted at 15 000*g* for 30 min at 4 °C and removed. Induced yeast were washed once with PBSA, then incubated with cell lysate and mouse anti-c-Myc antibody (2.5 μg/mL) simultaneously for 2 h at 4 °C with rotation. Yeast were washed with 1 mL of ice cold PBS containing 1% (v/v) Triton-X 100 and then with 1 mL of ice cold PBSA. Cells were incubated with goat antimouse Alexa Fluor 647 conjugate (10 μg/mL) and streptavidin Alexa Fluor 488 conjugate (2 μg/mL) at 4 °C for 15 min and washed with 1 mL of ice cold PBSA. Cells with the highest binding/ligand display ratio (AlexaFluor488/AlexaFluor647) were sorted using a FACS Aria II.

2.6.6 Yeast Cell Panning Selections

Cell panning selections were carried out essentially as described[65]. Mammalian cells were grown in six-well plates to approximately 90% confluence. Culture medium was removed, and cells were washed three times with ice cold PBSA with 1 mM $CaCl_2$ and 0.5 mM Mg_2SO_4 (PBSACM). For the first round of selection, 2.4×10^9 yeast (3-fold diversity of fibronectin library, 6-fold diversity of affibody library) were washed once with ice cold PBSACM, resuspended to 1×10^8 yeast/mL in ice cold PBSACM, and

applied to mammalian cells in 1 mL aliquots dropwise. Cells were incubated without shaking for 2 h at 4 °C, and unbound yeast were removed by aspiration. Cells were washed with 1 mL of ice cold PBSACM four times with 25 gentle tilts and 5 nutations and one time with 10 nutations. Bound yeast were recovered by scraping cell monolayers and resuspending them in SD-CAA growth medium. Yield was quantified by dilution plating on YPD plates. For each subsequent round, at least 15-fold of the recovered yield was washed and resuspended to no more than 1×10^8 yeast/mL in ice cold PBSACM. Yeast were panned, in parallel, against one target-positive and two target-negative cell lines.

2.6.7 Clonal Characterization of Sorted Populations by Yeast-Cell Panning

Forty-eight colonies from each selection campaign, obtained by plating yeast populations on SD-CAA, were picked and resuspended in 1 mL of SG-CAA in deep-well 96-well plates. Plates were covered and grown at 30 °C with shaking for at least 8 h.

Target-positive and target-negative mammalian cells were grown to approximately 80% confluence in 24-well plates. Cells were washed three times with ice cold PBSACM. Aliquots of 250 μL of induced clonal yeast were added dropwise directly to one well of target-positive and one well of target-negative mammalian cells. Cells were incubated without shaking for at least 2 h at 4 °C. Cells were washed with 250 μL of ice cold PBSACM twice with 25 gentle tilts and five nutations and once with 10 nutations. Yeast binding was visualized using the EVOS FL Cell Imaging System (Thermo Fisher Scientific) at 40× total magnification.

Individual clone binding strength was categorized as −, + , ++, or +++ through counting associated yeast in a random microscope field. Clones were characterized as "–"

if fewer than 15 yeast were observed, "+" if 15 to 50 yeast were observed, "++" if greater than 50 yeast were observed but mammalian cells were still visible, and "+++" if yeast were the dominant organism seen in the frame.

2.6.8 DNA Sequencing

Plasmid DNA from yeast clones that bound target-positive but not target-negative cells was recovered by a Zymoprep of 200 μL of each individual clone. Ligand sequences were amplified in 50 μL of PCR mixtures containing 2 μL of Zymoprep DNA, 1× Phusion High Fidelity buffer, 0.5 μM each of primers W5 and W3[151], 0.2 mM dNTP mixture, and 2.5 U Phusion polymerase (New England Biolabs). PCR products were purified by agarose gel electrophoresis and Sanger sequenced with GeneAmp5 primer (5′-CGACGATTGAAGGTAGATACCCATACG-3′; Eurofins MWG Operon).

2.6.9 Error-Prone PCR of Fibronectin and Affibody Domains

Random mutation of fibronectin domains and affibodies was performed essentially as described[151] by error-prone PCR with nucleoside analogs[152]. Zymoprepped plasmid DNA was mutated by error-prone PCR of full fibronectin domain or affibody genes using primers W5/W3; fibronectin loops using primers BCHPEP5/BCHPEP3, DEHPEP5/DEHPEP3, and FGHPEP5/FGHPEP3; and affibody helices using primers ABY1F-b/ABY1R and ABY2F/ABY2R-b (Table 2-3). PCR products were purified by agarose gel electrophoresis, amplified in four 200 μL PCR mixtures, concentrated by ethanol precipitation, and resuspended in 30 μL of buffer E (1 M sorbitol, 1 mM $CaCl_2$) several hours before electroporation. Mutated sublibraries were homologously recombined with linearized pCT-Gene (cut with *Nde*I, *Pst*I-HF, and *Bam*HI-HF), pCT-40-FnHP-Loop (cut with *Sma*I, *Nco*I-HF, and *Nde*I) for fibronectin loop shuffling, or

pCT-40-Helix (cut with *Sma*I, *Nco*I-HF, and *Nde*I) for affibody helix shuffling in EBY100 yeast by electroporation transformation as described[70].Transformation efficiency was quantified by dilution plating on SD-CAA plates.

W5	5'-CGACGATTGAAGGTAGATACCCATACGACGTTCCAGACTACGCTCTGCAG-3'
W3	5'-ATCTCGAGCTATTACAAGTCCTCTTCAGAAATAAGCTTTTGTTCGGATCC-3'
BCHPEP5	5'-CTGGAGGTTACCAACGCAACTCCGAACTCTCTGACTATTTCTTGG-3'
BCHPEP3	5'-CGGAACAGTGAATTCCTGGCTCGGGGAGTTACCACCAGTTTCGCCGTAGGTGATACGGTA-3'
DEHPEP5	5'-TACCGTATCACCTACGGCGAAACTGGTGGTAACTCCCCGAGCCAGGAATTCACTGTTCCG-3'
DEHPEP3	5'-TACAGCGTACACGGTAATGGTATAATCCTGGCCCGGTTTCAGACCGCTGATGGTCGC-3'
FGHPEP5	5'-AAACCGGGCCAGGATTATACCATTACCGTGTACGCTGTA-3'
FGHPEP3	5'-GTCGATTTCGGTGCGATAATTGATGCTGATTGG-3'
ABY1F-b	5'-TTCTGGTGGTGGTGGTTCTGCTAGCGCCGAAGCAAAATAC-3'
ABY1R	5'-GGTCAGGTTCGGCAG-3'
ABY2F	5'-CTGCCGAACCTGACC-3'
ABY2R-b	5'-TTTCTTCGCCTCAGACAGGAGTTCAGAGCTCTGGGACGGGTC-3'

Table 2-3. Error-Prone PCR Oligonucleotide Sequences

2.6.10 Expression Plasmids for Depletion Model

CD276-specific or nonspecific affibody clones were chosen from populations selected to bind either soluble CD276 extracellular domain or MS1-CD276 cells with relative binding strength defined with a phase microscopy assay. Clones HS (high-yield specific) and LS (low-yield specific) bind MS1-CD276 cells as "+++" and "+," respectively while binding MS1-Thy1 as "–" when assessed by microscopy (Table 2-4). Clones HN (high-yield non target-specific) and LN (low-yield non target-specific) bind both MS1-CD276 and MS1-Thy1 as "+++" and "+," respectively (Table 2-4). Clones HS and LS were cloned into pCT-40 vector by NheI and *Bam*HI restriction sites. Nontarget specific affibody clones HN and LN were cloned into pCT-40V[66] vector (pCT-40 with the c-Myc tag replaced by a V5 tag) by NheI and *Bam*HI restriction sites. Affibody clone

A5[24], an affibody with no known binding partner, was cloned into pCT-40E[66] vector (pCT-40 with the c-Myc tag replaced by an E-tag) by NheI and *Bam*HI restriction sites (Table 2-4).

HS	AEAKYTKEKANAIVQILVLPNLTVSQLHAFLSALHNDPSQSSELLSEAKKLNDSQAPK
HN	AEAKYAKESSYASLYIGILPNLTHSQYYAFIYALQDDPSQSSELLSEAKKLNDSQAPK
LS	AEAKYNKELANAALSIVYLPNLTGDQKSAFWLALQDDPSQSSELLSEAKKLNDSQAPK
LN	AEAKYAKERHRAWMEITGLPNLTRPQRIAFILALRDDPSQSSELLSEAKKLNDSQAPK
A5	AEAKYAKENFNATSEIYYLPNLTHFQRSAFSNALFDDPSQSSELLSEAKKLNDSQAPK

Table 2-4. Sequences for Depletion Model System

2.6.11 Determination of Optimal Incubation Time for Cellular Selections

MS1-CD276 was grown to approximately 90% confluence in 12-well plates. Culture medium was removed, and cells were washed three times with 500 μL of ice cold PBSACM.

A total of 5×10^7 yeast expressing CD276-specific affibody clone HS or LS were pelleted at 8000*g* for 1 min, washed once with ice cold PBSACM, and resuspended in 500 μL of ice cold PBSACM. Yeast were then applied to MS1-CD276 monolayers dropwise and incubated at 4 °C without shaking for 15, 30, 45, 60, or 120 min. Cells were washed five times with 500 μL ice cold PBSACM as described[65]. Briefly, cells were tilted 25 times and rotated five times for the first four washes and rotated 10 times only for the fifth wash. A total of 500 μL of SD-CAA was added dropwise to the washed wells, and cells were recovered by scraping. Yeast recovery was quantified by dilution plating on YPD plates (10 g/L yeast extract, 20 g/L peptone, 20 g/L dextrose, 16 g/L agar).

2.6.12 Depletion of Nonspecific Clones with Sequential Depletion

Mixtures of 0.2 ± 0.1% CD276-specific, 3 ± 2% nonspecific, and 97 ± 2% nonbinding affibody-displaying yeast were generated, and compositions were quantified by flow cytometry analysis. Yeast were pelleted and washed once with ice cold PBSACM, then resuspended to a concentration of 1×10^8 yeast/mL in ice cold PBSACM.

MS1-Thy1 and MS1-CD276 were grown to approximately 90% confluence in 12-well plates. Culture medium was removed and cells were washed three times with 500 μL of ice cold PBSACM. A total of 500 μL of yeast mixture were added to MS1-Thy1 monolayers dropwise and incubated at 4 °C for 15 min without rotation. The binding buffer containing unbound yeast were collected. Monolayers were washed four times as described in the previous section, with unbound yeast collected and pooled. The collected yeast were concentrated into 500 μL of ice cold PBSACM and applied to the next washed MS1-Thy1 monolayer. This process was repeated for zero, two, four, or six depletion steps against MS1-Thy1 monolayers. Recovered yeast were then applied to an MS1-CD276 monolayer and incubated at 4 °C for 120 min. Monolayers were washed five times, and bound yeast were recovered by scraping as before. Yeast recovery was quantified by dilution plating on YPD plates. Recovered yeast were grown in 5 mL of SD-CAA at 30 °C with shaking. Protein expression was induced by resuspending a portion of the outgrowth in SG-CAA at $OD_{600\ nm} < 1$ and growing these yeast for at least 8 h at 30 °C with shaking.

Mixture compositions were quantified by flow cytometry analysis. Yeast were pelleted and washed once with 1 mL PBSACM. Yeast were then labeled with 20 μL of goat anti-c-myc FITC conjugate (Bethyl Laboratories, Cat: A190–104F, 2 μg/mL), goat

anti-V5 FITC conjugate (Bethyl Laboratories, Cat: A190–119F, 2 μg/mL), or goat anti-E-tag FITC conjugate (Bethyl Laboratories, Cat: A190–132F, 2 μg/mL) for 20 min at room temperature. Yeast were then pelleted and washed once with PBSACM. Fluorescence was analyzed using an Accuri C6 (BD Biosciences). Enrichment ratios were determined by dividing the percentage positive for one tagged construct by the total percentage of induced yeast.

2.6.13 Depletion of Nonspecific Clones by Pre-Blocking with Disadhered Mammalian Cells

MS1-Thy1 was grown to approximately 90% confluence in a 75 cm^2 tissue culture-treated flask. Culture medium was removed, and cells were washed once with 5 mL of PBS. Cells were disadhered by trypsin-EDTA treatment for 6 min, then quenched by the addition of serum-containing culture medium. Cells were then pelleted at 500*g* for 3 min, trypsin-containing culture medium was removed, and cells were resuspended in fresh culture medium for counting using a Countess II FL (Thermo Fisher Scientific).

Mixtures of 0.3 ± 0.1% CD276-specific, 1.9 ± 0.8% nonspecific, and 98 ± 0.7% nonbinding affibody-displaying yeast were generated, and compositions were quantified by flow cytometry analysis. Yeast were pelleted and washed with ice cold PBSACM and resuspended to 5×10^7 yeast in 500 μL of ice cold PBSACM containing 1×10^6 MS1-Thy1. Yeast and MS1-Thy1 were incubated at 4 °C with rotation for 2 h. After incubation, samples were added dropwise to washed MS1-CD276 monolayers in 12-well plates and incubated at 4 °C without rotation for 15 min. Monolayers were washed five times with 500 μL of ice cold PBSACM as described above. Bound yeast were recovered by scraping. Yeast recovery was quantified by dilution plating on YPD plates. Recovered

yeast were grown, protein expression was induced, and final mixture composition was determined by flow cytometry as described above.

2.6.14 Helix Walking Library Construction

CD276 rational mutagenesis libraries were constructed using an analogous method to CDR-walking[84,149,150]. The first affibody helix was diversified at seven sites using degenerate oligonucleotides while retaining the parental sequence in the second helix. Separately, the second affibody helix was diversified at six sites using degenerate oligonucleotides while retaining the parental first helix. The diversified oligonucleotide for one helix and parental oligonucleotide for the other helix were assembled by overlap extension PCR and homologously recombined into pCT-Helix yeast surface display vector within yeast strain EBY100 by electroporation transformation. Transformation efficiency was quantified by dilution plating on SD-CAA agar plates. Full-length library construction was characterized by flow cytometry as previously described.

2.6.15 Protein Production

Gel-purified PCR amplicons were digested by *Nhe*I-HF and *Bam*HI-HF and ligated into a pET-22b vector containing a C-terminal His_6 tag (Novagen, EMD Millipore) using T4 DNA ligase (New England Biolabs). Plasmids were transformed via heat-shock into T7 Express *E. coli* (New England Biolabs) and plated on lysogeny broth (LB; 10.0 g/L tryptone, 5.0 g/L yeast extract, 10.0 g/L sodium chloride) agar plates containing kanamycin (50 mg/L). Clones were verified by Sanger sequencing of plasmids recovered by bacterial miniprep (Epoch Life Science).

E. coli were grown to saturation in 5 mL of LB containing kanamycin at 37 °C with shaking. Cultures were diluted to $OD_{600\,nm}$ = 0.03 with 100 mL of LB in 250 mL of

baffled culture flasks. At $OD_{600\,nm}$ = 0.5–1.0, protein expression was induced with 0.5 mM isopropyl β-d-1-thiogalactopyranoside overnight at 30 °C with shaking. Cells were pelleted at 3220*g* for 20 min, resuspended in bacterial lysis buffer (50 mM sodium phosphate (pH 8.0), 0.5 M sodium chloride, 5% glycerol, 5 mM CHAPS, and 25 mM imidazole supplemented with protease inhibitor) and subjected to four to five freeze–thaw cycles. Insoluble cell debris was removed by centrifugation at 12 000*g* for 10 min followed by filtration (0.2 μm). Protein was purified by metal affinity chromatography on 2 mL of Cobalt HisPur Resin (Thermo Fisher Scientific) or HisPur Cobalt Resin Spin Columns (Thermo Fisher Scientific) according to the manufacturer's protocol. Eluted fractions were pooled and buffer exchanged by HPLC prior to lyophilization. Lyophilized protein was resuspended in PBS, and protein concentration was quantified by absorbance at 280 nm[153]. Protein identity was verified by MALDI-TOF-MS using a 5800 matrix-assisted laser desorption ionization mass spectrometry.

2.6.16 Affinity Titration of Affibody Domains

Detached MS1-Thy1 and MS1-CD276 cells were washed and individually labeled with varying concentrations of purified affibody for 25 min at 4 °C with rotation unless additional time was needed to approach binding equilibrium. Cells were pelleted at 500*g* for 3 min and washed with 1 mL of ice cold PBSACM prior to labeling with 50 μL of anti-His_6 FITC conjugate (Abcam ab1206; 10 μg/mL) for 25 min at 4 °C. Cells were again pelleted and washed with 1 mL of ice cold PBSACM. Fluorescence was analyzed using an Accuri C6. The dissociation constant was calculated by nonlinear least-squares regression using a 1:1 binding model.

2.6.17 Thermal Stability of Affibody Domains

Secondary structure, midpoint of thermal denaturation (T_m), and protein refolding were determined using circular dichroism spectroscopy performed on a Jasco-815 spectrophotometer. Purified and lyophilized protein was resuspended in PBS to a concentration of 20 μM and placed in a 1 mm path length quartz cuvette. Ellipticity was measured between 200 and 260 nm wavelengths at 20 °C before and after heating to 98 °C in order to observe secondary structure of the folded affibody. Samples were then heated at 1 °C/min from 20 to 98 °C, while the ellipticity was monitored at 220 nm. The midpoint of thermal denaturation was calculated by nonlinear least-squares regression using a two-state protein unfolding model.

Chapter 3 – Magnetic Bead-Immobilized Mammalian Cells Are Effective Targets to Enrich Ligand-Displaying Yeast

Adapted with permission from "Lown, P.S; Hackel, B.J. "Magnetic Bead-Immobilized Mammalian Cells Are Effective Targets to Enrich Ligand-Displaying Yeast" *ACS Comb. Sci.* **2020**, 22 (5), 274-284" Copyright 2020 American Chemical Society

3.1 Summary

Yeast surface display empowers selection of protein binding ligands, typically using recombinant soluble antigens. However, ectodomain fragments of transmembrane targets may fail to recapitulate their true, membrane-bound form. Direct selections against adhered mammalian cells empower enrichment of genuine binders yet benefit from high target expression, robustly adherent mammalian cells, and nanomolar affinity ligands. This study evaluates a modified format with mammalian cells immobilized to magnetic beads; yeast-displayed fibronectin domain and affibody ligands of known affinities and cells with expression ranges of epidermal growth factor receptor (EGFR) and CD276 elucidate important parameters to ligand enrichment and yield in cell suspension panning with comparison to adherent panning. Cell suspension panning is hindered by significant background of nondisplaying yeast but exhibits yield advantages in model EGFR systems for a high affinity (K_d = 2 nM) binder on cells with both high (10^6 per cell) target expression (9.6 ± 0.6% vs 3.2 ± 0.4%, $p < 0.0001$) and mid (10^5) target expression (2.3 ± 0.5% vs 0.41 ± 0.09%, $p = 0.0008$), as well as for a low affinity (K_d > 600 nM) binder on high target expression cells (2.0 ± 0.5% vs 0.017 ± 0.005%; $p = 0.001$). Significant enrichment was observed for all EGFR systems except the low-

affinity, high expression system. The CD276 system failed to provide significant enrichment, indicating that this technique may not be suitable for all targets. Collectively, this study highlights new approaches that yield successful enrichment of yeast-displayed ligands via panning on immobilized mammalian cells.

3.2 Introduction

Protein ligands have been engineered[10,28,127] to clinically treat diseases with altered biomarker expression through direct inhibition, targeted drug/radioisotope delivery, and immune system engagement[1,154]. Similar ligands have been used for diagnostic purposes, such as targeted molecular imaging[128] and biomarker detection in blood and urine[155–158]. Recent advances in clinical biomarker discovery, such as next-generation sequencing[159], mass spectrometry-based proteomics[160,161], and other chemical biology techniques, have drastically increased the number of well-characterized, clinically relevant targets. This has resulted in a growing demand for engineered ligands to target these new biomarkers.

Common high-throughput methods, such as yeast[60,61,162] and phage[42,43,122] display technologies linking genotype to phenotype, coupled with selections via magnetic bead capture[20,48,163–165] and fluorescence activated cell sorting (FACS)[55,80], have been used to address this demand. Experimental screening strategies require the use of the biomarker to isolate binding ligands; however, many clinically relevant biomarkers possess hydrophobic transmembrane domains, making them difficult to work with in an aqueous environment. In lieu of full-length proteins, recombinantly produced soluble ectodomains are often used as analogs during ligand selections. While this strategy has proven successful[68,70,81–84,111], many engineered ligands fail to bind to genuine antigen on target-

expressing cells (Chapter 2)[166]. As negative results may be less likely to be published[167], there is a lack of research thoroughly investigating this problem, thus understating the need for more reliable methods of translatable ligand discovery.

The failure of recombinant soluble ectodomain-based selection methods indicates that these ectodomain fragments may not fully recapitulate the protein in its true, membrane-bound form. While this issue remains largely unstudied, a number of factors may cause this failure, including the improper folding and aggregation of the soluble ectodomains[87,89,130,131], non-natural post-translational modification due to the production host cell type[88,91], the addition of biological or chemical tags for purification and selection[71], and the absence of a transmembrane domain or cell membrane. All of these factors may create epitopes that are masked or not present in the true, membrane-bound antigen.

To avoid these issues, a number of selection techniques utilizing target-expressing cells have been developed, including FACS using detergent-solubilized cell lysate[99,110,162] or whole cells[112,168] and panning on adherent cell monolayers[65,98,99]; however, these techniques leave room for improvement. While FACS with cell lysate or whole cells is an effective method for enrichment, its throughput (10^7–10^8 per hour) is substantially below current display library sizes[20,44,56,70] and its lack of avidity limits the enrichment of weaker affinity ligands, such as those isolated from some de novo libraries. While adherent cell panning has been employed successfully in multiple scenarios[100,102–109,122,169], a study using EGFR-binding fibronectins found that enrichment is hindered when using cells with low-to-moderate ($\leq 10^5$ targets/cell) expression or ligands of micromolar or weaker affinity[65].

The use of cells in suspension has been investigated as an alternative method of cell panning in phage display libraries[101,112,123,170] and has shown success in isolating binding ligands to cell biomarkers[171,172]. There is also some evidence that cell suspension panning may outperform adherent cell panning in the phage display context, as two phage library campaigns against cells in suspension succeeded after equivalent campaigns against adherent cells failed[117,118]. This success motivates adaptation of these methods to yeast surface display libraries; however, cell suspension panning methods for phage display use differential centrifugation to separate cell-bound phages from nonbinding phages, which has been limitedly studied in yeast surface display[119]. Selections using mammalian cells conjugated to magnetic beads is an attractive alternate method of sorting because of the effectiveness of conjugation[173], as well as the high capacity (10^6 binding yeast per 10^6 magnetic beads), throughput (10^{10} cells per selection), and established reliability of isolating specific binders to the immobilized target associated with magnetic bead selections[48,79].

This study aims to evaluate a new method of ligand selection using suspended mammalian cells immobilized to magnetic beads as a selection agent in comparison to traditional adherent mammalian cell panning. It is hypothesized that the use of suspended mammalian cells may aid in enrichment and enhance capacity by increasing the exposed mammalian-cell surface area for ligand binding while potentially enabling ligand campaigns against cell lines that cannot be cultured adherently for traditional cell panning.

To optimize and better understand the parameters for successful cell-based selections using yeast surface display in this new system, washing stringency, target expression on mammalian cells, ligand binding affinity, ligand protein scaffold, and target of interest were systematically varied to understand how each parameter affects enrichment ratio and yield of ligand-displaying yeast in EGFR-expressing and CD276-expressing systems. While a significantly increased background yield of nondisplaying yeast limits the effectiveness of cell suspension panning, it shows a significant increase in the yield of binding yeast compared to adherent panning. In addition, cell suspension panning demonstrates substantially increased throughput, which allows the sorting of larger libraries in shorter timespans. The use of a CD276-expressing model failed to provide effective enrichment, indicating that not all targets may be suitable for this technique. Together, these results advance understanding and development of protocols for ligand selection experiments.

3.3 Results

Two different magnetic beads were used to generate bead-mammalian cell conjugates for testing in yeast-displayed ligand selections: a carboxylic acid-functionalized magnetic bead that was covalently conjugated to amines present on the mammalian cell surface and a streptavidin-functionalized magnetic bead that was noncovalently conjugated to biotinylated cells. These bead-cell conjugates were used as a pulldown agent to test enrichment of high affinity binder-displaying yeast from nondisplaying yeast. In parallel, conventional adherent mammalian cell panning was used to compare the ability of cell suspension panning to enrich ligand-displaying yeast relative to established techniques.

3.3.1 Streptavidin and Carboxylic Acid Beads Both Effectively Conjugate Mammalian Cells

A431 cells were conjugated, in a 1:1 mixture at 5×10^6 cells or beads per mL, to carboxylic acid-functionalized magnetic beads in moderate, albeit highly variable, yield (29 ± 7%) (Figure 3-1A). Examination of conjugated cells visualized by phase contrast microscopy showed individual cells attached to several (3.3 ± 0.4) beads with no observable aggregation of cells and beads (Figure 3-1B). A431 cells conjugated in this manner showed fluorescence similar to unconjugated cells when labeled with an anti-EGFR antibody, indicating that EGFR expression was not appreciably blocked (Figure 3-1C).

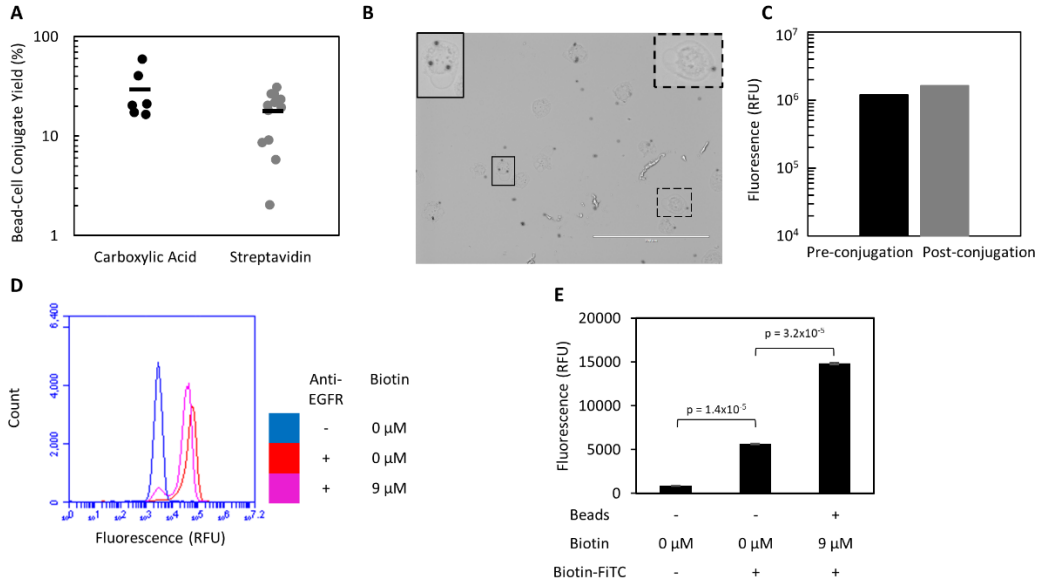

Figure 3-1. Mammalian cells can be efficiently conjugated to magnetic beads. (A) Beads and A431 cells were incubated in a 1:1 ratio prior to washing on a magnet to remove all unbound cells. The yield of conjugates was quantified by flow cytometry. (B) Bead-A431 conjugates (n = 39) were visualized to ensure proper conjugation. Carboxylic acid beads (black spheres) can be seen attached to the majority of A431 cells. Scale bar is 200 µm. Two cells (outlined) are enlarged and contrast-enhanced to show detail. (C) A431 cells were labeled with an anti-EGFR antibody and their fluorescence quantified by flow cytometry before and after conjugation to carboxylic

acid beads to assess whether EGFR expression was extensively masked by conjugation to beads. (D) A431 cells were labeled with an anti-EGFR antibody and their fluorescence quantified by flow cytometry before and after biotinylation to assess whether EGFR expression was extensively masked. A small number of cells had their expression masked by the labeling with 9 μM biotin. (E) Unbiotinylated A431 cells with no beads and biotinylated A431 cells conjugated to streptavidin beads were labeled with biotin-FITC and the fluorescence of the cell population (as gated by scatter) was analyzed to detect the presence of streptavidin beads attached to A431 cells. While biotin-FITC significantly labels the cell surface in the absence of streptavidin beads, a further significant increase in signal is observed after conjugation occurs. Fluorescence is presented as mean ± standard error of three trials.

To explore an alternative method of conjugation, A431 cells were biotinylated for capture by streptavidin-functionalized magnetic beads. Sulfo-NHS-LC-biotin with a 22.3 Å linker failed to provide substantial conjugation to streptavidin beads (data not shown), despite substantial biotinylation of the cell surface. The use of an analogous sulfo-NHS biotin with a 20,000 Da PEG linker provided significantly enhanced conjugate yield, perhaps due to the increased accessibility of the biotin moiety to the extracellular space. This increase allowed streptavidin bead conjugation to become comparable to the carboxylic acid beads (Figure 3-1A). Varying biotin labeling concentrations from 0.9–90 μM were tested, with all conditions providing similar yield (Figure 3-2A). Nine micromolar was chosen as a conservative balance between limiting material consumption and ensuring sufficient biotinylation. No significant difference in yield was observed for labeling times varied from 30 min to 2 h (Figure 3-2B). Thus, a 30 min labeling time was selected for subsequent experiments. Biotinylated A431 cells showed a similar fluorescence to unbiotinylated cells when labeled with an anti-EGFR antibody, indicating that EGFR expression was not masked on the majority of cells (Figure 3-1D). Streptavidin bead-cell conjugates exhibited significantly increased signal relative to unbiotinylated cells when labeled with biotin-FITC and analyzed for fluorescence by

flow cytometry (gating for mammalian cells by scatter), confirming the presence of streptavidin beads (Figure 3-1E).

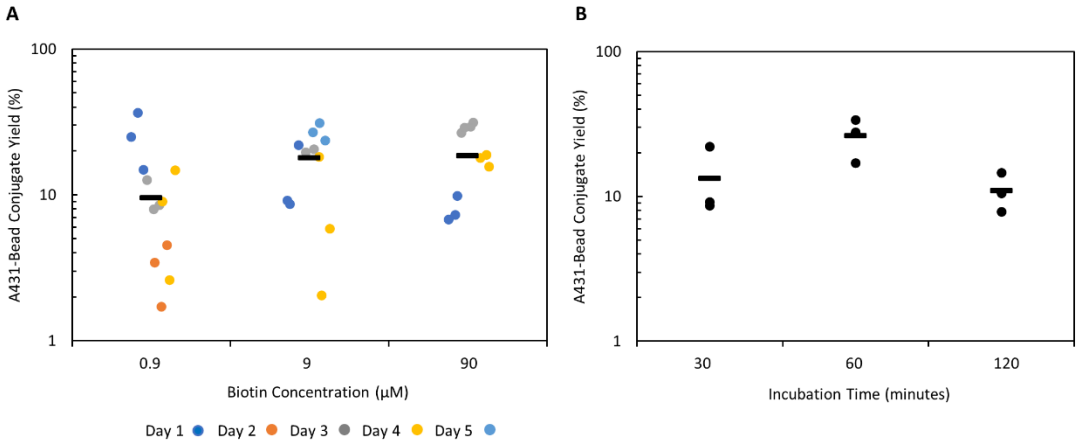

Figure 3-2. Biotinylated mammalian cell conjugation to streptavidin beads is relatively insensitive to biotin concentration or mammalian cell-biotin incubation time. (A) A431 cells were labelled with various concentrations of biotin for 30 minutes prior to conjugation to streptavidin beads. The yield of conjugates was quantified by flow cytometry. (B) A431 cells were labelled with 9 μM biotin and rotated for various time periods prior to conjugation to streptavidin beads. The yield of conjugates was quantified by flow cytometry.

In summary, both carboxylic acid bead capture using native cellular amines and streptavidin bead capture using biotinylated cells were relatively effective. In cases where cell supply is limited, thereby motivating higher yield, increased concentrations or stoichiometric excess of beads could be evaluated.

3.3.2 Cell Suspension Panning Enriches Yeast-Displayed EGFR-Binding Fibronectin Domains

Target-expressing mammalian cells conjugated to magnetic beads were assessed for their ability to effectively enrich yeast displaying binding ligands. A mixture of 10^6 yeast harboring display plasmids encoding for a fibronectin domain with high affinity for EGFR (E6.2.6′ K_d = 2 ± 2 nM)[81] and 10^8 plasmidless EBY100 were panned against

bead-immobilized A431 cells, which express $4 \pm 1 \times 10^6$ EGFR/cell. The mixture of yeast and bead-cell conjugates was incubated, placed on a magnet to collect bead-cell conjugates along with bound yeast and washed twice. This baseline condition resulted in an enrichment that was highly variable but significantly greater than unity (9 ± 1 with carboxylic acid beads, $p < 0.0001$; 11 ± 2, $p = 0.0004$ with streptavidin beads) of binding yeast relative to nondisplaying yeast with high yield of binding yeast ($19 \pm 6\%$ with carboxylic acid beads; $10 \pm 2\%$ with streptavidin beads). Binder yields were comparable or moderately lower for the less stringent one-wash condition as well as with three to five washes (Figure 3-3A). Surprisingly, the yield of nondisplaying yeast did not decrease as expected across sequential washes in the streptavidin bead system and only slightly decreased in the carboxylic acid bead system, suggesting some form of interaction prevented the effective removal of nondisplaying yeast from the system by washing (Figure 3-3B). As a result, the enrichment did not exhibit a substantial increase at any alternate washing conditions (Figure 3-3C).

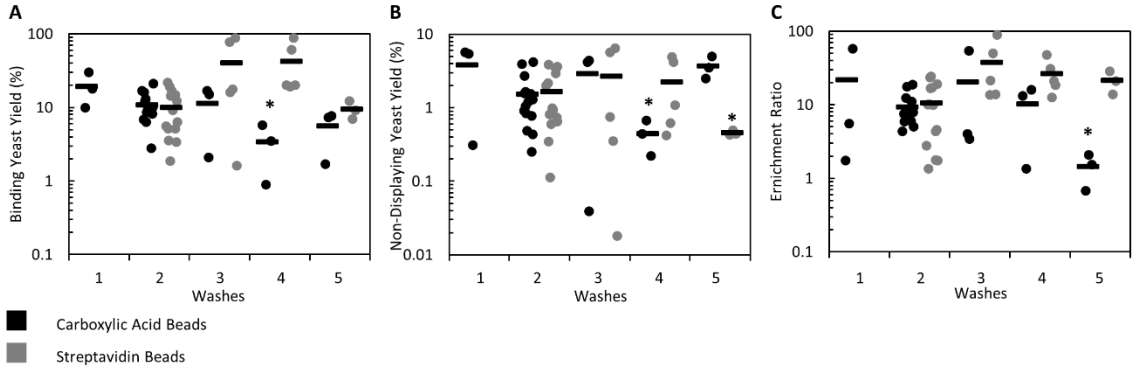

Figure 3-3. Cell suspension panning enrichment is relatively insensitive to washing conditions. Mixtures of yeast displaying E6.2.6′ and nondisplaying EBY100 yeast were incubated with bead-A431 conjugates and washed 1–5 times. (A) Binding yeast yield, (B) nondisplaying yeast yield, and (C) enrichment ratio were quantified. An asterisk (*) indicates $p < 0.05$ (with Bonferroni correction) relative to the 2-wash baseline.

To further probe the unexpected result of sustained yield of nondisplaying yeast even with extensive washing, 10^8 nondisplaying yeast were mixed with bare beads and the yield quantified after washing. In the case of the carboxylic acid bead system, bare beads resulted in a high yield of nondisplaying yeast compared to the streptavidin bead system (2.2 ± 0.8% vs 0.19 ± 0.06%), indicating that the retention of nondisplaying yeast on the carboxylic acid bead system may be due to yeast-bead interactions, despite extensive quenching of beads after mammalian cell conjugation (Figure 3-4A). When nondisplaying yeast were mixed with bead-A431 conjugates, the yield of nondisplaying yeast rose significantly (2.8 ± 0.9%) in the streptavidin system while remaining similar in the carboxylic acid system (1.2 ± 0.1%) relative to bare beads (Figure 3-4B). This appears to indicate that an underlying yeast-A431 interaction may also be preventing proper removal of nondisplaying yeast. While these results were obtained with 0.1% (w/v) bovine serum albumin to limit nonspecific interactions, more complex inhibitors, 1% (w/v) milk powder or 1% (v/v) fetal bovine serum, were tested to further screen any potential nonspecific interactions. Only the addition of serum in the carboxylic acid system resulted in a significant decrease in the yield of nonbinding yeast, and this decrease was not nearly as substantial as expected if nonspecific interactions were being effectively screened. Combined, this indicates that even the addition of complex blocking mixtures was not sufficient to hinder nonspecific yeast recovery (Figure 3-4B).

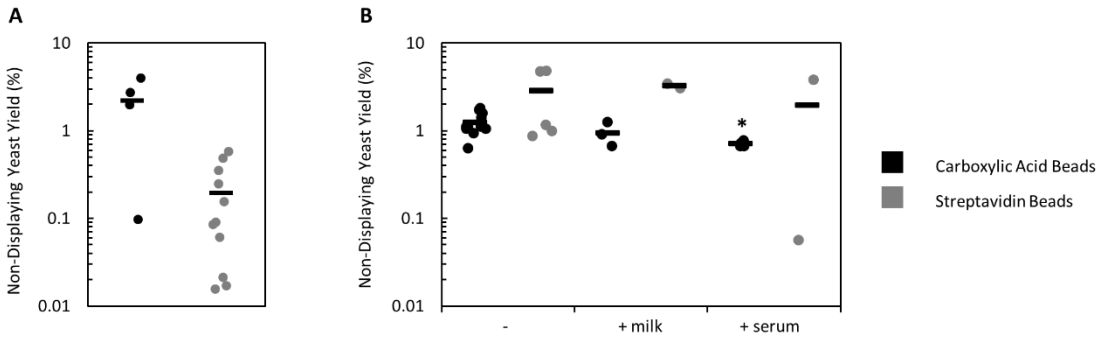

Figure 3-4. Nondisplaying yeast show nonspecific interactions with both beads and bead-cell conjugates. Nondisplaying yeast were incubated with (A) bare magnetic beads or (B) bead-A431 conjugates and washed twice with PBSACM or alternate buffers prior to quantifying yield. An asterisk (*) indicates $p < 0.05$ (with Bonferroni correction) relative to washing with PBSACM.

3.3.3 Cell Suspension Panning Enriches EGFR-Binding Fibronectins with High Throughput and Capacity

One of the potential benefits of the suspension cell panning approach is to efficiently process a large library of yeast cells. To assess the throughput of the bead-cell conjugate system, increasing amounts of nondisplaying yeast were incubated with bead-cell conjugates while holding the number of binding yeast constant at 10^6, which mimics an initial sort of a naïve library with a moderate number of binders within a large pool of nonfunctional clones. The highest tested condition (10^{10} nondisplaying yeast) showed no significant difference in the yield of binding yeast compared to 100-fold fewer nondisplaying yeast (16 ± 3% vs 15 ± 2%, $p = 0.67$; Figure 3-5A). Moreover, the yield of nondisplaying yeast decreased slightly, thereby resulting in nominally increased enrichment given constant binder yield (Figure 3-5B). This result of up to 10^{10} yeast panned per 10^6 target mammalian cells compares favorably to adherent panning recommendations which limit the number of panned yeast to 5×10^7 yeast per cm^2 or about 4×10^8 yeast per 10^6 mammalian cells, given an estimate of 1.2×10^6 cells per well

in a 6-well plate[106]. This is comparable to magnetic bead selections with soluble recombinant target[48]. The capacity for recovering binding yeast was also tested by incubating increasing amounts of binding yeast with bead-cell conjugates, while holding the number of nondisplaying yeast constant. While a 10-fold increase in the amount of binding yeast resulted in a similar yield, the use of 10^8 binding yeast did have a significantly decreased yield relative to baseline (9 ± 2% vs 2.1 ± 1.2%, $p = 0.004$; Figure 3-5C), meaning that there are limitations to panning populations containing greater than 10^7 binding yeast per 10^6 input mammalian cells. While there is a significant increase in the number of binding yeast recovered across all tested conditions, the reduction in yield at 10^8 input binding yeast may indicate that a recovery of roughly 10^6 binding yeast per 10^6 input mammalian cells may be at or approaching the system capacity (Figure 3-5D).

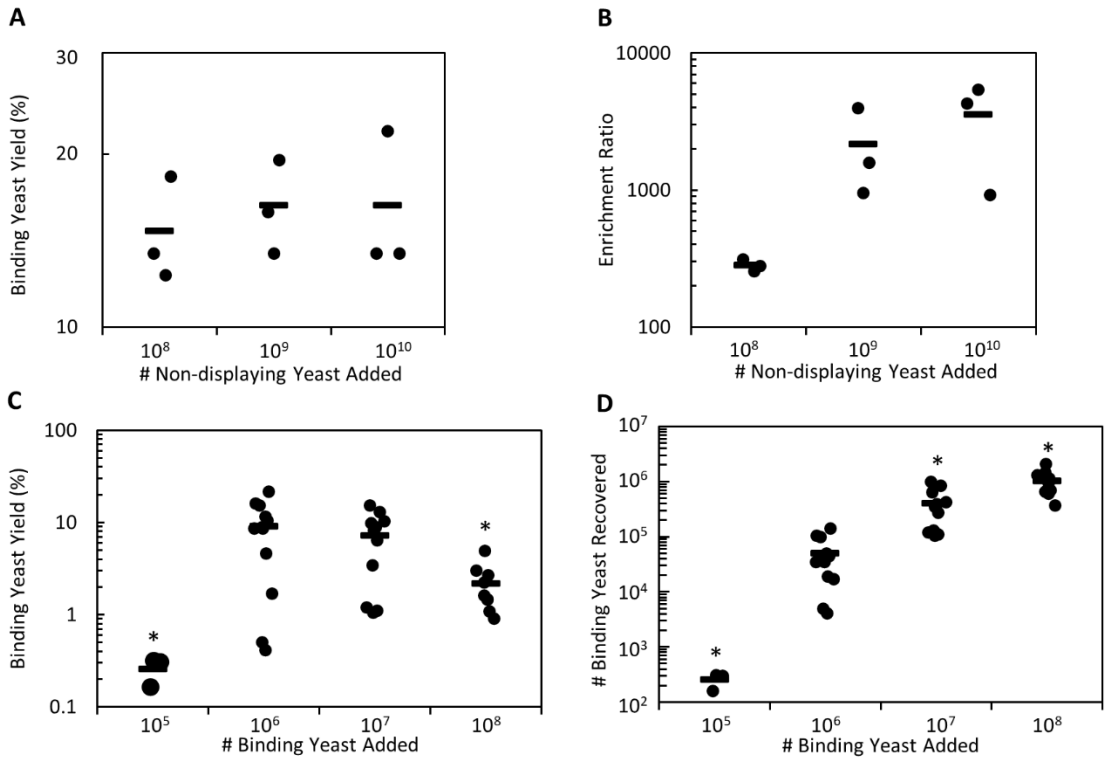

Figure 3-5. Cell suspension panning shows high binding yeast capacity and throughput. (A and B) Mixtures of 10^6 binding yeast and increasing numbers of nondisplaying yeast were sorted against bead-A431 conjugates and the yield of binding yeast and enrichment ratio were quantified. (C and D) Mixtures of 10^8 nondisplaying yeast and increasing numbers of binding yeast were sorted against bead-A431 conjugates and the yield of binding yeast and absolute number of binding yeast were quantified. An asterisk (*) indicates $p < 0.05$ (with Bonferroni correction) compared to the baseline conditions. The reduced yield of the 10^5 binding yeast conditions is hypothesized to be due to a small nonspecific loss of yeast due to binding to the tube surface that is negligible at all other conditions.

3.3.4 Cell Suspension Panning Provides Higher Binder Yield and Lower but Effective Enrichment Relative to Adherent Cell Panning

To compare the efficacy of this system relative to traditional adherent cellular panning, 18 replicates of both cell suspension and adherent cell panning were conducted in parallel over 3 days using the highly EGFR-expressing cell line A431 and high affinity E6.2.6′ ligand with carboxylic acid beads. Compared to adherent panning, cell suspension panning showed higher yield of binding yeast (12 ± 3% vs 3.4 ± 0.4%, $p = 0.005$; Figure 3-6A) and lower yield of nondisplaying yeast (0.043 ± 0.009% vs 0.15 ± 0.03%, $p = 0.001$; Figure 3-6B), resulting in an increase in enrichment (500 ± 200 vs 160 ± 50, $p = 0.01$; Figure 3-6C).

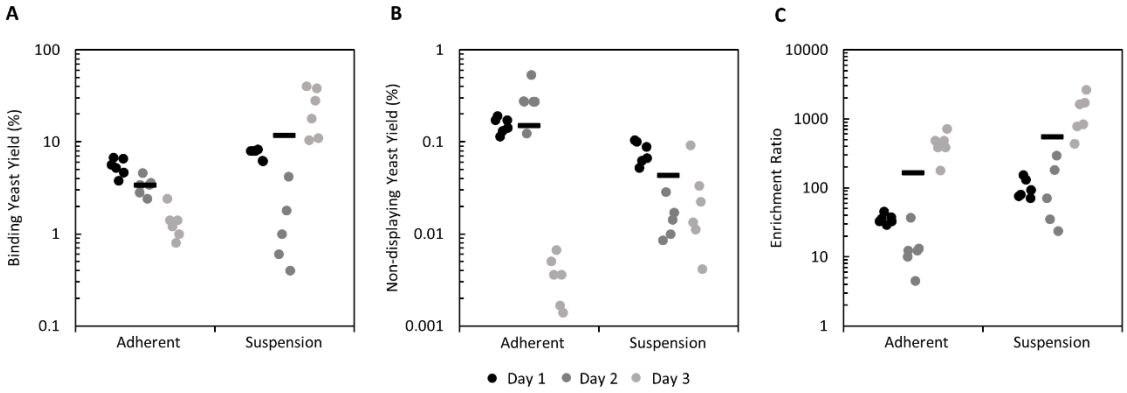

Figure 3-6. Initial cell suspension panning data demonstrates enhanced yield and enrichment compared to adherent cell panning in a high affinity, high target expression system. Mixtures of yeast displaying E6.2.6′ and nondisplaying yeast were sorted in suspension and adherently in parallel using bead-A431 conjugates as a pulldown agent. (A) Binding yeast yield, (B) nondisplaying yeast yield, and (C) enrichment ratio were quantified.

Initially, this data suggested that, while variable, suspension cell panning could provide more effective enrichment compared to traditional adherent panning. However, the exceptionally low yield of nondisplaying yeast in the cell suspension panning system contradicted our earlier results (Figures 3-3 and 3-4). To investigate this discrepancy, two additional sets of experiments were run using both carboxylic acid and streptavidin beads. These results were consistent with the earlier analysis, with cell suspension panning showing an increase in the yield of binding yeast (9.6 ± 0.6% vs 3.2 ± 0.3% with carboxylic acid beads, $p < 0.0001$; 9 ± 1% vs 3.8 ± 0.2% with streptavidin beads, $p = 0.002$; Figure 3-7A and D) along with an increase in the yield of nondisplaying yeast (1.0 ± 0.1% vs 0.08 ± 0.01% with carboxylic acid beads, $p < 0.0001$; 2.0 ± 0.3% vs 0.051 ± 0.007% with streptavidin beads, $p < 0.0001$; Figure 3-7B and E), which results in a decrease in the enrichment (11 ± 2 vs 60 ± 20 with carboxylic acid beads, $p = 0.006$; 10 ± 3 vs 100 ± 20 with streptavidin beads, $p < 0.001$; Figure 3-7C and F) relative to adherent cell panning but still allows for enrichment significantly greater than unity ($p < 0.001$ with carboxylic acid beads, $p = 0.0006$ with streptavidin beads), enabling practical use of this system.

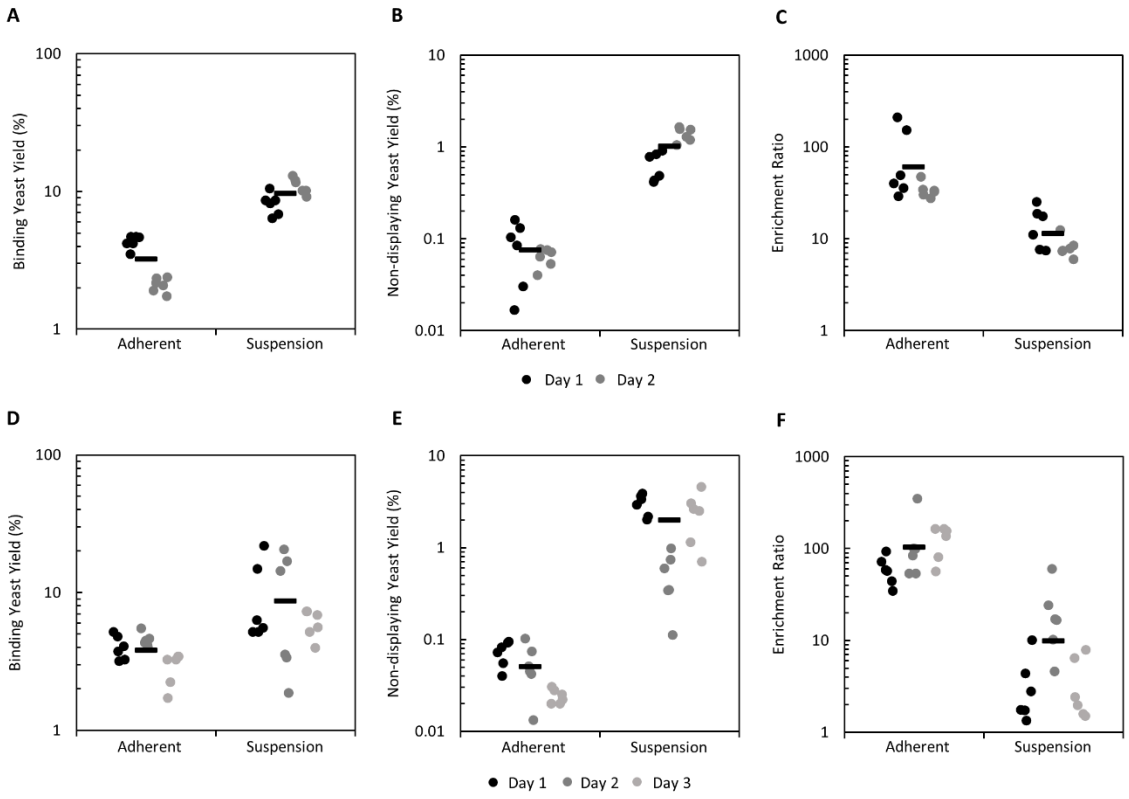

Figure 3-7. Further cell suspension panning data shows enhanced yield relative to adherent cell panning but does not recapitulate the increased enrichment. Mixtures of yeast displaying E6.2.6′ and nondisplaying yeast were sorted in suspension and adherently in parallel using bead-A431 conjugates using (A–C) carboxylic acid beads or (D–F) streptavidin beads as a pulldown agent. (A and D) Binding yeast yield, (B and E) nondisplaying yeast yield, and (C and F) enrichment ratio were quantified.

The variability regarding the yield of nondisplaying yeast across the multiple data sets was unable to be explained. All experiments were conducted by the same researcher, with cells displaying similar EGFR expression from the same master stock, and using the procedures listed herein. Nonetheless, the variability observed with the method is important to note. The results place a lower limit, which is still in the functional regime, on the enrichment while also offering optimism for even stronger performance. The relative bimodality of the nondisplaying yield suggests impact of an undefined parameter

without adequate experimental control. However, at this time, no speculation regarding this possible parameter is evident.

3.3.5 Cell Suspension Panning Enhances Binder Yield Relative to Adherent Cell Panning Robustly Across Ligand Affinities and Target Expressions but Not to All Targets

The effect of lower ligand affinity or cellular target expression on yield and enrichment in cell suspension panning was studied, as well as how this effect compared to adherent panning. Because of the similar results observed in the high affinity, high target expression system these experiments were conducted only in the carboxylic acid bead system. Similar to the high expression system, yeast displaying E6.2.6′ panned on midexpressing cells MDA-MB-231 ($2.9 \pm 1.7 \times 10^5$ EGFR/cell) showed a higher binding yeast yield compared to adherent panning (2.3 ± 0.5% vs 0.41 ± 0.09%, p = 0. 0008; Figure 3-8A) but lower enrichment (2.0 ± 0.3 vs 8 ± 2, p = 0.006; Figure 3-8C). Though lower, the enrichment was still significantly greater than unity (p = 0.007). Low affinity ligand AASV (K_d > 600 nM for EGFR) panned on high-expressing A431 cells yielded more binding yeast than observed for adherent panning (2.0 ± 0.5% vs 0.017 ± 0.005%, p = 0.001; Figure 3-8D), but a higher yield of nondisplaying yeast resulted in similar enrichment compared to adherent panning (1.5 ± 0.3 vs 1.7 ± 0.8, p = 0.79; Figure 3-8F), neither of which was significantly greater than unity (p = 0.053 and 0.20, respectively). Thus, weaker affinity ligands remain challenging for cellular panning enrichment.

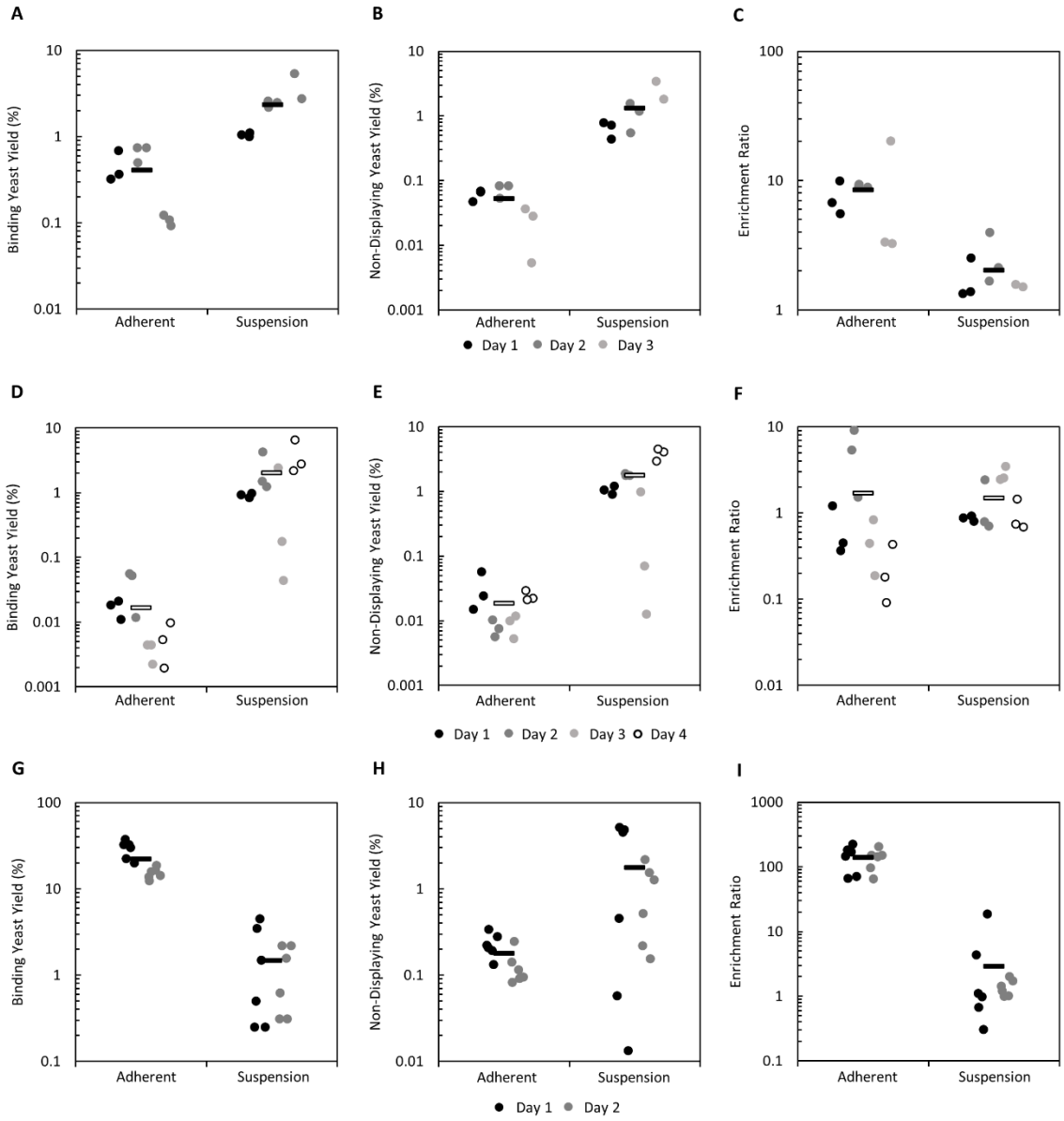

Figure 3-8. Effect of ligand affinity, target expression, and target/protein type on yield and enrichment. Mixtures of binding and nonbinding yeast were sorted in parallel by cell suspension and adherent panning and binding yeast yield, nondisplaying yeast yield, and enrichment ratio were quantified. (A–C) Ligand: E6.2.6′. Cell Line: MDA-MB-231. (D–F) Ligand: AASV. Cell Line: A431. (G–I) Ligand: AC2 Cell Line MS1-CD276.

To test how cell suspension panning compares to adherent panning in a system with an alternative protein scaffold and target, sorts in parallel with a cell line that highly expresses CD276 (MS1-CD276; $1.2 \pm 0.1 \times 10^6$ CD276/cell) and a midaffinity affibody

ligand AC2 (K_d = 310 ± 75 nM for CD276) were conducted. Surprisingly, cell suspension panning displayed both lower binding yeast yield (1.5 ± 0.4% vs 22 ± 4%, $p < 0.0001$ Figure 3-8G) and enrichment (3 ± 1 vs 140 ± 20, $p < 0.0001$; Figure 3-8I) relative to adherent panning and was unable to provide significant effective enrichment ($p = 0.11$). This result suggests that, while cell suspension panning provides a yield advantage to fibronectin domains in an EGFR model system, this might not translate to all protein scaffolds or targets.

3.4 Discussion

Existing high-throughput methods have successfully isolated binding ligands to soluble ectodomain analogs; however, difficulties translating binding to genuine antigen on target-expressing cells have hampered the clinical development and use of such molecules. The failure of such recombinant soluble ectodomain-based selection methods to generate ligands that bind to full-length, membrane-bound target indicate that these ectodomains may not fully recapitulate protein expressed on the cell surface. Surface display library selection techniques using target-expressing cells have been developed and successfully employed in many cases to overcome translatability issues but could be further improved. FACS-based selections employing target-expressing mammalian cells or cell lysate provide effective enrichment but are limited by throughput and lack avidity for weak affinity ligand enrichment. Adherent cell panning, on the other hand, provides high-throughput, avid selections with effective enrichment in a variety of cases; although prior work with EGFR-binding fibronectins indicate limited effectiveness in weak affinity or low expression conditions, motivating further improvement[65,106]. Likewise, the effective selection of binding ligands from a phage display library using cells in

suspension and anecdotal evidence of cell suspension panning campaigns succeeding in cases where adherent panning failed provide motivation to adapt these methods to yeast surface display libraries[117,118]. This adaptation, utilizing target-expressing mammalian cells immobilized to magnetic beads, was compared to adherent cell panning and displayed yield advantages and functional enrichment using a high affinity binder on cells with both high and mid target expression and provided only a yield advantage using a low affinity binder on cells with high target expression.

The conjugation of A431 cells to both carboxylic acid- and streptavidin-functionalized magnetic beads was accomplished in sufficient yield to produce a functional number of conjugates with limited optimization. No extensive networking of cells and beads was observed, and the target expression was essentially maintained across both conjugation methods. In both cases, it remains possible that higher concentrations or stoichiometric excess of beads could enhance conjugate yield. Additionally, while the 20,000 Da PEG biotin employed aided in enhancing conjugate yield, the optimal linker length to enable a biotinylated cell-bead linkage was not studied. Combined, this provides several avenues for further improving conjugation yield.

Cell suspension panning provided functional enrichment in an EGFR system using a high affinity binder and a high expression cell line with increased throughput relative to adherent panning. The high yield and relative insensitivity of nondisplaying yeast to washing was apparently due to a combination of bead-yeast and mammalian cell-yeast interactions that were not appreciably mitigated by buffers that have been previously used to screen nonspecific interactions. This limits the possible enrichment of the system which, while still functional, could be improved by further depletion of

nondisplaying yeast. While not tested in this study, it is possible that the use of mild surfactants or a presort against bare beads or target-negative bead-cell conjugates could help mitigate these interactions.

The first set of experiments performed using carboxylic acid beads in the high affinity, high target expression system showed a consistent, lower yield of nondisplaying yeast that was not replicated across any other experiment, which all showed a consistent, moderate yield of nonbinding yeast. Despite not knowing the precise parameter inducing this bimodality in the data, the observed variability provides a lower bound for performance with the potential that further optimization can promote even higher enrichment.

Follow-up experiments conducted with a high affinity ligand on high and mid target-expression cell lines and a low affinity ligand on a high target-expression cell line showed a significant increase in the yield of binding yeast across all conditions compared to adherent panning. In addition, all conditions with the exception of low affinity, high target-expression produced functional enrichment. This indicates that, while enrichment of weaker affinity ligands remains challenging in cell panning selections, cell suspension panning is a practical alternative selection across a wide range of ligand affinities and target expressions.

When testing cell suspension panning using a midaffinity CD276-binding affibody and a high CD276-expressing cell line, we found that cell suspension panning failed to provide the yield advantage or functional enrichment observed in the EGFR system. It is unclear whether the protein scaffold, cellular target, or another uncontrolled parameter is responsible for this reversal in the observed trend of binding yeast yield, but

this result indicates that cell suspension panning may not be appropriate for all protein scaffolds or targets.

While expression was measured biweekly over the course of this study and observed to remain consistent, it is possible that the use of presort analysis of mammalian cell target expression could yield additional insight regarding the interday variability observed in cell suspension panning. Target expression on mammalian cells has been previously shown to strongly impact the yield of binding yeast in adherent mode panning[65]. Additionally, the use of sequential sorts is expected to also aid in the reduction of interday variability through the averaging of enrichment values.

3.5 Conclusion

In conclusion, the above work presents and characterizes a new system for translatable ligand selection using suspended mammalian cells immobilized on magnetic beads. Both streptavidin and carboxylic acid beads can be used to effectively conjugate mammalian cells without forming large aggregates or masking native cell expression. Optimization of washing conditions enabled a system that can effectively enrich binding yeast relative to nondisplaying yeast; however, an unexplained high background of nondisplaying yeast is present that was not able to be reduced with increased washing or alternate buffers to screen nonspecific interactions. While these interactions seem to be both yeast-bead and yeast-cell driven, their exact cause is still unknown. Despite this, cell suspension panning provides practical enrichment to high affinity ligands on cell lines expressing 10^5–10^6 targets per cell, while low affinity ligands fail to be effectively enriched due to the increased background. Cell suspension panning also compared favorably to traditional adherent panning with a significant yield advantage in both high

and low affinity ligand cases, as well as increased throughput allowing up to 10^{10} cells to be sorted in a single tube. However, cell suspension panning failed to provide a benefit in a CD276 system, indicating that this panning approach may not be suitable for all targets or protein scaffolds. Ultimately, the findings of this study provide an alternate, higher throughput method for translatable selection to increase the efficiency of translatable ligand discovery and motivating further study into the limiting factors of this mode of selection.

3.6 Materials and Methods

3.6.1 Cells and Cell Culture

MDA-MB-231 were provided by Professor Jayanth Panyam (Department of Pharmaceutics, University of Minnesota–Twin Cities). A431 were provided by Professor Daniel Vallera (Department of Therapeutic Radiology, University of Minnesota–Twin Cities). Miles Sven 1 cells stably transfected to express human CD276 (MS1-CD276)[139] were provided by Juergen Willmann (Department of Radiology, Stanford University). All cell lines were grown with DMEM containing 4.5 g/L d-glucose, sodium pyruvate, and l-glutamine and supplemented with 10% (v/v) fetal bovine serum and 1% (v/v) 10 000 U/mL penicillin–streptomycin. All cell lines were stored in an incubator at 37 °C in a humidified atmosphere with 5% CO_2.

Yeast surface display was performed essentially as previously described[132]. Expression plasmids, detailed below, were transformed into *Saccharomyces cerevisiae* yeast strain EBY100 by EZ-Yeast Transformation (Zymo Research, Irvine, CA). Yeast harboring expression plasmids were grown in SD-CAA medium (20.0 g/L dextrose, 16.8 g/L sodium citrate dihydrate, 6.7 g/L yeast nitrogen base, 5.0 g/L casamino acids, and 3.9

g/L citric acid in deionized H_2O) at 30 °C with shaking. Protein expression was induced by transferring yeast cells in logarithmic phase (OD_{600nm} < 6) into SG-CAA medium (19.0 g/L galactose, 10.2 g/L sodium phosphate dibasic heptahydrate, 8.6 g/L sodium phosphate monobasic monohydrate, 6.7 g/L yeast nitrogen base, 5.0 g/L casamino acids, and 1.0 g/L dextrose in deionized H_2O) and growing at 20 °C overnight. EBY100 without plasmid were grown in YPD medium (20.0 g/L peptone, 20.0 g/L dextrose, and 10.0 g/L yeast extract in deionized H_2O) at 30 °C with shaking.

3.6.2 Expression Plasmids

The pCT-80 plasmid was used as the expression vector for yeast surface display on the C-terminus of Aga2p. The vector encodes for Aga2p followed by an 80-amino acid linker (comprising a Factor Xa cleavage site, an HA epitope, a proline/alanine/serine peptide based on the PAS#1 motif[174], and a glycine-rich peptide), the ligand, and a C-terminal Myc epitope. In essence, this is the classic pCT yeast surface display plasmid[60] with the addition of the 40-amino acid proline/alanine/serine peptide (as such, it was previously named pCT-40[65]). Genes were cloned into pCT-80 vector by NheI and *Bam*HI restriction sites: EGFR-binding fibronectin domains E6.2.6′[81] and E6.2.6′ AASV[65], and CD276-binding affibody clone AC2[166].

3.6.3 Receptor Expression Quantification

Polystyrene beads with known quantities of immobilized antimouse IgG (Bangs Laboratories, Inc., Fishers, IN) were used to construct a calibration curve from which the EGFR and CD276 expression of cell lines was quantified. Beads or cells were labeled with either mouse anti-EGFR clone ab30 (4 μg/mL) or mouse anti-CD276 clone 185504 (4 μg/mL) for 30 min at 4 °C. Beads or cells were washed once with phosphate-buffered

saline with 0.1% (w/v) bovine serum albumin, 1 mM $CaCl_2$, and 0.5 mM Mg_2SO_4 (PBSACM) and pelleted at 500*g* for 3 min. The beads or cells were then labeled with goat antimouse Alexa Fluor 647 conjugate (Life Technologies, Carlsbad, CA) for 30 min at 4 °C, washed once with PBSACM, and again pelleted at 500*g* for 3 min. Fluorescence was analyzed by flow cytometry using an Accuri C6 Plus (BD Biosciences, San Jose, CA).

3.6.4 Mammalian Cell-Magnetic Bead Conjugation

Mammalian cells were grown to approximately 70–90% confluency in 75 cm^2 tissue culture-treated flasks. The culture medium was removed, and the cells were washed once with 5 mL of PBS. The cells were then detached by trypsin-EDTA treatment for 10 min, followed by the addition of culture medium with serum. The detached cells were then pelleted at 500*g* for 3 min. The trypsin-containing medium was removed, and the cells were resuspended in fresh culture medium for counting using a Countess II FL (Thermo Fisher Scientific). The cells were pelleted at 500*g* for 3 min at 4 °C and washed twice with ice cold PBS before being pelleted again, and the supernatant was removed.

For streptavidin bead conjugation, washed cells were resuspended in 1 mL of a 9 μM solution of 20 kDa biotin-PEG-SVA (Laysan Bio Inc., Arab, AL) in PBS per 10^6 mammalian cells and rotated for 30 min at room temperature. The biotinylated cells were washed five times with ice cold PBSACM to quench and remove excess biotin prior to incubation with an equimolar amount of streptavidin-coated Dynabeads (Thermo Fisher Scientific, Cat: 11205D) in 50 μL of PBSACM at 4 °C for an hour. The bead-cell conjugates were then placed on a DynaMag-2 magnet (Thermo Fisher Scientific, Cat:

12321D) for 2 min to capture all conjugated cells and washed once with PBSACM to remove any unconjugated cells.

For carboxylic acid bead conjugation, carboxylic-acid-coated Dynabeads (Thermo Fisher Scientific, Cat: 14305D) were mixed with 200 μL of a 10 mM sodium hydroxide solution per 10^6 beads and rotated at room temp for 10 min. The beads were placed on a DynaMag-2 magnet for 2 min and washed twice with 200 μL of 4 °C deionized water per 10^6 beads, then resuspended in 200 μL of a 4 °C, 50 mg/mL 1-ethyl-3-(3-(dimethylamino)propyl)carbodiimide solution per 10^6 beads. This mixture was allowed to rotate at room temperature for 30 min before being placed again on the magnet and washed once with 200 μL of 4 °C deionized water and twice with 200 μL of 100 mM MES. An equimolar amount of activated beads was added to the pelleted cells and mixed thoroughly prior to rotating at room temperature for 30 min. The bead-cell conjugates were placed on the magnet and washed once with 500 μL of 0.05 M Tris and once with 500 μL of PBSACM.

For both types of bead-cell conjugation, reaction yield was quantified by flow cytometry on an Accuri C6 Plus to count the number of cells in both the pre- and postconjugation mixtures.

3.6.5 Cell Suspension Panning

Yeast mixtures containing 1×10^8 plasmidless EBY100 and 1×10^6 yeast harboring ligand display plasmids were washed in PBSACM and added to a 1.7 mL tube containing 10^6 mammalian cells conjugated to either streptavidin or carboxylic-acid-coated beads in 1 mL of ice cold PBSACM. This mixture was rotated for 15 min at 4 °C. The mixture was placed on a magnet, unbound yeast were aspirated, and bead–cell

conjugates were washed twice with 1 mL of ice cold PBSACM. The yield of plasmid-harboring yeast was quantified by dilution plating on SD-CAA plates, while the yield of total yeast was quantified by dilution plating on YPD. Enrichment ratio was calculated as the yield of plasmid-harboring yeast divided by the yield of plasmidless yeast.

3.6.6 Adherent Mammalian Cell Panning

Adherent cell panning selections were carried out essentially as described[65]. Mammalian cells were grown in 12-well plates to approximately 70–90% confluency. The culture medium was aspirated, and the cells were washed once with ice cold PBSACM. Yeast mixtures containing 1×10^8 plasmidless EBY100 and 1×10^6 yeast harboring ligand display plasmids were washed in PBSACM and added dropwise to each well in 1 mL of ice cold PBSACM. Cells were incubated without shaking for 15 min at 4 °C and unbound yeast were aspirated. Cells were washed with 1 mL of ice cold PBSACM four times with 25 gentle tilts and 5 nutations and one time with 10 mutations. Bound yeast were removed by scraping cell monolayers and resuspending them in 1 mL of PBSACM. The yield of plasmid-harboring yeast was quantified by dilution plating on SD-CAA plates, while the yield of total yeast was quantified by dilution plating on YPD. Enrichment ratio was calculated as the yield of plasmid-harboring yeast divided by the yield of plasmidless yeast.

3.6.7 Optimization of Washing Conditions

The washing conditions of adherent mammalian cell panning have been optimized in prior work[65,99,166]. To determine the optimal number of washes for the cell suspension panning, the baseline conditions described above were repeated while varying the number

of washes from one to five. Yield and enrichment were quantified by dilution plating on YPD and SD-CAA plates.

3.6.8 Quantification of System Capacity and Nonbinding Yeast Blocking

The capacity of cell suspension panning was determined by conducting sorts using the baseline conditions above while varying the number of initial displaying yeast from 10^5 to 10^8. The ability of nonbinding yeast to block binding yeast was determined by conducting sorts using the baseline conditions above while varying the number of initial nondisplaying yeast from 10^8 to 10^{10}. In both cases, yield and enrichment were quantified by dilution on YPD and SD-CAA plates.

3.6.9 Statistical Analysis

Washing data and functional enrichment were tested for significance using Welch's *t* test, while comparisons between cell suspension and adherent panning were binned by day and method prior to significance testing by two-way ANOVA with only main effects. Samples containing greater than six replicates were subjected to Grubb's test to remove potential outliers. All statistics are reported as the mean ± standard error.

Chapter 4 – Extended Yeast Surface Display Linkers Enhance the Enrichment of Ligands in Direct Mammalian Cell Selections

Adapted with permission from "Lown, P.S; Cai, J.J., Ritter, S.C., Otolski, J.J., Wong, R., Hackel, B.J. "Extended Yeast Surface Display Linkers Enhance the Enrichment of Ligands in Direct Mammalian Cell Selections" *Protein Engineering, Design and Selection* **2021**, 34, 1-9" Copyright 2021 Oxford University Press. The pCT-641 plasmid was constructed by Dr. Seth C. Ritter.

4.1 Summary

Selections of yeast-displayed ligands on mammalian cell monolayers benefit from high target expression and nanomolar affinity, which are not always available. Prior work extending the yeast–protein linker from 40 to 80 amino acids improved yield and enrichment but is hypothesized to be below the optimal length, prompting evaluation of an extended amino acid linker. A 641-residue linker, chosen to be roughly an order of magnitude longer than the existing linkers, provided enhanced enrichment with a 2-nM affinity fibronectin ligand and 10^5 epidermal growth factor receptors (EGFR) per cell (14 ± 2 vs. 8 ± 1, $p = 0.008$) and a >600-nM affinity ligand, 10^6 EGFR per cell system (23 ± 7 vs. 0.8 ± 0.2, $p = 0.004$). Enhanced enrichment was also observed with a 310-nM affinity affibody ligand and 10^4 CD276 per cell, suggesting a generalizable benefit to other scaffolds and targets. Spatial modeling of the linker suggests that improved extracellular accessibility of ligand enables the observed enrichment under conditions not previously possible.

4.2 Introduction

Protein scaffolds have enabled the efficient engineering of specific molecular binding activity while maintaining desirable biophysical properties for both therapeutic and diagnostic applications[10,127]. Often, the discovery of binding ligands to clinically relevant biomarkers is conducted through the generation of large combinatorial libraries[68,70,175,176]. To effectively screen these libraries, high-throughput selection strategies including magnetic bead capture[20,48,163,164] and fluorescence-activated cell sorting[55,60] have been coupled with yeast[60,61,162] and phage[42,43,122] display technologies. These strategies often use recombinantly produced, soluble ectodomains as analogs for full-length proteins. While proven successful[177], these methods may generate ligands that bind strongly to the biomarker analogs yet fail to translate binding to genuine antigen on target-expressing cells[166] (Chapter 2). As a solution, several selection techniques utilizing target-expressing cells have been developed to use full-length, native biomarkers to aid in translatable ligand selection, including biopanning on adherent cell monolayers[65,98,99], magnetic bead-immobilized cells[178,179] (Chapter 3), or flow cytometry with suspended cells[168]. Adherent cell panning has isolated high-affinity, translatable binders in multiple scenarios[100,102–109,122]. Yet studies conducted using epidermal growth factor receptor- (EGFR-) binding fibronectins found that enrichment—the ratio of the yields (fractions of yeast collected) of ligand-displaying and nondisplaying yeast in a sort and a metric for the relative increase in frequency of ligands with desired target-binding relative to nonbinding background—is hindered when using cells with low-to-moderate ($\leq 10^5$ targets/cell) expression or ligands of micromolar or weaker affinity in both adherent and suspension systems[65,179] (Chapter 3).

One hypothesis for the inability of these studies to effectively enrich ligands in nonideal systems is due to limited ligand–target binding. The yeast cell wall is ~115 nm thick[180], throughout which the yeast surface display construct is distributed by glycosylphosphatidylinositol (GPI)-mediated anchoring[64,181]. Previous research with similar constructs indicated that cell wall glycans cause steric occlusion of ligand binding, with a 649-amino acid linker providing consistent molecular engagement regardless of target molecular weight[182]. Similarly, a 122-nm linker was required for a plasma membrane-tethered yeast surface construct to reliably contact an extracellular molecular probe[180]. The linker of the classic pCT yeast surface display construct is 40 amino acids with a maximum end-to-end distance of 15 nm (assuming an average distance of 3.8 Å between alpha-carbons)[183], far below either studied limit. This may decrease the number of yeast-displayed ligands able to access the extracellular space and engage with their target, lowering the effective avidity of the system. Further supporting this, a study that appended an additional 40-amino acid flexible linker showed enhanced binding of high- and low-affinity EGFR-binding fibronectins on high-expressing cells[65]. However, even this 80-amino acid linker is expected to be far under the length for optimal mammalian cell surface engagement, thus motivating the creation of even longer yeast surface display linkers for the purpose of adherent mammalian cell panning.

This study aims to evaluate the effectiveness of a substantially extended linker, 8-fold longer at 641 amino acids, in providing more robust ligand-biomarker interaction in the context of adherent mammalian cell panning in comparison to the previously established 80 amino acid linker. To create a generalizable comparison, parameters including mammalian cell target expression, ligand binding affinity, ligand protein

scaffold, and target biomarker were studied. Sorting mixtures containing a low frequency of yeast expressing pCT-80 or pCT-641 display plasmids and a majority of plasmidless EBY100 were used to mimic *de novo* selection from naïve libraries and panned in parallel. The longer linker significantly increased enrichment in both high affinity, moderate target expression and low affinity, high target expression EGFR systems. In the latter case, the longer linker provided significant effective enrichment whereas the shorter linker could not. However, the longer linker did not provide significant enrichment in the low affinity, moderate target expression system, indicating that further modifications to the yeast surface display may be needed to enrich low affinity ligands in non-ideal conditions. Significantly increased enrichment was also observed in a low affinity, low expression CD276 system, indicating this benefit may be generalizable to other protein scaffolds and biomarkers. This increased enrichment was observed despite significantly decreased display levels of the pCT-641 construct on the yeast surface. Modeling the dynamics of the two linkers as stiffness-modified Gaussian chains[183–185] uniformly distributed throughout the cell wall indicated that the longer linker spends more time extended into the extracellular environment, supporting the hypothesis that the increased performance is a result of more robust ligand accessibility to the extracellular space. Combined, these results advance understanding of the factors that dictate binding ligand yield and enrichment in adherent mammalian cell panning and provide tools for isolating binding ligands in conditions not previously possible.

4.3 Results

Iterative restriction enzyme digestion and destructive ligation[186] were used to exponentially expand the existing pCT-80 linker (SI Table 1)[65]. In short, the existing vector was digested in parallel by *Avr*II and *Bam*HI to generate an insert and by *Nhe*I and *Bam*HI to create an acceptor vector. While compatible for ligation, the resulting hybrid recognition site of *Avr*II and *Nhe*I cannot be digested by either enzyme, effectively breaking the recognition site while doubling the linker region. To achieve the desired 8-fold increase in linker length, this process was repeated over sufficient iterations to create a 641 amino acid linker (Figure 4-1). This new linker, containing a truncated version of the original linker with 18 amino acids of a proline-alanine-serine rich segment (based on PAS#1)[174] and $(G_4S)_3$ bridged by alanine and arginine encoded for by the broken restriction site (Table 4-1), was expected to have similar conformational flexibility and secondary structure due to its similar composition. However, detailed characterization was outside the scope of this study.

	Name	Sequence
Repeat Sequences	PAS_{38}	PAAPAPASPAAPAPSAPAASPAAPAPASPAAPAPSAPA
	PAS_{18}	PAAPAPASPAAPAPSAPA
	$(G_4S)_3$	GGGGSGGGGSGGGGS
Linkers	pCT-80	[Aga2p] - KDNSSTIEGRYPYDVPDYALQAS - PAS_{40} - $(G_4S)_3$ - AS
	pCT-641	[Aga2p] - KDNSSTIEGRYPYDVPDYALQAS - PAS_{40} - $(G_4S)_3$ - APR - $[PAS_{18}$ - $(G_4S)_3$ - AR$]_{15}$ – PAS_{18} - $(G_4S)_3$ - AS

Table 4-1. A list of repetitive amino acid sequences and linker sequences used in pCT-80 and pCT-641.

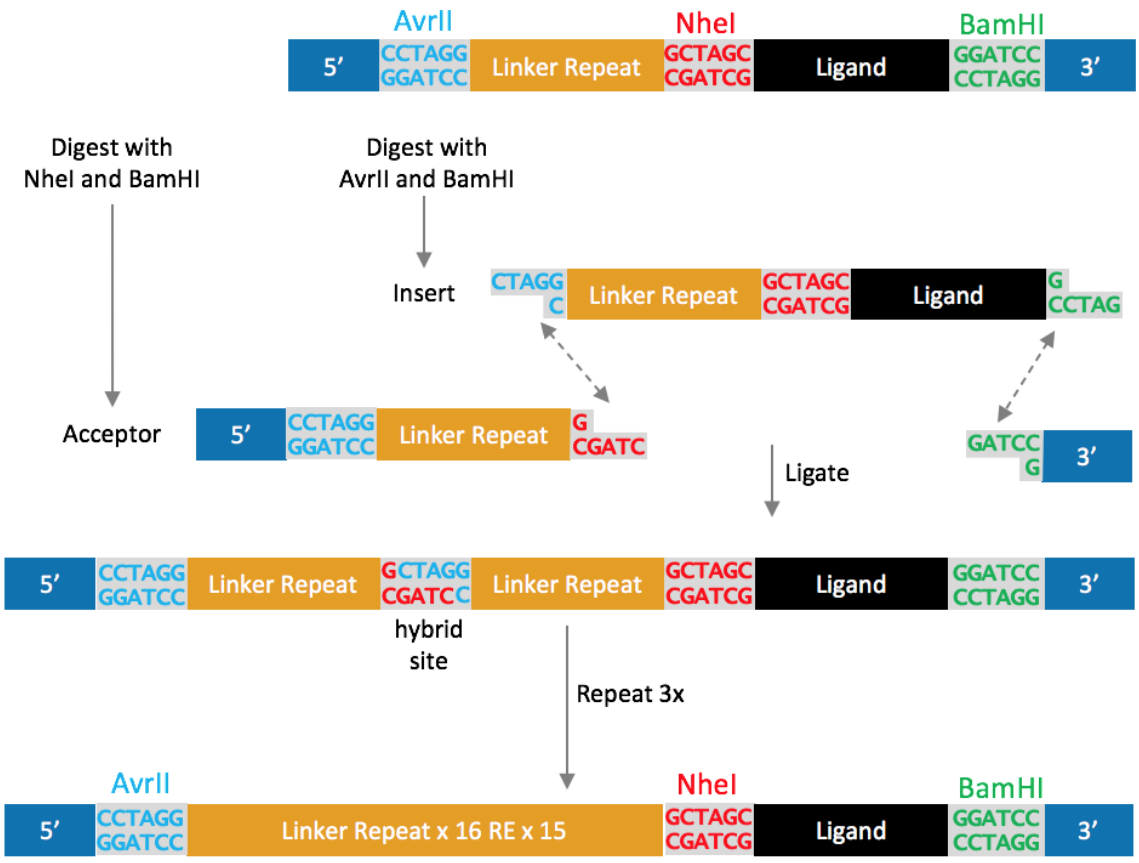

Figure 4-1. Exponential expansion of repetitive linker by iterative restriction enzyme digest and destructive ligation. Digesting the initial construct in parallel creates an insert and acceptor with compatible overlaps. Ligation results in a hybrid sequence of NheI and AvrII that is recognized by neither restriction enzyme, preventing further digestion and a doubling of the linker region. Each repetition of the procedure doubles the existing linker region.

4.3.1 Longer Linkers Increase the Yield of Displaying Yeast and Enrichment in Low Affinity or Moderate Target Expression Systems

To compare the efficacy of the extended linker in enriching binding ligands, adherent cell panning was conducted in parallel with both the 80- and 641-residue linkers. The A431 cell line, which highly overexpresses EGFR ($4 \pm 1 \times 10^6$ EGFR/cell), was the panning target for a mixture of yeast containing plasmidless EBY100 yeast and yeast expressing display plasmids encoding high affinity ($K_d = 2 \pm 2$ nM) EGFR-binding fibronectin domain E6.2.6'[81] from either the pCT-80 or pCT-641 construct. Upon

selection, the yield of nondisplaying and ligand-displaying yeast were measured via dilution plating, and ligand enrichment was computed. Compared to the pCT-80 construct, pCT-641 showed a higher yield of ligand-displaying yeast (7.5 ± 1.0% vs. 2.8 ± 0.5%, $p < 0.0001$; Figure 4-2B) accompanied with a moderate increase in the yield of nondisplaying yeast (0.15 ± 0.03% vs. 0.10 ± 0.03%, $p = 0.05$; Figure 4-2C), resulting in a nominal, statistically insignificant elevation in enrichment (120 ± 40 vs. 50 ± 10, $p = 0.12$; Figure 4-2A).

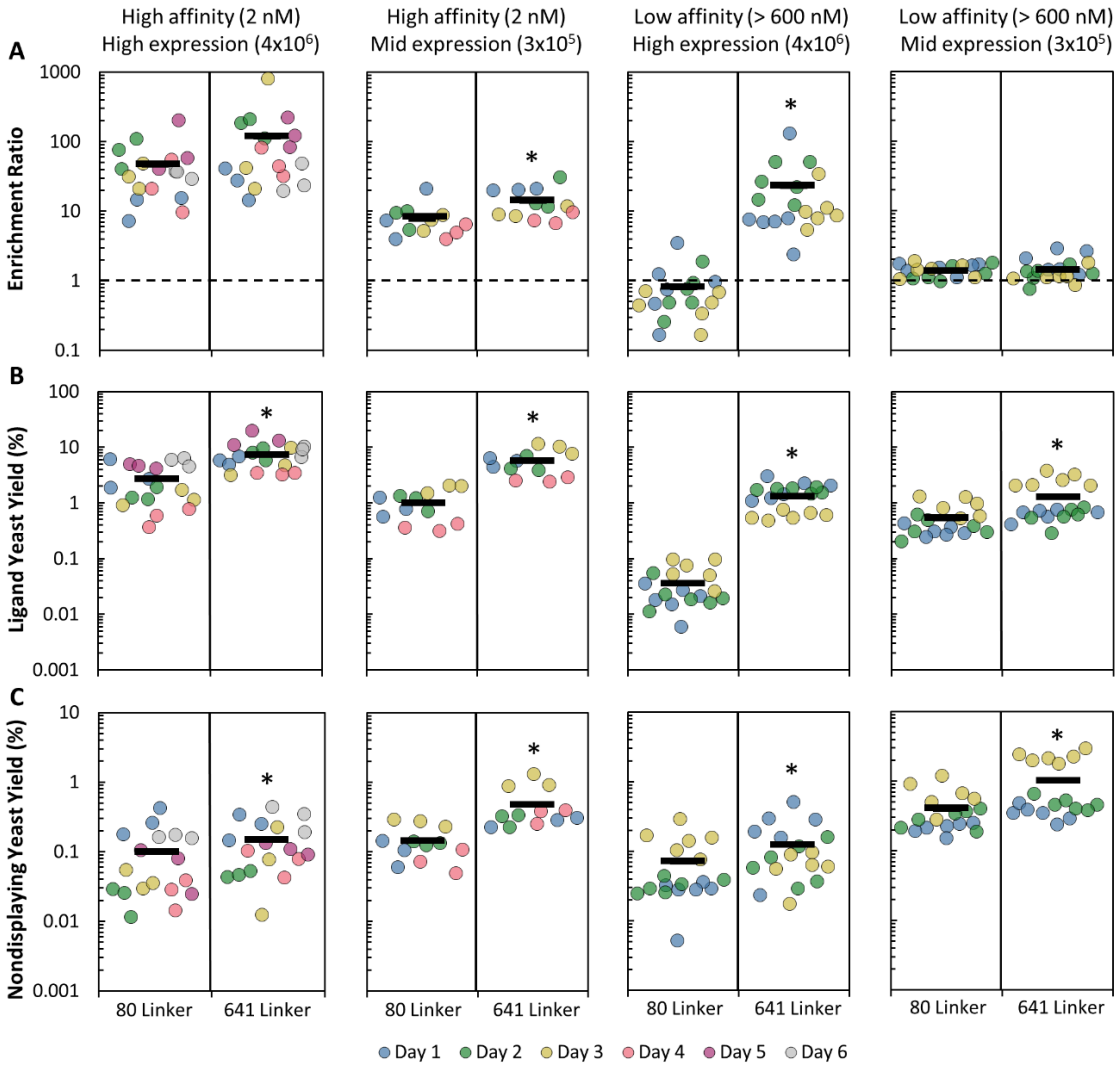

Figure 4-2. The effect of ligand affinity and target expression on yield and enrichment across 80- and 641- amino acid linkers in an EGFR system. Yeast displaying either pCT-80 or pCT-641 tethered ligands were mixed with nondisplaying yeast and sorted in parallel by adherent cell panning. (A) Enrichment ratio (B) ligand-displaying yeast yield, and (C) nondisplaying yeast yield were quantified on both high- (E6.2.6') and low- (E6.2.6' AASV) affinity ligands as well as high- (A431) and mid- (MDA-MB-231) expressing cell lines. Dotted lines (A) indicate the limit of functional enrichment. * indicates $p < 0.05$ relative to the 80-amino acid linker.

The lack of a significant increase in enrichment suggested that, while the extended linker may effectively increase avidity, E6.2.6' is sufficiently high affinity that very little avidity is needed to provide consistent attachment of displaying yeast to the highly-expressing mammalian cell surface. Thus, it was decided to move to more challenging systems, which is also where more technological advancement is needed for binder isolation. On mid-expressing MDA-MB-231 cells ($2.9 \pm 1.7 \times 10^5$ EGFR/cell) the longer linker improved enrichment of the high affinity E6.2.6' (14 ± 2 vs. 8 ± 1, $p = 0.008$; Figure 4-2A) as well as yield ($5.6 \pm 0.8\%$ vs. $1.0 \pm 0.2\%$, $p < 0.0001$; Figure 4-2B). The increased stringency of panning with the roughly 14-fold reduction in mammalian cell expression between the mid- and high-expressing system is sufficient to reveal the extended linker's avidity advantage. Even more striking, for low affinity ligand E6.2.6' AASV ($K_d > 600$ nM for EGFR)[65] panned on high-expressing A431 cells the 641-residue linker increased ligand-displaying yeast enrichment from non-functional 0.8 ± 0.2 to highly effective 23 ± 7 ($p = 0.004$; Figure 4-2A). This was driven by an increased yield ($1.4 \pm 0.2\%$ vs. $0.036 \pm 0.007\%$, $p < 0.0001$; Figure 4-2B).

However, while E6.2.6' AASV panned on mid-expressing MDA-MB-231 cells provided significantly higher ligand-displaying yeast yield ($1.3 \pm 0.2\%$ vs. $0.53 \pm 0.08\%$, $p < 0.0001$; Figure 4-2B) for the longer linker, this did not translate to significantly increased enrichment (1.4 ± 0.1 vs. 1.39 ± 0.07, $p = 0.73$; Figure 4-2A), indicating that

any potential increase in ligand accessibility by the longer linker is not enough to overcome a combination of low ligand affinity and limited biomarker expression. Thus, enriching weaker affinity ligands on all but the highest expressing cell lines remains challenging in adherent cell panning. Additionally, the moderate but significant increase in nondisplaying yeast yield, seen for the longer linker across all model EGFR systems, somewhat hindered enrichment. The increased accessibility may allow additional nonspecific interactions between the linker and/or ligand with nondisplaying yeast, which could potentially be ameliorated using blocking agents such a milk powder or fetal bovine serum; however, this has not been evaluated.

4.3.2 Improved Linker Performance is Generalizable to CD276 and Affibodies

To assess whether the increased performance of the pCT-641 construct was target or ligand dependent, further sorts were conducted with a cell line that has low expression of CD276 (MDA-MB-231: $4 \pm 2 \times 10^4$ CD276/cell) and a low affinity affibody ligand: AC2 (K_d = 310 nM; 240-390 nM 68% CI)[166]. This system showed similar trends to the EGFR system, with an increase in ligand-displaying yeast yield (0.9 ± 0.1% vs. 0.6 ± 0.1%, p = 0.003; Figure 4-3B) and enrichment (7.5 ± 0.8 vs. 4.3 ± 0.4, p = 0.0003; Figure 4-3A) of the pCT-641 construct relative to pCT-80. This indicates that the observed benefit of a longer linker is not limited to EGFR and fibronectin domains and may be generalizable to other targets and protein scaffolds. Cell panning is a potential method for screening libraries for ligands of micromolar affinity on cell lines expressing on the order of millions of targets per cell or libraries of ligands of up to 300 nM affinity on cell lines expressing tens-to-hundreds of thousands of targets per cell. Despite this, nonspecific

interactions remain a significant issue in cell panning screens and sufficient depletion strategies should be employed when conducting cell panning.

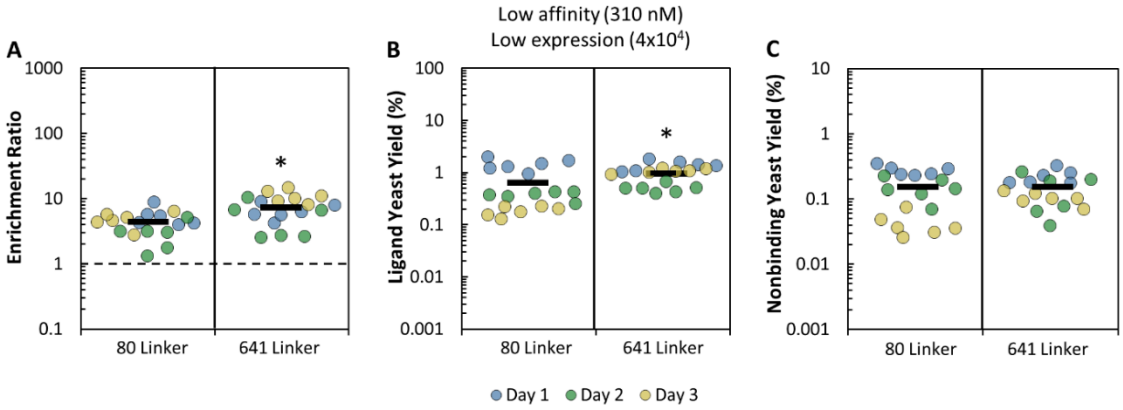

Figure 4-3. Yield and enrichment of 80- and 641-amino acid linkers in a CD276 system. Yeast displaying either pCT-80 or pCT-641 tethered ligands were mixed with nondisplaying yeast and sorted in parallel by adherent cell panning. (A) Enrichment ratio, (B) ligand-displaying yeast yield, and (C) nondisplaying yeast yield were quantified. Ligand: AC2 Cell Line: MDA-MB-231. The dotted line (A) indicates the limit of functional enrichment. * indicates $p < 0.05$ relative to the 80-amino acid linker.

4.3.3 Improved Linker Performance is Observed Despite Lower Yeast Cell Surface Expression

We hypothesize that the increased binding and enrichment for the extended linker results from improved ligand accessibility, which translates to elevated functional valency. Yet it is possible that the extended linker constructs achieved higher valency by simply expressing more abundantly on the yeast surface. To assess this possibility, the amount of surface displayed ligand was quantified using a single aliquot of each population after induction and before sorting (apart from AC2, which used a different induction). Yeast containing the pCT-641 plasmid were found to express significantly fewer ligands per cell relative to yeast containing pCT-80 (25% fewer for E6.2.6′, 10% fewer E6.2.6’ AASV and 34% fewer for AC2) (Figure 4-4A). This lower expression

indicates that the longer linker allowed the ligand to engage more reliably with its molecular target despite decreased ligand surface expression. Additionally, if a large portion of ligand-negative yeast cells contain plasmid offering antibiotic resistance, a lower percent induction could artificially deflate the displaying yeast yield, and therefore the enrichment ratio, of the assay. However, enrichment benefit was observed despite the percent induction of pCT-641 being comparable or moderately lower compared with the pCT-80 counterparts (Figure 4-4B). Additional experiments evaluating per cell expression and percent of cells displaying ligand, while displaying a differing trend of per cell expression, indicated that the induction conditions used to generate data were roughly optimal for both linkers (Figure 4-5).

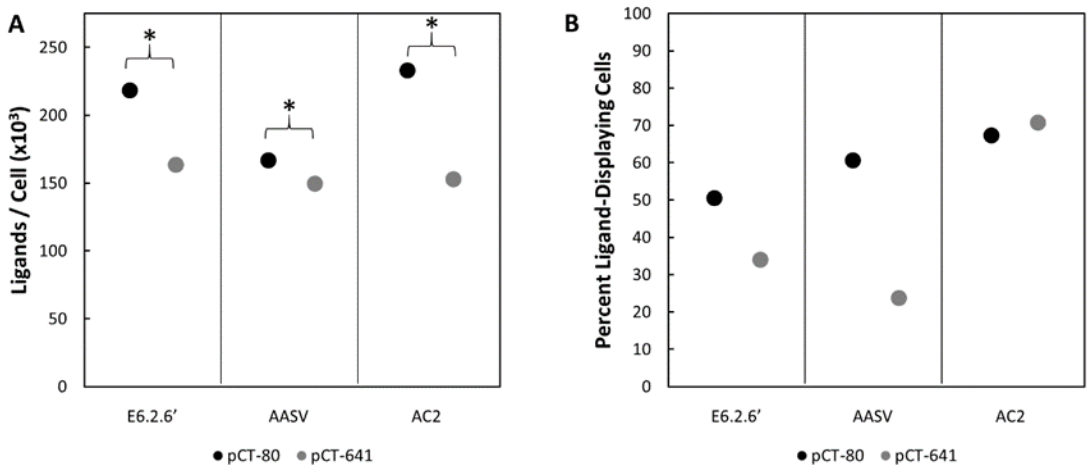

Figure 4-4. Yeast populations displaying ligands via pCT-641 have a lower surface expression and induction percentage. Yeast containing pCT-80 or pCT-641 and encoding for E6.2.6′, E6.2.6’ AASV or AC2 were labeled with an anti-C-Myc antibody and FITC secondary. Their fluorescence was analyzed by flow cytometry and compared to a quantitative bead standard labeled with the same antibody mixture to determine ligand expression. The same induction of E6.2.6′ and E6.2.6’ AASV ligands were used to generate the sorting data in Figure 4-2. (A) Ligand expression is presented as the mean of >10,000 events from a single culture. 95% CIs were calculated but are <0.8% of the mean and therefore not visible. $P < 0.05$ difference in expression levels. (B) The percent of ligand-displaying cells (fluorescein isothiocyanate [FITC] positive) in each sample

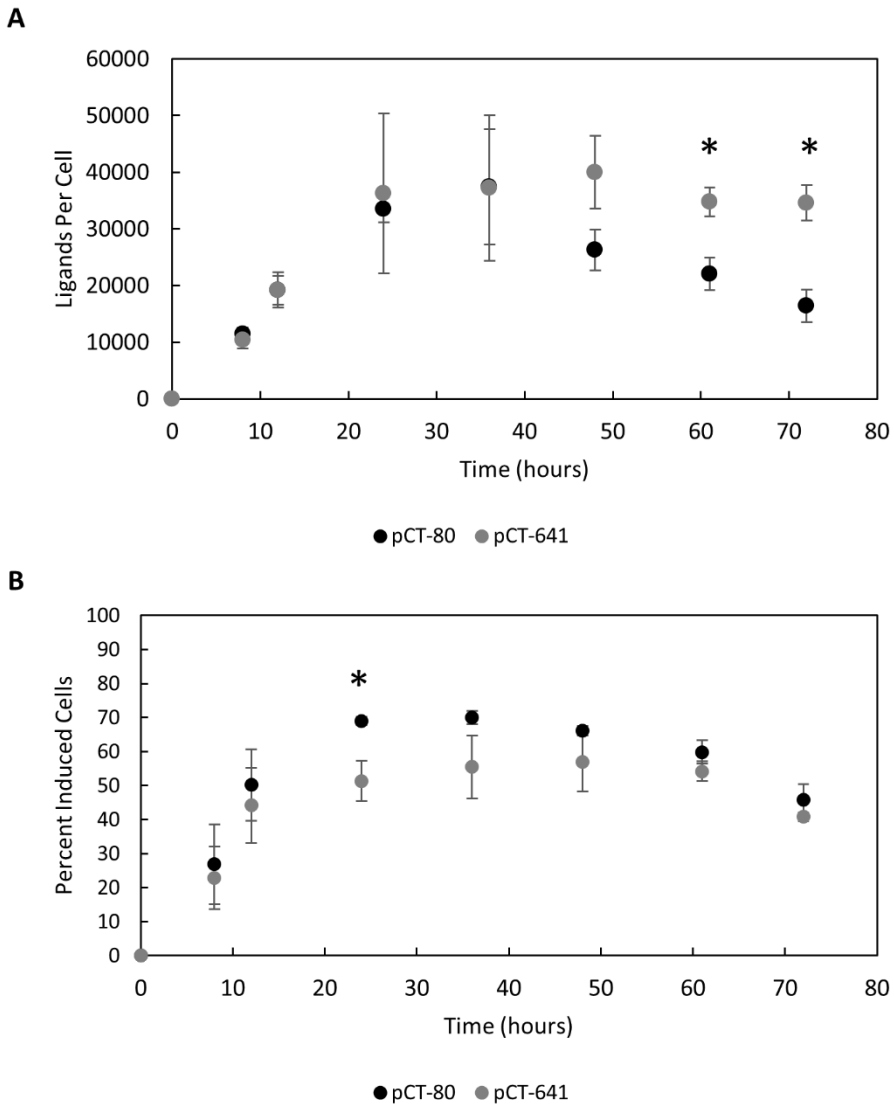

Figure 4-5. The effect of induction time on surface display levels and percentage of induced yeast for populations displaying E6.2.6' via pCT-80 and pCT-641. Yeast containing pCT-80 or pCT-641 expression plasmids encoding for E6.2.6' were grown at 30 °C and induced at 20 °C. Aliquots were taken from each sample at specified timepoints and labelled with an anti-c-myc antibody and anti-mouse-FITC secondary antibody. Their fluorescence was analyzed by flow cytometry and compared to a quantitative bead standard labelled with the same antibody mixture to determine ligand expression. Ligand expression (A) and percent induction (B) are presented as the mean of three samples ± standard deviation. * indicates $p < 0.05$ difference between pCT-80 and pCT-641.

4.3.4 Gaussian chain model shows linker stiffness and length drives extracellular accessibility

To further understand the impact of the yeast surface display linkers and the parameters that affect extracellular accessibility, we constructed and evaluated geometric models of the two linker systems. Both GGSGGS and PAS#1, polypeptides of similar composition to the $(G_4S)_3$ and PAS#1-based repeats that primarily make up the pCT-80 and pCT-641 linkers, have been previously described as random coil structures [187,188]. This guided the selection of the Gaussian chain model to describe both linkers[183–185]. To account for the nonideal behavior of real polypeptide chains, the model was modified with a characteristic ratio correction factor, using homopolymer values for glycine, alanine, and proline[189,190]. While experimental characterization of the characteristic ratios for the 80 and 641 amino acid linkers is outside the scope of this study, GGSGGS linkers have a characteristic ratio similar to polyglycine[187], and PAS#1 has been described as having a stiffness between polyalanine and polyproline[188]. This indicates that, while not experimentally determined, the characteristic ratio of the linkers should fall within the range of values provided, thus allowing for a semi-quantitative framework for comparison of length distributions between both linkers. To account for the GPI-mediated attachment of Aga1p, the model allowed linkers to anchor anywhere within the cell wall (assumed to be 115 nm thick)[180]. Lacking any prior knowledge of the distribution of Aga1p in the cell wall, a uniform distribution was chosen for simplicity.

With this model, we calculated the probability distribution of ligand distance from the yeast cell surface, assuming the linker is a homopolymer consisting of either poly-glycine, poly-alanine, or poly-proline. This reveals a relatively constant probability

within the cell wall, due to the homogenous distribution of the yeast surface display construct, with a sharp decrease across the boundary of the cell wall (Figure 4-6A). The fraction of ligands in the extracellular space correlated with both length and stiffness, with pCT-641 having a higher fraction of extracellular ligands compared to pCT-80 regardless of stiffness. Increasing the number of linker amino acids from 80 to 641 provided a 2.8-3.2 fold increase in the fraction of ligands in the extracellular space, supporting our hypothesis that the improved performance of pCT-641 is more consistent ligand-target engagement as a result of increased ligand accessibility to the extracellular space (Figure 4-6B).

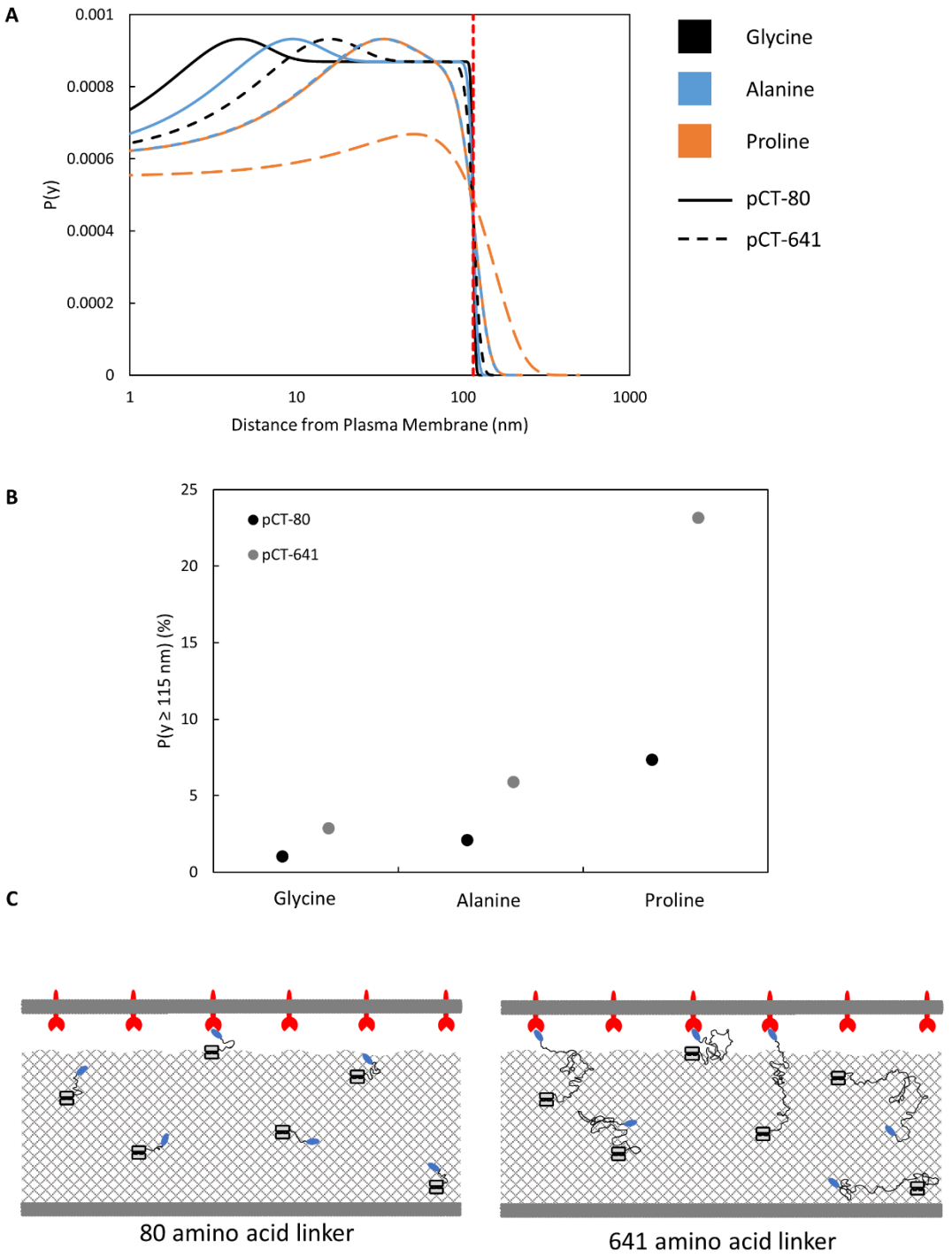

Figure 4-6. pCT-641 extends farther than pCT-80, on average, regardless of material composition. (A) Probability distribution functions of ligand distance from the cell surface were constructed for pCT-80 and pCT-641 using a characteristic ratio corrected Gaussian chain model. Curves were constructed for the characteristic ratios of glycine, alanine, and proline. The vertical dotted line indicates the approximate boundary between

the cell wall and the extracellular space. (B) The area under each curve beyond the cell wall boundary was integrated to determine the percentage of total ligand accessible to the extracellular space. (C) Schematic of a yeast cell and mammalian cell in close contact. Aga1p–Aga2p anchor complexes are uniformly distributed throughout the cell wall with ligands tethered through representative linkers to illustrate how increased length relates to extracellular accessibility

While the model does not take into account the observed expression levels or the exact stiffness of the linker, we can make a reasonable approximation for the number of ligands with accessibility to the extracellular space by estimating the fraction of accessible ligands for each linker as a linear combination of the values from Figure 4-6B weighted by the fractional composition of glycine, alanine, and proline, using expression levels from Figure 4-4A, and assuming a yeast cell to be an 8 μm diameter sphere. This estimate suggests 24-36 accessible ligands per μm^2 for yeast expressing pCT-80 versus 63-69 accessible ligands per μm^2 for pCT-641, a moderate increase in spite of the expression difference. Dependent upon cell-cell shape complementarity and target density, these estimates make it reasonable that the longer linker transitions these interactions from monovalent to multivalent

Our model theoretically suggests an infinite length linker to maximize ligand-target engagement but does not account for several factors including genetic efficiency, extracellular shuttling, and stability. These factors may restrict the length of realistically functional linkers and reduce ligand expression that would create an optimum that is not readily extractable from our existing data. However, the inability of a 40, 80, or 641 flexible linker to effectively enrich the low affinity linker in low expression conditions[65] either suggests that the length needed for effective avidity may be prohibitively long or that other approaches may be needed to enhance the extracellular exposure of ligands. For instance, stiffer linkers provide a higher fraction of accessible ligands relative to

flexible linkers with the same number of residues. This could potentially motivate the design of a hybrid linker with a stiff base to allow extracellular access and a flexible distal portion to allow the ligand to sample space. Another suggestion is to pre-treat the yeast with Zymolyase to effectively thin the cell wall[180], although this may also result in the removal of ligand attached to the degraded portion of the cell wall.

While the above data highlights the usefulness of extended linkers in yeast surface display systems when conducting cell panning, recommendations for linker length in other display platforms (ribosome, phage, and mammalian cell) are less clear. In the case of ribosome and phage display, the small size of the display platform limits steric hinderance between the platform and target cell. In these cases, short linkers are often incorporated more to aid in the stability of the displayed protein fusion. However, it remains possible that the analytical study of linker length in these systems could see a useful improvement. While there is no need to penetrate through a cell wall in mammalian cell display, the size of yeast and mammalian cells remain similar. Thus, a similar level of steric hindrance could be expected, which motivates the switch from existing linkers to one similar in length to those mentioned above and a more thorough investigation of the effect of linker length on cell panning performance in mammalian cell display systems.

4.4 Conclusion

A dramatically extended yeast surface display linker provides more robust extracellular engagement with cell surface biomarkers. The 641-amino acid linker provided significantly improved ligand yield and enrichment in adherent cell panning for both high affinity ligands on cells with moderate target expression and low affinity

ligands on cells with high target expression relative to the existing 80-amino acid linker. This enhanced yield and enrichment was observed despite 10-34% fewer ligands displayed per yeast cell and was observed with multiple scaffolds and targets. In addition, modelling the linkers suggests pCT-641 has a higher fraction of extracellularly accessible ligands, which suggests the observed performance benefits are due to more consistent ligand-target interactions. Ultimately, the findings of this study provide a new yeast surface display construct for use in adherent cell panning while motivating further study into other construct improvements.

4.5 Materials and Methods

4.5.1 Cells and Cell Culture

A431 cells were provided by Professor Daniel Vallera (Department of Therapeutic Radiology, University of Minnesota – Twin Cities). MDA-MB-231 were provided by Professor Jayanth Panyam (Department of Pharmaceutics, University of Minnesota – Twin Cities). All cell lines were grown with DMEM containing 4.5 g/L D-glucose, sodium pyruvate, and L-glutamine and supplemented with 10% (v/v) fetal bovine serum and 1% (v/v) 10,000 U/mL penicillin-streptomycin. All cell lines were incubated at 37 ºC in a humidified atmosphere with 5% CO_2.

Yeast surface display was performed largely as previously described.[132] Expression plasmids, explained below, were transformed into *Saccharomyces cerevisiae* yeast strain EBY100 by EZ-Yeast Transformation (Zymo Research, Irvine, CA). Yeast harboring expression plasmids were grown in SD-CAA medium (16.8 g/L sodium citrate dihydrate, 3.9 g/L citric acid, 20.0 g/L dextrose, 6.7 g/L yeast nitrogen base, and 5.0 g/L casamino acids in deionized H_2O) at 30 ºC with shaking for at least 7 hours. Protein

expression was induced on the yeast surface by transferring yeast cells in logarithmic phase (OD_{600nm}<6) into SG-CAA medium (10.2 g/L sodium phosphate dibasic heptahydrate, 8.6 g/L sodium phosphate monobasic monohydrate, 19.0 g/L galactose, 1.0 g/L dextrose, 6.7 g/L yeast nitrogen base, and 5.0 g/L casamino acids in deionized H_2O) and growing at 20 ºC for 24 to 48 hours. EBY100 without expression plasmids were grown in YPD medium (20.0 g/L peptone, 20.0 g/L dextrose, and 10.0 g/L yeast extract in deionized H_2O) at 30 °C with shaking.

4.5.2 Expression Plasmids

The pCT-80 and pCT-641 plasmids were used as the expression vectors for yeast surface display on the C-terminus of Aga2p. pCT-80 encodes for Aga2p followed by an 80-amino acid linker (composed of a Factor Xa cleavage site, an HA epitope, a proline/alanine/serine peptide based upon the PAS#1 motif [PAS40], a glycine-rich peptide [$(G_4S)_3$], and an NheI recognition site), the ligand, a BamHI recognition site, and a C-terminal Myc epitope (SI Table 1). This is, essentially, the classic pCT yeast surface display plasmid with the addition of a 40-amino acid PAS#1-based domain.

To further extend the linker, the latter 38 amino acids of PAS40 (PAS38), the ligand, and C-terminal Myc epitope were PCR amplified with the addition of an AvrII recognition site 5' of PAS38. This construct was inserted into NheI and BamHI digested pCT-80 by HiFi DNA Assembly (New England Biolabs), creating the starting construct for further expansion. The linker was then exponentially expanded through iterative restriction enzyme digestion and destructive ligation, as previously described [186]. The construct was digested with AvrII (New England Biolabs) and BamHI (New England Biolabs) to generate an insert containing PAS38, $(G_4S)_3$, an NheI recognition site, and the

ligand. The same plasmid was separately digested with NheI and BamHI to create an acceptor vector. Ligation resulted in the duplication of PAS38-$(G_4S)_3$ as well as the destruction of the cut NheI and AvrII sites. This process was repeated three additional times. Each plasmid was digested by AvrII and BamHI before being analyzed by gel electrophoresis to confirm proper duplication of the linker. The longest plasmid constructed was named pCT-641 as it is, essentially, the classic pCT yeast surface display plasmid with the addition of a 601-amino acid linker (Table 4-1).

4.5.3 Receptor Expression Quantification

Cellular expression of EGFR, CD276, and yeast-displayed ligand were quantified using polystyrene beads with known quantities of immobilized anti-mouse IgG (Bangs Laboratories, Inc., Fishers, IN) to construct a calibration curve. Beads and cells were separately labelled with either mouse anti-EGFR clone ab30 (4 µg/mL) (Abcam), mouse anti-CD276 clone 185504 (4 µg/mL) (Biotechne), or anti-c-Myc clone 9E10 (4 µg/mL) (BioLegend) for 30 minutes at 4 ºC. Beads and cells were washed once with phosphate-buffered saline with 0.1% (w/v) bovine serum albumin, 1 mM $CaCl_2$ and 0.5 mM Mg_2SO_4 (PBSACM) and pelleted at 500g for 3 minutes. The beads and cells were then labelled with goat anti-mouse Alexa Fluor 647 conjugate (10 µg/mL) (Life Technologies A-21235) or goat anti-mouse FITC conjugate (10 µg/mL) (Sigma-Aldrich F0257) for 30 minutes at 4 ºC, washed once with PBSACM, and again pelleted at 500 g for 3 minutes. Fluorescence was analyzed by flow cytometry using an Accuri C6 Plus (BD Biosciences). Bead fluorescence was used to construct a calibration curve from which the EGFR, CD276, or yeast-displayed ligand expression was quantified

4.5.4 Adherent Mammalian Cell Panning

Adherent cell panning selections were carried out with minor modifications from previous literature[65]. Mammalian cells were grown in 12-well plates to approximately 70-90% confluency. The culture medium was aspirated, and cells washed once with ice cold PBSACM. Yeast mixtures containing $1x10^6$ or $1x10^7$ ligand-displaying yeast and $1x10^8$ EBY100 were washed in PBSACM and added dropwise to each well in 1 mL of ice cold PBSACM. Plates were incubated statically for 15 minutes at 4 °C and the unbound yeast were removed. Wells were washed with 1 mL of ice cold PBSACM four times with 25 gentle tilts and 5 gentle nutations and a fifth time with 10 nutations. Cell monolayers with bound yeast were removed by scraping and resuspended in 1 mL of PBSACM. The yield of plasmid-harboring yeast was quantified by plating mixture dilutions on SD-CAA plates, while the yield of total yeast was quantified by plating mixture dilutions on YPD plates. Enrichment ratio was calculated as the yield of plasmid-harboring yeast divided by the yield of plasmidless yeast.

4.5.5 Modeling Ligand Distribution on the Yeast Cell Surface

Linker length was substantially shorter than yeast cell radius; thus, curvature was neglected and the cell surface was approximated as an impermeable plane. The linker was modelled as a 1-D Gaussian chain model and $P(z)$, the probability distribution function of the linker extending an end-to-end distance z in the direction perpendicular to the cell surface, is given by:

$$P(z) = \sqrt{\frac{3}{2\pi\langle r^2\rangle}}\, e^{-3z^2/2\langle r^2\rangle}$$

where $\langle r^2\rangle$ is the mean-square end-to-end length of the peptide chain and is given by:

$$\langle r^2 \rangle = C_\infty n l^2$$

where C_∞ is the length-independent characteristic ratio, n is the number of peptide bonds, and l is the average distance between adjacent C_α atoms (3.8 Å) [183]. The linker was assumed to be uniformly distributed within the cell wall (estimated as 115 nm) [180] and the conditional probability of the linker ending a distance y from the plasma membrane given that the linker starts a distance a from the plasma membrane is given by:

$$P(y|a) = \sqrt{\frac{6}{\pi\langle r^2 \rangle}} \frac{1}{1 + \mathrm{erf}\left(\sqrt{\frac{3a^2}{2\langle r^2 \rangle}}\right)} e^{\frac{-3(y-a)^2}{2\langle r^2 \rangle}}$$

This equation was multiplied by the probability distribution of linker in the cell wall and numerically integrated to generate the probability distribution function $P(y)$ using the law of total probability. The characteristic ratios for polyglycine (2.16), polyalanine (9.27), and polyproline (116)[189,190] were used to generate curves for polypeptides of 80 and 641 residues and the fraction of ligands extending beyond the cell wall.

4.5.6 Statistical Analysis

All cell panning was binned by day and linker prior to significance testing by two-way ANOVA with only main effects. Significance testing of yeast surface display levels was conducted by constructing 95% confidence intervals. All statistics are reported as mean ± standard deviation except for the following: yeast surface display levels were reported as 95% confidence intervals and AC2 affinity was reported as a 68% confidence interval.

Chapter 5 – Combined Differential Yeast Biopanning and Deep Sequencing Enables Highly Specific Ligand Discovery in the Context of Oncology Biomarkers IGF1R and InsRA

5.1 Summary

Protein ligand selection strategies often utilize recombinantly-produced extracellular domains in-lieu of full-length protein targets. Such selections have been successfully applied against a variety of targets but may result in ligands that fail to translate binding to full-length target on expressing cells. As an alternative, selections utilizing target-expressing cells have been investigated. However, the heterogenous nature of the mammalian cell surface often results in the enrichment of non target-specific ligands that may dominate the population, thus hindering the isolation of target-specific ligands by traditional screening via binder enrichment and clonal analysis of specificity. This study evaluates the ability to identify specific binders by deep sequencing yeast populations sorted on either target-expressing cells or target-negative cells in the context of insulin-like growth factor receptor (IGF1R) and insulin receptor isoforms A (InsRA) and B (InsRB). Sorting of affibody libraries yielded preferential enrichment on IGF1R-expressing cells relative to IGF1R-negative cells, which translated to affibodies with significant specificity towards IGF1R-expressing cells being identified through deep sequencing. Additionally, both fibronectin and affibody libraries yielded preferential enrichment on both InsRA- and InsRB-expressing cells relative to parental HEK293T cells but showed little isoform specificity. Combined, these results motivate the evaluation of a subset of the identified IGF1R-specific sequences by traditional clonal

specificity screening to verify the accuracy of this new method, along with the deep sequencing of the InsRA and InsRB sorted populations to identify rare clones with isoform specificity.

5.2 Introduction

Protein ligands have been previously engineered with high affinity, specific binding activity to a wide range of clinically relevant biomarkers while maintaining desirable characteristics for diagnostic and therapeutic applications[10,127]. Binding ligands are often generated from engineered naïve libraries or libraries isolated from immunized animals presented using surface display technologies – such as phage[42–44] or yeast[60–62] surface display – and selected using techniques including target immobilized to microwell plates[44], magnetic-activated cell sorting (MACS)[48,78,79], or fluorescence-activated cell sorting (FACS)[60,80]. Many biomarkers of interest are transmembrane proteins, therefore possessing transmembrane domains that are insoluble in an aqueous environment. While progress has been made in stabilizing membrane proteins in phospholipid bilayer nanodiscs[73,74], relatively few targets are commercially available in this format, with the preparation of new targets requiring either expensive custom synthesis or using protocols that have not been robustly optimized relative to existing recombinant production strategies. Thus, these selections are often conducted using recombinantly-produced extracellular domains. While proven successful in numerous discovery campaigns[81–86], campaigns utilizing solely recombinant extracellular domains may produce ligands that bind to recombinant target but not full-length, membrane-bound target on expressing cells due to missing native epitopes or the addition of non-native epitopes[166] (Chapter 2).

As a solution, whole cells and detergent-solubilized cell lysates expressing full-length target have been implemented as antigen sources in MACS[178,179,191] (Chapter 3) and FACS[99,111,112,166,168] (Chapter 2), with success in yielding binders that translate to target-expressing cells and tissues. Yet, it has been shown that campaigns conducted in this manner, despite extensive depletion by a number of different strategies including panning against target-negative cells[109,122–124,166] (Chapter 2), masking with polyclonal mixtures enriched for binding to a target-negative cell line[125], or sequential selections with recombinant extracellular domains and target-expressing cells[166] (Chapter 2), can enrich high frequencies of off-target or nonspecific ligands, making the identification of specific ligands difficult by conventional clonal testing[109,166] (Chapter 2).

This problem motivates the investigation of alternative methods to increase the throughput of the specificity screening of ligands to difficult targets, such as transmembrane proteins. A compelling approach involves the use of massively parallel sequencing (also known as deep sequencing), which allows the sequencing of millions of ligand variants. Deep sequencing of library populations after the application of selection pressure allows the correlation of sequence abundance and function[192–194]. This sequence-function mapping has been utilized to identify ligands with target specificity. Such methods commonly involve either sorting in parallel against a panel of fluorescently-labelled recombinant proteins by FACS[195,196] or the sorting an already matured population by competitive labelling FACS with fluorescently-labeled target and unlabeled non-target proteins[197]. Deep sequencing of these populations allows identification of specific variants through the frequency of sequences in the target-positive pool relative to the off-target pools in the former case and the enrichment of

sequences in the post-sort population relative to the pre-sort population in the latter case. These successes, combined with the increased translatability of ligands discovered by cell-based methods and increased throughput of adherent cell panning, make the adaptation of these methods to cell panning campaigns compelling.

This study applies the principles of ligand specificity engineering through parallel deep sequencing of yeast surface display populations differentially sorted on target-expressing and target-negative cells via panning on adherent cell monolayers in the context of insulin-like growth factor receptor (IGF1R) and insulin receptor (InsR). IGF1R is commonly overexpressed in breast, prostate, and thyroid cancers and negatively associated with patient outcome[198,199]. Additionally, InsR has been shown to be overexpressed in breast and thyroid cancers, with the A isoform (InsRA) being the predominant isoform over the B isoform (InsRB) in these cancers[199]. Combined, this makes the discovery of panels of ligands with binding to IGF1R or InsR – with a focus on InsRA – compelling. Ligands with specific binding to IGF1R and InsRA could provide more efficient screening for cancers associated with IGF1R and InsRA overexpression via molecular imaging[128]. As well, the use of ligands to detect IGF1R and InsR expression on patient biopsies would also allow effective treatment stratification based upon tumor molecular profiling, since the lack of IGF1R expression has been associated with tamoxifen resistance[200] and the co-expression of IGF1R and InsR is associated with resistance to IGF1R-targeted therapies in mouse models[201]. InsRA-binding ligands could also aid in treating cancer cells or resensitize cancer cells to IGF1R-targetted therapies[201] while limiting side effects of inhibiting InsRB in normal tissues. The combined inhibition of IGF1R and InsR by a tyrosine kinase inhibitor

showed promise in antitumoral activity[202], highlighting the potential for treatment using both IGF1R- and InsRA-binding ligands. The discovery of InsRA specific ligands is also motivated by a prior study, which used a Gp2 library[71] to isolate InsR-specific ligands with high affinity binding[111]. However, these molecules showed low isoform specificity (unpublished) despite InsRA being the major isoform used for selections, indicating that additional methods may be required to screen for isoform specific molecules.

In this study, naïve fibronectin domain[70] or affibody[68] libraries were initially sorted via adherent cell panning on cells expressing either IGF1R or an InsRA-mCherry fusion protein to enrich IGF1R and InsRA binding ligands. Yeast populations enriched against IGF1R were then sorted in parallel on either IGF1R-negative or IGF1R-expressing cells, while yeast populations enriched against InsRA were sorted in parallel on either InsRA-mCherry expressing, InsRB-EGFP expressing, or parental HEK293T cells. Significant yield preference was noted in several of the IGF1R and InsRA campaigns, suggesting the presence of target-specific – but not necessarily isoform-specific – ligands within the sorted populations. Populations from the IGF1R campaigns were deep sequenced and the relative frequencies of sequences in the populations from both the IGF1R-negative and IGF1R-expressing sorts were compared, with the hypothesis that clones with a significantly higher frequency in the IGF1R-expressing sorts possess specificity to IGF1R. Deep sequencing revealed 174 affibody sequences and 1 fibronectin domain sequence that were significantly more frequent in populations resulting from IGF1R-expressing sorts relative to IGF1R-negative sorts, further suggesting that this sorting strategy can identify ligands with target-specific binding.

Future work should focus on deeper sequencing of the IGF1R populations to discover additional IGF1R-enriched affibodies and fibronectins along with a similar analysis of the InsRA campaigns. To confirm the hypothesis that sequences preferentially observed in target-expressing sorts are specific, a subset of sequences observed at a significantly higher frequency in either the IGF1R or InsRA sorts along with several sequences with no observed frequency preference should be produced as soluble ligands and tested for binding to target-expressing and target-negative cells in order to experimentally determine clonal specificity and verify the accuracy of this method

5.3 Results

5.3.1 Differential Panning Shows Affibody Specificity Towards IGF1R-Overexpressing Cells

Four selection campaigns were carried out to select ligands with binding to IGF1R. Two scaffolds – fibronectin and affibody – were expressed using yeast surface display constructs with either an 80-amino acid linker (pCT-80) or a 641-amino acid linker (pCT-641). Fibronectin domain and affibody libraries using pCT-80 were previously used to isolate ligands with binding to CD276 and Thy1[166] (Chapter 2), while pCT-641 showed improved enrichment in adherent cell panning sorts with limited avidity[203] (Chapter 4) which may potentially allow the enrichment of lower affinity ligands from the naïve library. All four libraries were initially panned against mouse embryonic fibroblast cells with a homozygous disruption of IGF1R (R-)[204] that were stably transfected with cDNA encoding for human IGF1R (R-/IGF1R)[200] to remove any nonbinding yeast and limit the population to a size that could be efficiently deep sequenced, while acknowledging that IGF1R-specific ligands are likely coenriched with

off-target specific and nonspecific ligands. pCT-641 libraries were then sorted via FACS for full-length ligand expression. All four populations were then panned in triplicate against either R- or R-/IGF1R cells (Figure 5-1).

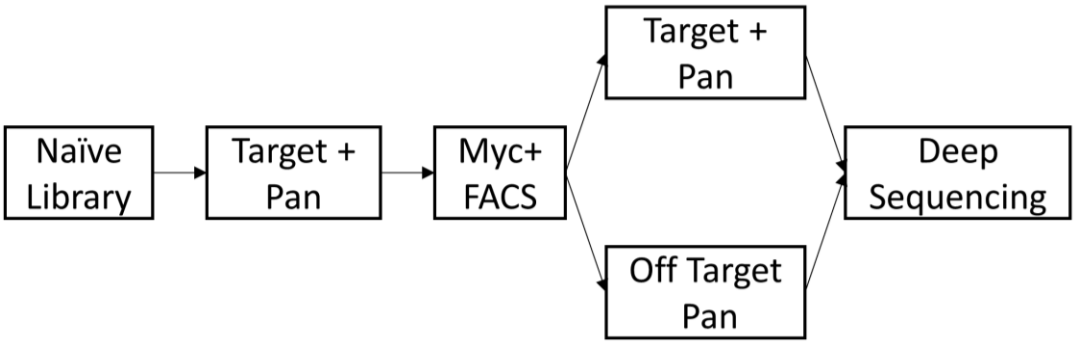

Figure 5-1. Overview of differential cell panning. Naïve fibronectin domain and affibody libraries are initially screened by panning on target-overexpressing, adherent cell monolayers. The resultant population is then selected for full-length ligands via FACS using a C-terminal Myc-tag (Myc+ FACS). The target-positive cell enriched population is then split and panned in parallel either a second time on target-overexpressing cells or one of several additional cell lines (target-negative cells, cells overexpressing an additional target, or parental cells with basal level target expression).

While neither fibronectin campaign showed a significant yield preference for R-/IGF1R cells over R- cells (pCT-80: 0.09 ± 0.02% vs. 0.05 ± 0.01%, $p = 0.19$; pCT-641: 0.15 ± 0.04% vs. 0.0033 ± 0.0008%, $p = 0.07$; Figure 5-2), both affibody campaigns showed a significantly increased yield on R-/IGF1R cells (pCT-80: 0.57 ± 0.05% vs. 0.15 ± 0.02%, $p = 0.01$; pCT-641: 0.100 ± 0.001% vs. 0.017 ± 0.004%, $p = 0.001$; Figure 5-2), suggesting that the affibody populations may contain a substantial subset of IGF1R-specific ligands. Interestingly, despite our previous observation that pCT-641 aids enrichment in sub-optimal model cell panning systems[203] (Chapter 4), the pCT-641 fibronectin domain library showed no significant advantage over pCT-80 on either cell line ($p = 0.3$ for R-/IGF1R; $p = 0.06$ for R-; Figure 5-2) while the pCT-80 affibody

library showed significantly increased yields on both cell lines compared to pCT-641 (p = 0.01 for R-/IGF1R; p = 0.02 for R-; Figure 5-2). However, each library is a separate transformation from DNA with a diversity far exceeding the capacity of yeast surface display libraries, which makes it difficult to make a direct comparison between the two linkers.

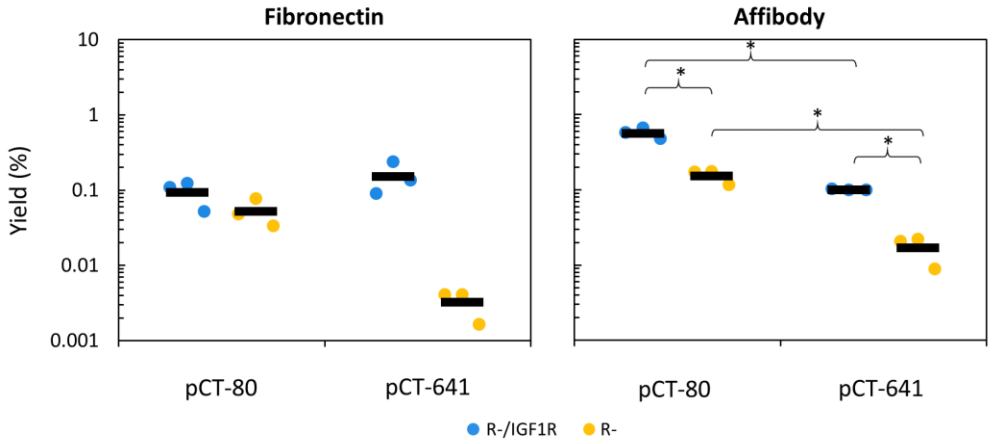

Figure 5-2. Differential cell panning on R- and R-/IGF1R cells exhibit modest, and sometimes significant, yield preference to IGF1R-overexpressing cells. Fibronectin domain and affibody ligands tethered to the yeast surface by either an 80-amino acid linker (pCT-80) or a 641-amino acid linker (pCT-641) were enriched in a single round of panning on R-/IGF1R cell monolayers and subjected to an additional round of panning on either R-/IGF1R (blue) or R- (yellow) cell monolayers in triplicate, denoted by the two strip plots for each library. Yield was quantified by plating on SD-CAA plates. An asterisk (*) represents $p < 0.05$ difference in yields.

5.3.2 Campaigns Conducted on IRA-Overexpressing Cells Shows High IR-Expressing Cell Specificity but Low Isoform Specificity

Fibronectin domain and affibody libraries expressed using pCT-641 were similarly panned on HEK293T cells stably transfected to overexpress an InsRA-mCherry fusion protein (HEK-InsRA) and sorted for full-length ligand expression by FACS prior to parallel sorting in triplicate on either HEK-InsRA cells, HEK293T cells stably transfected to overexpress an InsRB-EGFP fusion protein (HEK-InsRB), or parental

HEK293T cells with basal levels of InsR expression. Despite being initially sorted on HEK-InsRA cells, the fibronectin domain campaign showed significantly higher yield on HEK-InsRB cells (0.54 ± 0.03% vs. 0.32 ± 0.02%, $p = 0.008$; Figure 5-3) and both InsR cell lines exhibited higher yield relative to parental HEK293T cells (0.14 ± 0.02%, $p = 0.004$ for HEK-InsRA and $p = 0.0006$ for HEK-InsRB). On the other hand, the affibody campaign did not show a significant increase in yield on HEK-InsRA cells relative to HEK-InsRB cells (2.4 ± 0.3% vs. 1.8 ± 0.3%, $p = 0.2$), but only the yield on HEK-InsRA cells were significantly higher than on HEK293T cells (1.0 ± 0.1%, $p = 0.02$ for HEK-InsRA and $p = 0.08$ for HEK-InsRB). Combined, this seems to indicate that there may be a substantial number of InsR-binding ligands in the populations, but without a preponderance of ligands with substantial specificity towards InsRA.

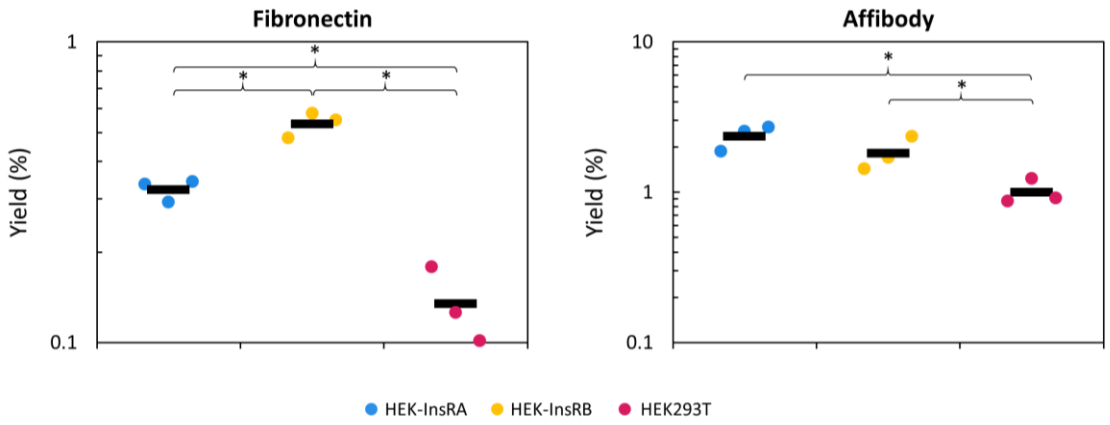

Figure 5-3. Differential cell panning on InsR-overexpressing and HEK293T cells exhibits limited InsRA specificity, but high InsR cell line binding. Fibronectin domain and affibody ligands tethered to the yeast surface by 641-amino acid linker (pCT-641) were enriched in a single round of panning on HEK-InsRA cell monolayers and subjected to an additional round of panning on either HEK-InsRA (blue), HEK-InsRB (yellow), or HEK293T (magenta) cell monolayers in triplicate, denoted by the three strip plots for each library. Yield was quantified by plating on SD-CAA plates. An asterisk (*) represents $p < 0.05$ difference in yields.

5.3.3 Deep Sequencing Aids in the Identification of Sequences That Are Preferentially Enriched on IGF1R-Overexpressing Cells

With the encouraging yield data from the IGF1R campaigns suggesting that the pCT-80 and pCT-641 affibody campaigns contained IGF1R-specific ligands, both the affibody and fibronectin domain campaigns were deep sequenced to provide clonal frequency data from both R-/IGF1R and R- cell pans. In general, the deep sequencing data showed good correlation with the preliminary yield data, with the majority of sequences being only observed in the R-/IGF1R cell pans, suggestion some degree of IGF1R specificity (Figure 5-4). However, a mixture of low sequencing depth and high variance of sequence frequency across replicates limited the number of clones with significant frequency preference. The pCT-80 and pCT-641 affibody populations contained 44 and 130, respectively, sequences that had significantly higher frequencies in the R-/IGF1R cell pans with few clones showing significantly higher frequencies in the R- cell pans (Table 5-1). The pCT-80 and pCT-641 fibronectin domain populations only yielded a single clone from pCT-641 with any frequency preference towards R-/IGF1R cells (Table 5-1). Notably, the most frequent clone in the pCT-80 affibody R-/IGF1R population is also the most frequent clone in the R- populations (shown in the upper right corner of Figure 5-4A), indicating both that it is likely non target-specific and the clone most likely to be selected by traditional clone picking. This highlights the strength of this deep sequencing approach to identify rare, yet potentially IGF1R-specific clones. While not confirmed to be IGF1R-specific, the preliminary yield data, along with the significant enrichment observed in deep sequencing provides strong evidence that the panel of affibodies identified by deep sequencing have preferential binding to R-/IGF1R cell lines.

	Affibody		Fibronectin	
	pCT-80	pCT-641	pCT-80	pCT-641
R-/IGF1R specific	44	130	0	1
R- specific	4	3	0	0
Nonspecific	3,952	6,833	2,328	5,515

Table 5-1. Deep sequencing results show ligands with specificity towards R-/IGF1R cells. All IGF1R campaigns were deep sequenced and the resulting reads paired and filtered for quality. MATLAB was used to eliminate any truncated reads, calculate the frequency of each sequence in each cell sort population, and test for statistical difference in frequency between the frequency in the pools. Nonspecific reads may be truly nonspecific, specific to a target on both cell lines, or nonbinding ligands that were not thoroughly eliminated from the sort.

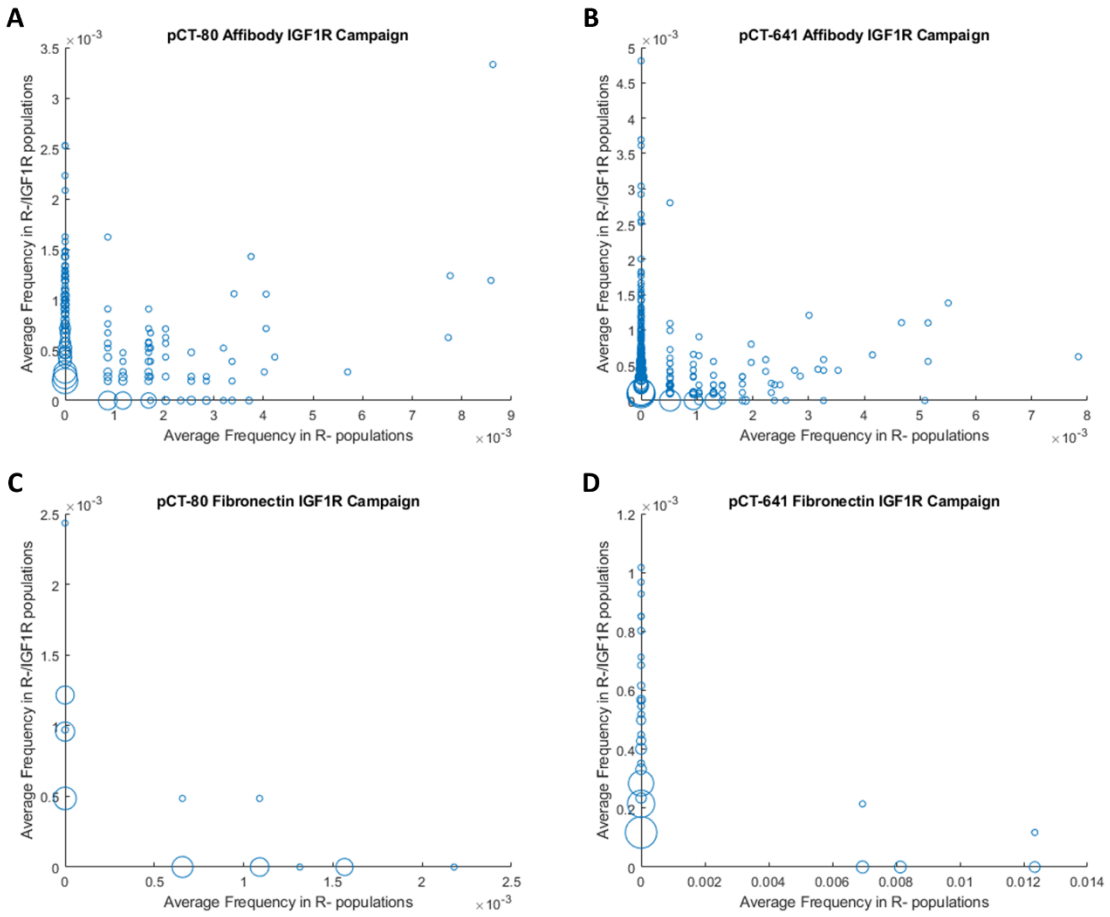

Figure 5-4. Affibody populations show a preference for R-/IGF1R cells. Sequences were plotted by frequency in both the R- and R-/IGF1R panned populations. Sequences with the same frequencies were combined into a single point, with the point size increasing as the square root of the number of sequences.

5.3.4 Low Avidity Sorting Conditions Result in a Reduction of High Yield, InsRA-Binding Ligands

Given the relatively high diversity of ligands collected from each cell line in the InsR campaigns and limited number of sequences with significant frequency preference to the R-/IGF1R cell pans observed in the R-/IGF1R deep sequencing, we desired the ability to increase the selection pressure of the cell panning to winnow the population down to the highest affinity ligands. Prior work showed that reducing the disulfide bonds of the Aga1p-Aga2p yeast surface display construct using dithiothreitol (DTT) was effective in reducing the valency of ligands on the yeast surface, thus increasing the selection pressure of adherent cell panning and preferentially enriching high affinity ligands[66]. The affibody and fibronectin domain yeast populations that were enriched with a single round of adherent panning on HEK-InsRA cells were incubated with DTT to reduce the number of ligands on the yeast surface by roughly 4-5 fold. These yeast were then sorted as previously in parallel on either HEK-InsRA, HEK-InsRB, or HEK293T cells. As expected, these sorts yielded fewer ligands on average in each case, with no significant difference in yield between cells panned on HEK-InsRA, HEK-InsRB, or HEK293T, thus making the estimation of potential specificity difficult (Figure 5-5).

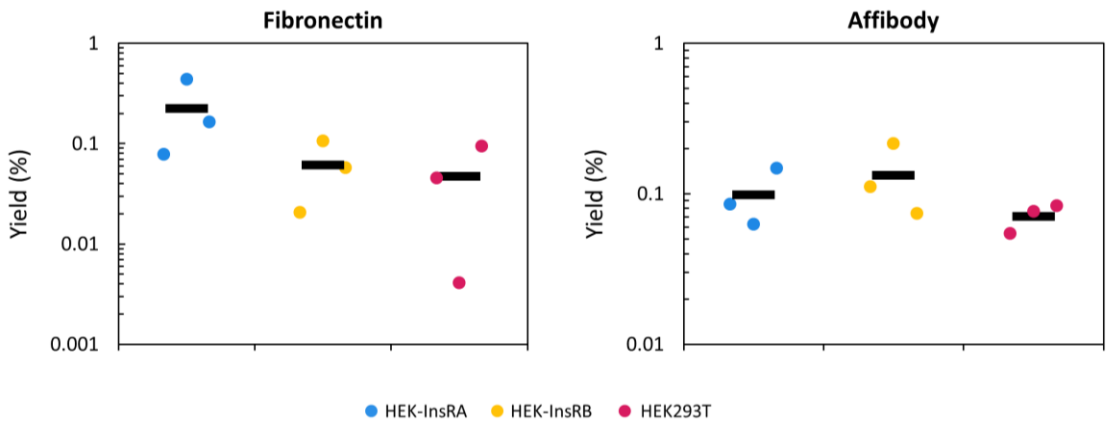

Figure 5-5. Differential cell panning on InsR-overexpressing and HEK293T cells under reduced avidity conditions displays no significant yield preference. Fibronectin domain and affibody ligands tethered to the yeast surface by 641-amino acid linker (pCT-641) were enriched in a single round of panning on HEK-InsRA cell monolayers and subjected to an additional round of panning after using DTT to reduce the number of ligands on the yeast surface by 4-5 fold. Selections were conducted on either HEK-InsRA (blue), HEK-InsRB (yellow), or HEK293T (magenta) adherent cell monolayers in triplicate, denoted by the three strip plots for each library. Yield was quantified by plating on SD-CAA plates. An asterisk (*) represents $p < 0.05$ difference in yields.

5.4 Discussion

Cell-based panning methods have shown efficacy in isolating ligands that translate to binding on full-length target on target-expressing cells or tissues where recombinantly-produced extracellular domains have failed[166]. However, the heterogeneous nature of the mammalian cell surface often results in non target-specific ligands either co-enriching or out-enriching specific ligands, resulting in difficulties isolating specific ligands by traditional clonal screening methods[166]. While a variety of depletion methods have been devised, few provide any significant ability to limit the enrichment of non target-specific ligands in the context of yeast surface display[109,122–125,166]. This study explored an alternative, bioinformatics-based method of screening for target-specific ligands by enriching naïve fibronectin domain and affibody libraries in a

single round of adherent cell panning on target-expressing cells to eliminate the majority of nonbinding ligands while retaining the majority of binding ligands and limiting the likelihood of non target-specific ligands dominating the ligand pool. These populations were then sorted in parallel on either target-expressing and target-negative cells in the IGF1R campaign and target-expressing, off-target expressing, or parental cells in the InsRA campaign. The affibody libraries showed substantially higher binding on R-/IGF1R cells, while the fibronectin domain libraries did not, suggesting that the potential binding epitopes of IGF1R are more amenable to the flatter helix paratope of affibody than the convex paratope of fibronectin domains. As well, the longer pCT-641 linker failed to provide any substantial advantage over the pCT-80 linker in either fibronectin domain or affibody campaign, However, the library transformations (on the order of 10^8 for each yeast library) is vastly smaller than the actual amino acid diversity of the underlying libraries (on the order of 10^{17} for the second-generation sitewise gradient affibody library, 10^{20} for the second-generation sitewise gradient fibronectin library, and 10^{19} for the third-generation sitewise gradient fibronectin library), making it highly unlikely that the pCT-80 and pCT-64 yeast libraries possess any clones in common and thus limiting the ability to directly compare the linkers.

The resultant populations were then deep sequenced and their frequencies compared under the hypothesis that clones significantly more prevalent in the target-positive sort relative to other sorts possess target-specific binding. The deep sequencing frequencies showed general agreement with the yield data, with a higher number of cell-line specific clones observed in the affibody deep sequencing populations mirroring the observed higher yield of the affibody population on R-/IGF1R cells relative to R- cells.

Combined, these data suggests the IGF1R specificity of the identified clones but further work is needed to confirm their specificity.

First, while deep sequencing identified a panel of affibodies with significantly higher frequency in the target-positive pool, most of the sequences in all libraries were single reads (83.7% of pCT-80 affibody, 81.3% of pCT-641 affibody, 99.7% of pCT-80 fibronectin, and 97.5% of pCT-641 fibronectin). This suggests that the depth of sequencing is shallow relative to the estimated underlying diversity of the populations, and that deeper sequencing will discover more sequences and adjust the frequency of existing sequences to align more closely with the actual population frequency. While this is unlikely to alter the significance of the higher frequency R-/IGF1R-specific clones, it is possible that deeper sequencing might reveal additional R-/IGF1R-specific clones that are lower frequency. Additionally, while having a significantly higher frequency in the R-/IGF1R pool suggests that a clone has specificity to IGF1R, experimental clonal screening is required to determine the accuracy of this new method, which could be succinctly determined by taking a selection of the highest frequency (and therefore likely the highest affinity) R-/IGF1R-specific and non cell line specific clones and labelling R- and R-/IGF1R cells with the same concentration of His-tagged soluble ligand followed by an anti-His tag antibody. Analyzing cellular fluorescence by flow cytometry would provide an experimental measure of ligand specificity, which could then be compared to the deep sequencing specificity scoring.

Additionally, the higher yield of fibronectin- and affibody-expressing yeast when panned against adherent HEK-InsRA and HEK-InsRB cell monolayers relative to parental HEK293T cells, thus suggesting the population contains InsR-specific ligands,

creates makes conducting a similar analysis to identify InsRA-specific ligands compelling. Deep sequencing of the HEK-InsRA, HEK-InsRB, and HEK293T population to generate sequence frequency data will allow the identification of sequences that are likely InsR-specific by comparing their frequency on HEK-InsRA and HEK-InsRB to HEK293T, while isoform specificity can be determined for those same sequences by comparing the frequencies on HEK-InsRA and HEK-InsRB. Similarly, experimental verification of potential InsRA-specific, InsR-specific, and nonspecific clones will be necessary to determine the accuracy of this methodology.

5.5 Conclusion

In conclusion, the above work provides a method of clonal specificity analysis that allows the screening of potentially millions of clones simultaneously, with the caveat that further deep sequencing is likely required to better determine the specificity of clones and additional experimental clonal specificity screening of a subset of target-specific and non target-specific ligands is needed to determine the accuracy of this new method. Initial panning of affibody and fibronectin domain libraries on adherent target-expressing cell monolayers prior to parallel sorting either on target-expressing cells or target-negative cells showed substantially increased yield of affibodies on IGF1R-expressing cells compared to IGF1R-negative cells. Similarly, both affibodies and fibronectin domains exhibited substantially increased yields on InsR-expressing cells compared to parental HEK293T cells with basal levels of InsR expression, although no InsR isoform specificity was observed. This limited level of sorting was used to ensure a high diversity of clones in each library and prevent non target-specific ligands from dominating the pool. Deep sequencing identified a panel of affibodies hypothesized to be IGF1R-

specific, while the limited sequencing depth and highly variable frequency of fibronectin domains in the deep sequencing data likely explain the failure to identify any significant clonal specificity. It is hypothesized that a similar analysis on the InsRA campaign will result in the identification of InsR-specific ligands that can be further analyzed for isoform specificity, potentially resulting in a panel of IGF1R-specific and InsRA-specific ligands that can be further applied for imaging and therapeutic applications.

5.6 Materials and Methods

5.6.1 Cells and Cell Culture

Mouse embryonic fibroblast cells with a homozygous disruption of IGF1R (R-)[204] and R- cells that were stably transfected with cDNA encoding for human IGF1R (R-/IGF1R)[200] were a generous gift from Professor Deepali Sachdev (Department of Medicine, Pharmacology, and Cancer Center, University of Minnesota – Twin Cities). HEK293T cells stably transfected to overexpress an InsRA-mCherry fusion protein (HEK-InsRA) and HEK293T cells stably transfected to overexpress an InsRB-EGFP fusion protein (HEK-InsRB) were a generous gift from Professor Douglas Yee (Department of Medicine, Pharmacology, and Cancer Center, University of Minnesota – Twin Cities). HEK-InsRA and HEK-InsRB cells were grown in DMEM containing 4.5 g/L D-glucose, L-glutamine, and 110 mg/L sodium pyruvate supplemented with 10% (v/v) fetal bovine serum and 1% (v/v) 10,000 U/mL penicillin–streptomycin (supplemented DMEM). R- cells were grown in supplemented DMEM with 50 µg/mL G418 (Geneticin) added. R-/IGF1R cells were grown in supplemented DMEM with 50 µg/mL G418 (Geneticin) and 100 µg/mL hygromycin B. All mammalian cells were cultured at 37 °C in a humidified atmosphere with 5% CO_2

Yeast surface display was performed essentially as described[132]. EBY100 strain yeast without expression plasmids were grown in autoclaved YPD (10 g/L yeast extract, 20 g/L bacto peptone, and 20 g/L dextrose) at 30 °C with shaking. EBY00 strain yeast containing expression plasmids were grown in sterile-filtered SD-CAA medium (16.8 g/L sodium citrate dihydrate, 3.9 g/L citric acid, 20 g/L dextrose, 6.7 g/L yeast nitrogen base, and 5 g/L casamino acids) at 30 °C with shaking for at least 7 hours prior to induction. Yeast in logarithmic phase growth ($OD_{600nm} < 6$) were transferred to sterile-filtered SG-CAA medium (10.2 g/L sodium phosphate heptahydrate, 8.6 g/L sodium phosphate monohydrate, 19 g/L galactose, 1 g/L dextrose, 6.7 g/L yeast nitrogen base, and 5 g/L casamino acids) and grown at 20 °C with shaking for at least 24 hours to induce protein expression on the yeast surface.

5.6.2 Naïve Library Construction and Characterization

Oligonucleotides encoding for the third-generation sitewise gradient fibronectin domain library (unpublished) and second-generation sitewise gradient affibody library[68] (Integrated DNA Technologies) were amplified by overlap extension PCR. The resulting gene fragments were incorporated into yeast surface display vector pCT-641[203] by homologous recombination within yeast strain EBY100 through electroporation transformation as previously described[70]. Transformation efficiencies were quantified by serial dilution of transformation mixtures and plating on SD-CAA plates. Proper library construction was verified by Sanger sequencing of yeast clones.

Proper expression of ligands on the yeast surface was characterized by simultaneous labelling of the N-terminal hemagglutinin (HA) and C-terminal c-Myc epitope. One million yeast were pelleted at 1,500*g* for 3 minutes and washed once with

phosphate-buffered saline with 0.1% (w/v) bovine serum albumin, 1 mM $CaCl_2$ and 0.5 mM Mg_2SO_4 (PBSACM) before being labelled with a monoclonal mouse anti-c-Myc antibody 9E10 (4 µg/mL, MilliporeSigma, Cat# OP10) and a chicken anti-HA polyclonal antibody (10 µg/mL, Abcam, Cat# ab9111). The cells were then incubated for 30 minutes at 4 °C, pelleted again, washed once with PBSACM, and labelled with a goat anti-mouse Alexa Fluor 647 conjugate antibody (20 µg/mL, Invitrogen, Cat# A21235) and goat anti-chicken Alexa Fluor 488 conjugate antibody (20 µg/mL, Invitrogen, Cat# A11039) prior to being incubated for 30 minutes at 4 °C. The labeled cells were then pelleted, washed once with PBSACM, and resuspended in PBSACM before being filtered through a 35 µm nylon filter. Cells were analyzed for fluorescence using a Accuri C6 Plus (BD Biosciences).

5.6.3 Mammalian Cell FACS

To improve cellular InsR expression, HEK-InsRA and HEK-InsRB cells were sorted for receptor expression. The cell culture media was aspirated from HEK-InsRA and HEK-InsRB cells adherently cultured in T75 flasks. Cell cultures were washed with 5 mL of PBS prior to the addition of 3 mL of 0.05% trypsin-EDTA (Gibco). Cells were incubated at 37 °C for 3 minutes to promote dissociation and then the trypsin-EDTA mixture was neutralized with 6 mL of supplemented DMEM. Cells in suspension were aspirated, pelleted at 500*g* for 3 minutes, and washed with fresh supplemented DMEM to neutralize any remaining trypsin. The cells were again pelleted and washed once with PBSACM prior to being labelled with a monoclonal mouse anti-InsR antibody 83-7[111] (4.83 µg/mL, provided by the Yee Lab), incubated for 30 minutes at 4 °C, and washed once again with PBSACM. Cells were then labelled with a goat anti-mouse Alexa Fluor

647 conjugate antibody (20 µg/mL, Invitrogen A21235), incubated for 30 minutes at 4 °C, and washed once with PBSACM. Labeled cells were resuspended in PBSACM and filtered through a 35 µm nylon filter. Cells with the highest InsR and fluorescent protein signal (mCherry for InsRA, EGFP for InsRB) were sorted under aseptic conditions using a FACS Aria II (BD Biosciences).

5.6.4 Yeast-Displayed Ligand Avidity Reduction with DTT

The reduction of ligand avidity on the yeast surface was conducted essentially as previously described[66]. 5×10^8 yeast were pelleted at 1,500*g* for 3 minutes and washed twice with 10 mM Tris buffer pH 7.5 (0.26 g/L Tris base, 1.24 g/L Tris-HCl). Dithiothreitol (DTT) was dissolved in 10 mM Tris buffer to a concentration of 7.5 mM and yeast were resuspended in 2 mL of the DTT solution and statically incubated for 20 minutes at 30 °C. The yeast were then pelleted and washed twice with ice cold PBSACM prior to use in adherent cell panning.

5.6.5 Adherent Mammalian Cell Panning

Adherent cell panning was conducted essentially as previously described[65,203]. R-/IGF1R and HEK-InsRA cells were seeded in 6-well plates and allowed to grow to between 70-90% confluency. The cell culture media was aspirated, and the mammalian cells were washed once with ice cold PBSACM.

For the initial round of selection, yeast were oversampled as allowed by the capacity of adherent cell panning (3-22 fold diversity). Yeast expressing either affibody or fibronectin domain ligands were washed once with ice cold PBSACM and resuspended at a concentration of fewer than 4×10^8 yeast/mL. 1 mL of the yeast mixture was added to each well dropwise. Plates containing yeast and mammalian cells were

statically incubated for 15 minutes at 4 °C and the unbound yeast aspirated. Wells were washed with 1 mL of ice cold PBSACM four times with 25 gentle tilts and 5 gentle nutations. Wells were washed a fifth time with 1 mL of ice cold PBSACM with 10 gentle nutations. Bound yeast were removed by scraping and resuspended in SD-CAA. The yield of plasmid-harboring yeast was quantified by plating dilutions of the final and initial mixtures on SD-CAA plates. The collected yeast were outgrown and reinduced prior to use in the next round of sorting.

For differential cell panning, yeast were oversampled at greater than 19-fold diversity to have a high confidence of library completeness in both the positive and negative cell pans. Yeast expressing either affibody or fibronectin domain ligands isolated from the R-/IGF1R sort were panned against either R-/IGF1R or R- cell monolayers in triplicate while yeast isolated from the HEK-InsRA sort were panned against either HEK-InsRA, HEK-InsRB, or HEK293T cell monolayers in triplicate.

5.6.6 Full-Length Ligand FACS

In order to isolate yeast with full-length ligand expression, yeast were simultaneously labelled at the N-terminal hemagglutinin (HA) and C-terminal c-Myc epitope. At least 20-fold diversity of ligand-displaying yeast were pelleted at 1,500*g* for 3 minutes, washed once with PBSACM, and labelled with a monoclonal mouse anti-c-Myc antibody 9E10 (4 µg/mL, MilliporeSigma, Cat# OP10) and a chicken anti-HA polyclonal antibody (10 µg/mL, Abcam, Cat# ab9111). The cells were then incubated for 30 minutes at 4 °C, pelleted, washed once with PBSACM, and labelled with a goat anti-mouse Alexa Fluor 647 conjugate antibody (20 µg/mL, Invitrogen, Cat# A21235) and goat anti-chicken Alexa Fluor 488 conjugate antibody (20 µg/mL, Invitrogen, Cat# A11039). The

yeast were then incubated for 30 minutes at 4 °C, pelleted, washed once with PBSACM, resuspended in PBSACM, and filtered through a 35 μm nylon filter. Labeled yeast were then sorted for Alexa Fluor 488 and Alexa Fluor 647 signal above nondisplaying yeast using a FACS Aria II (BD Biosciences).

5.6.7 Deep Sequencing of Yeast Populations

Yeast plasmid DNA from clones selected by differential cell panning was extracted by a Zymoprep of 4×10^7 yeast. Illumina barcodes and adapters were added to ligand genes by a two-step PCR. Ligand DNA was amplified by PCR with scaffold-specific primers prior to further amplification with primers encoding for Illumina barcodes and adapters. Deep sequencing was run on an Illumina MiSeq v3 in 300 bp paired end mode. Deep sequencing resulted in approximately 32,000 reads across all IGF1R populations. All reads were paired, searched for scaffold-specific sequences, and quality filtered by USEARCH[205]. The resulting high-quality reads were translated and dereplicated on an amino acid sequence basis.

5.6.8 Ligand Specificity Determination

Amino acid sequences and their number of occurrences in each cell panning population were imported into MATLAB and sequence frequencies were calculated for each population. To determine whether a given sequence was specific to a cell line, the frequency of the sequence in the R-/IGF1R populations was compared to the frequency of the sequence in the R- populations by significance testing.

5.6.9 Statistical Analysis

All adherent cell panning yield data is presented as mean ± standard error. Significance testing of yield data was conducted using Welch's t-test. All significance

testing to determine ligand specificity was conducted by Welch's t-test using MATLAB's two-sample t-test function, ttest2.

Chapter 6 – Conclusion and Future Work

The work presented in this thesis builds upon the adherent cell panning technique created by the Shusta lab, along with the significant advances made by prior members of the Hackel lab. This work provides new methods to significantly deplete nonspecific ligands (Chapter 2) or determine the specificity of ligands within a population (Chapter 5), along with a cell panning technique that increases selection throughput by an order of magnitude compared to adherent cell panning, putting it on par with recombinant MACS and allowing the screening of full-size yeast surface display libraries (Chapter 3). Finally, the new extended yeast surface display linker described herein provides effective enrichment of moderate affinity ligands (on the order of 100 nM) on low-expressing cells (on the order of 10^4 targets per cell) and micromolar affinity ligands on high-expressing cells (on the order of 10^6 targets per cell), drastically expanding the conditions under which ligand selection campaigns can be accomplished (Chapter 4).

Combined, these advances open avenues of possible innovation not previously possible. Primarily, the above advances motivate the discovery of ligands to difficult targets that are intractable to recombinant-based sorting, such as GPCRs, ion channels, and targets with unique post-translational modifications or structure. Pre-blocking with parental cells prior to sorting on cells transfected to express the target of interest would limit the enrichment of non target-specific ligands, while differential cell panning on cells transfected with several sub-family proteins followed by deep sequencing would allow the identification of ligands with specific binding to disease-implicated sub-family

members. After finding ligands with specific binding, mammalian cell-based FACS could be conducted to further isolate ligands with agonistic or antagonist activity[206].

Additionally, the ability of modest affinity ligands to be sorted on even low-expressing mammalian cells opens the possibility of ligand-biomarker co-discovery for both poorly characterized cell lines and patient biopsies. Sorting against these cell lines with some form of depletion (either pre-blocking or differential cell panning followed by deep sequencing) using cells with established proteomic profiles or normal tissue would result in a population of ligands with preferential binding to the target cell line. This population could then be labelled with a panel of recombinant targets and screened by FACS to identify the ligand's conjugate biomarker.

While the advancements made with the pCT-641 yeast surface display construct allows the enrichment of ligands in suboptimal systems, enrichment is still lacking on micromolar or weaker affinity ligands in cases where cells express fewer than 10^5 biomarkers per cell. Given that relatively few ligands in a naïve library possess binding activity to a given target but even weak ligands can readily be evolved into high affinity ligands through directed evolution methods, the ability to recover weak binding ligands is critical to discovery efforts. Further efforts to design effective yeast surface display linkers is stymied by the large space of potential linker designs and limited understanding of the distribution of display constructs on the yeast surface. One method of experimentally determining the distribution would be to take yeast populations expressing ligands attached to the yeast surface by linkers of varying length and label the ligands with a fluorescent antibody prior to analysis by confocal or TIRF microscopy. The spatial resolution of either technique would be able to map the distribution of ligands

on the cell surface. If most ligands still lack access to the extracellular environment in pCT-641, this would motivate the creation of even longer linkers. However, if ligands generally extend into the extracellular space, focus would need to shift to improving local avidity by boosting per cell ligand expression. Since pCT-641 suffered from lower yeast cell expression, likely due to the inefficiencies of producing and trafficking such a large construct, a linker with a similar physical length but fewer amino acids could be designed. This could be accomplished by building hybrid linkers that contain a stiff, N-terminal alpha-helical domain such as EAAAK to provide more extension per amino acid with a PAS-based C-terminus to provide conformational flexibility so that the ligand can sample the mammalian cell surface. Another potential method for boosting ligand display levels is to investigate the use of stronger promoters and secretion factors[207] or overexpress yeast proteins implicated in protein synthesis, secretion, or cell wall binding[208].

Finally, the collation of deep sequencing data garnered from multiple ligand discovery campaigns has shown great benefit in designing new combinatorial scaffold libraries to include broadly applicable binding motifs[70,84]. However, these studies used recombinantly-produced extracellular domains, whose binding epitopes are not necessarily the same as full-length target. This motivates the collective probing of the deep sequencing datasets of the CD276, Thy1, R-/IGF1R, and InsRA campaigns for ligands with cell line specificity. Analyzing the sitewise amino acid enrichment of these specific sequences could inform the design of new affibody and fibronectin domain libraries containing a higher frequency of ligand with binding to cell-bound targets. Conversely, probing these datasets for sequences prevalent in two or more campaigns

would provide information on what amino acids or motifs are associated with nonspecific binding and these motifs could be depleted from the library.

In conclusion, the above research provides a suite of tools that can be applied to utilize cell-based selections more effectively in ligand discovery campaigns, thus enhancing the ability of the field to generate ligands with translatable binding to target-expressing cells and tissues. This work also elucidates the key factors involved in successful yeast-mammalian cell engagement, providing a framework for further research to improve cell-based selections. Extension of this research has the potential to generate ligands with binding to targets, such as GPCRs and ion channels, that have evaded discovery by traditional selection techniques, co-discover ligands and targets on cancer cells, optimize the yeast surface display construct for low avidity conditions, and design new combinatorial libraries with ligands biased towards binding cell-based targets.

Chapter 7 – Bibliography

(1) Leader, B.; Baca, Q. J.; Golan, D. E. Protein Therapeutics: A Summary and Pharmacological Classification. *Nat. Rev. Drug Discov.* **2008**, *7* (1), 21–39. https://doi.org/10.1038/nrd2399.

(2) Wu, L.; Qu, X. Cancer Biomarker Detection: Recent Achievements and Challenges. *Chem. Soc. Rev.* **2015**, *44* (10), 2963–2997. https://doi.org/10.1039/C4CS00370E.

(3) Kwong, G. A.; Ghosh, S.; Gamboa, L.; Patriotis, C.; Srivastava, S.; Bhatia, S. N. Synthetic Biomarkers: A Twenty-First Century Path to Early Cancer Detection. *Nat. Rev. Cancer* **2021**, *21* (10), 655–668. https://doi.org/10.1038/s41568-021-00389-3.

(4) Lu, R.-M.; Hwang, Y.-C.; Liu, I.-J.; Lee, C.-C.; Tsai, H.-Z.; Li, H.-J.; Wu, H.-C. Development of Therapeutic Antibodies for the Treatment of Diseases. *J. Biomed. Sci.* **2020**, *27* (1), 1. https://doi.org/10.1186/s12929-019-0592-z.

(5) Mullard, A. FDA Approves 100th Monoclonal Antibody Product. *Nat. Rev. Drug Discov.* **2021**, *20* (7), 491–495. https://doi.org/10.1038/d41573-021-00079-7.

(6) Trkulja, C. L.; Jungholm, O.; Davidson, M.; Jardemark, K.; Marcus, M. M.; Hägglund, J.; Karlsson, A.; Karlsson, R.; Bruton, J.; Ivarsson, N.; Srinivasa, S. P.; Cavallin, A.; Svensson, P.; Jeffries, G. D. M.; Christakopoulou, M.-N.; Reymer, A.; Ashok, A.; Willman, G.; Papadia, D.; Johnsson, E.; Orwar, O. Rational Antibody Design for Undruggable Targets Using Kinetically Controlled Biomolecular Probes. *Sci. Adv.* **2021**, *7* (16), eabe6397. https://doi.org/10.1126/sciadv.abe6397.

(7) Finan, C.; Gaulton, A.; Kruger, F. A.; Lumbers, R. T.; Shah, T.; Engmann, J.; Galver, L.; Kelley, R.; Karlsson, A.; Santos, R.; Overington, J. P.; Hingorani, A. D.; Casas, J. P. The Druggable Genome and Support for Target Identification and Validation in Drug Development. *Sci. Transl. Med.* **2017**, *9* (383), 1–34. https://doi.org/10.1126/scitranslmed.aag1166.

(8) Romero, P. A.; Arnold, F. H. Exploring Protein Fitness Landscapes by Directed Evolution. *Nat. Rev. Mol. Cell Biol.* **2009**, *10* (12), 866–876. https://doi.org/10.1038/nrm2805.

(9) Gray, A. C.; Sidhu, S. S.; Chandrasekera, P. C.; Hendriksen, C. F. M.; Borrebaeck, C. A. K. Animal-Friendly Affinity Reagents: Replacing the Needless in the Haystack. *Trends Biotechnol.* **2016**, *34* (12), 960–969. https://doi.org/10.1016/j.tibtech.2016.05.017.

(10) Stern, L. A.; Case, B. A.; Hackel, B. J. Alternative Non-Antibody Protein Scaffolds for Molecular Imaging of Cancer. *Curr. Opin. Chem. Eng.* **2013**, *2* (4), 425–432. https://doi.org/10.1016/j.coche.2013.08.009.

(11) Sergeeva, A.; Kolonin, M.; Molldrem, J.; Pasqualini, R.; Arap, W. Display Technologies: Application for the Discovery of Drug and Gene Delivery Agents☆. *Adv. Drug Deliv. Rev.* **2006**, *58* (15), 1622–1654. https://doi.org/10.1016/j.addr.2006.09.018.

(12) Main, A. L.; Harvey, T. S.; Baron, M.; Boyd, J.; Campbell, I. D. The Three-Dimensional Structure of the Tenth Type III Module of Fibronectin: An Insight

into RGD-Mediated Interactions. *Cell* **1992**, *71* (4), 671–678. https://doi.org/10.1016/0092-8674(92)90600-H.
(13) Reiersen, H. Covalent Antibody Display--an in Vitro Antibody-DNA Library Selection System. *Nucleic Acids Res.* **2005**, *33* (1), e10–e10. https://doi.org/10.1093/nar/gni010.
(14) Odegrip, R.; Coomber, D.; Eldridge, B.; Hederer, R.; Kuhlman, P. A.; Ullman, C.; FitzGerald, K.; McGregor, D. CIS Display: In Vitro Selection of Peptides from Libraries of Protein-DNA Complexes. *Proc. Natl. Acad. Sci.* **2004**, *101* (9), 2806–2810. https://doi.org/10.1073/pnas.0400219101.
(15) Eldridge, B.; Cooley, R. N.; Odegrip, R.; McGregor, D. P.; FitzGerald, K. J.; Ullman, C. G. An in Vitro Selection Strategy for Conferring Protease Resistance to Ligand Binding Peptides. *Protein Eng. Des. Sel.* **2009**, *22* (11), 691–698. https://doi.org/10.1093/protein/gzp052.
(16) Roberts, R. W.; Szostak, J. W. RNA-Peptide Fusions for the in Vitro Selection of Peptides and Proteins. *Proc. Natl. Acad. Sci.* **1997**, *94* (23), 12297–12302. https://doi.org/10.1073/pnas.94.23.12297.
(17) Kamalinia, G.; Grindel, B. J.; Takahashi, T. T.; Millward, S. W.; Roberts, R. W. Directing Evolution of Novel Ligands by MRNA Display. *Chem. Soc. Rev.* **2021**, *50* (16), 9055–9103. https://doi.org/10.1039/D1CS00160D.
(18) Lipovsek, D.; Plückthun, A. In-Vitro Protein Evolution by Ribosome Display and MRNA Display. *J. Immunol. Methods* **2004**, *290* (1–2), 51–67. https://doi.org/10.1016/j.jim.2004.04.008.
(19) Mattheakis, L. C.; Bhatt, R. R.; Dower, W. J. An in Vitro Polysome Display System for Identifying Ligands from Very Large Peptide Libraries. *Proc. Natl. Acad. Sci.* **1994**, *91* (19), 9022–9026. https://doi.org/10.1073/pnas.91.19.9022.
(20) Dreier, B.; Plückthun, A. Rapid Selection of High-Affinity Binders Using Ribosome Display. In *Ribosome Display and Related Technologies*; Douthwaite, J. A., Jackson, R. H., Eds.; Springer Science+Business Media: New York, 2012; Vol. 805, pp 261–286. https://doi.org/10.1007/978-1-61779-379-0_15.
(21) Yan, X.; Xu, Z. Ribosome-Display Technology: Applications for Directed Evolution of Functional Proteins. *Drug Discov. Today* **2006**, *11* (19–20), 911–916. https://doi.org/10.1016/j.drudis.2006.08.012.
(22) Plückthun, A. Ribosome Display: A Perspective. In *Ribosome Display and Related Technologies*; Douthwaite, J. A., Jackson, R. H., Eds.; Methods in Molecular Biology; Springer New York: New York, NY, 2012; Vol. 805, pp 3–28. https://doi.org/10.1007/978-1-61779-379-0.
(23) Hillebrecht, J. R.; Chong, S. A Comparative Study of Protein Synthesis in in Vitro Systems: From the Prokaryotic Reconstituted to the Eukaryotic Extract-Based. *BMC Biotechnol.* **2008**, *8*, 1–9. https://doi.org/10.1186/1472-6750-8-58.
(24) Lamla, T.; Erdmann, V. A. Searching Sequence Space for High-Affinity Binding Peptides Using Ribosome Display. *J. Mol. Biol.* **2003**, *329* (2), 381–388. https://doi.org/10.1016/S0022-2836(03)00432-7.
(25) Wilson, D. S.; Keefe, A. D.; Szostak, J. W. The Use of MRNA Display to Select High-Affinity Protein-Binding Peptides. *Proc. Natl. Acad. Sci.* **2001**, *98* (7), 3750–3755. https://doi.org/10.1073/pnas.061028198.

(26) Hanes, J.; Schaffitzel, C.; Knappik, A.; Plückthun, A. Picomolar Affinity Antibodies from a Fully Synthetic Naive Library Selected and Evolved by Ribosome Display. *Nat. Biotechnol.* **2000**, *18* (12), 1287–1292. https://doi.org/10.1038/82407.
(27) Fukuda, I.; Kojoh, K.; Tabata, N.; Doi, N.; Takashima, H.; Miyamoto-Sato, E.; Yanagawa, H. In Vitro Evolution of Single-Chain Antibodies Using MRNA Display. *Nucleic Acids Res.* **2006**, *34* (19), e127–e127. https://doi.org/10.1093/nar/gkl618.
(28) Binz, H. K.; Amstutz, P.; Plückthun, A. Engineering Novel Binding Proteins from Nonimmunoglobulin Domains. *Nat. Biotechnol.* **2005**, *23* (10), 1257–1268. https://doi.org/10.1038/nbt1127.
(29) Grimm, S.; Yu, F.; Nygren, P.-Å. Ribosome Display Selection of a Murine IgG1 Fab Binding Affibody Molecule Allowing Species Selective Recovery Of Monoclonal Antibodies. *Mol. Biotechnol.* **2011**, *48* (3), 263–276. https://doi.org/10.1007/s12033-010-9367-1.
(30) Xu, L.; Aha, P.; Gu, K.; Kuimelis, R. G.; Kurz, M.; Lam, T.; Lim, A. C.; Liu, H.; Lohse, P. A.; Sun, L.; Weng, S.; Wagner, R. W.; Lipovsek, D. Directed Evolution of High-Affinity Antibody Mimics Using MRNA Display. *Chem. Biol.* **2002**, *9* (8), 933–942. https://doi.org/10.1016/S1074-5521(02)00187-4.
(31) Boublik, Y.; Bonito, P. Di; Jones, I. M. Eukaryotic Virus Display: Engineering the Major Surface Glycoprotein of the Autographa Californica Nuclear Polyhedrosis Virus (AcNPV) for the Presentation of Foreign Proteins on the Virus Surface. *Bio/Technology* **1995**, *13* (10), 1079–1084. https://doi.org/10.1038/nbt1095-1079.
(32) Oker-Blom, C. Baculovirus Display Strategies: Emerging Tools for Eukaryotic Libraries and Gene Delivery. *Briefings Funct. Genomics Proteomics* **2003**, *2* (3), 244–253. https://doi.org/10.1093/bfgp/2.3.244.
(33) Russell, S. J.; Hawkins, R. E.; Winter, G. Retroviral Vectors Displaying Functional Antibody Fragments. *Nucleic Acids Res.* **1993**, *21* (5), 1081–1085. https://doi.org/10.1093/nar/21.5.1081.
(34) Nolan, G. P. Retroviral Technology - Applications for Expressed Peptide Libraries. *Front. Biosci.* **2003**, *8* (4), 952. https://doi.org/10.2741/952.
(35) Buchholz, C.; Duerner, L.; Funke, S.; Schneider, I. Retroviral Display and High Throughput Screening. *Comb. Chem. High Throughput Screen.* **2008**, *11* (2), 99–110. https://doi.org/10.2174/138620708783744543.
(36) Müller, O. J.; Kaul, F.; Weitzman, M. D.; Pasqualini, R.; Arap, W.; Kleinschmidt, J. A.; Trepel, M. Random Peptide Libraries Displayed on Adeno-Associated Virus to Select for Targeted Gene Therapy Vectors. *Nat. Biotechnol.* **2003**, *21* (9), 1040–1046. https://doi.org/10.1038/nbt856.
(37) Perabo, L.; Büning, H.; Kofler, D. M.; Ried, M. U.; Girod, A.; Wendtner, C. M.; Enssle, J.; Hallek, M. In Vitro Selection of Viral Vectors with Modified Tropism: The Adeno-Associated Virus Display. *Mol. Ther.* **2003**, *8* (1), 151–157. https://doi.org/10.1016/S1525-0016(03)00123-0.
(38) Mäkelä, A. R.; Matilainen, H.; White, D. J.; Ruoslahti, E.; Oker-Blom, C. Enhanced Baculovirus-Mediated Transduction of Human Cancer Cells by Tumor-Homing Peptides. *J. Virol.* **2006**, *80* (13), 6603–6611.

https://doi.org/10.1128/JVI.00528-06.
(39) Nassal, M.; Skamel, C.; Kratz, P.; Wallich, R.; Stehle, T.; Simon, M. A Fusion Product of the Complete Borrelia Burgdorferi Outer Surface Protein A (OspA) and the Hepatitis B Virus Capsid Protein Is Highly Immunogenic and Induces Protective Immunity Similar to That Seen with an Effective Lipidated OspA Vaccine Formula. *Eur. J. Immunol.* **2005**, *35* (2), 655–665. https://doi.org/10.1002/eji.200425449.
(40) Buchholz, C. J.; Peng, K.-W.; Morling, F. J.; Zhang, J.; Cosset, F.-L.; Russell, S. J. In Vivo Selection of Protease Cleavage Sites from Retrovirus Display Libraries. *Nat. Biotechnol.* **1998**, *16* (10), 951–954. https://doi.org/10.1038/nbt1098-951.
(41) Urban, J. H. Selection of Functional Human Antibodies from Retroviral Display Libraries. *Nucleic Acids Res.* **2005**, *33* (4), e35–e35. https://doi.org/10.1093/nar/gni033.
(42) Smith, G. Filamentous Fusion Phage: Novel Expression Vectors That Display Cloned Antigens on the Virion Surface. *Science (80-.).* **1985**, *228* (4705), 1315–1317. https://doi.org/10.1126/science.4001944.
(43) Bratkovič, T. Progress in Phage Display: Evolution of the Technique and Its Applications. *Cell. Mol. Life Sci.* **2010**, *67* (5), 749–767. https://doi.org/10.1007/s00018-009-0192-2.
(44) Sachdev, S. S.; Lowman, H. B.; Cunningham, B. C.; Wells, J. A. Phage Display for Selection of Novel Binding Properties. *Methods Enzymol.* **2000**, *328*, 333–363.
(45) Cortese, R. Selection of Biologically Active Peptides by Phage Display of Random Peptide Libraries. *Curr. Opin. Biotechnol.* **1996**, *7* (6), 616–621. https://doi.org/10.1016/S0958-1669(96)80072-3.
(46) Hoogenboom, H. R. Overview of Antibody Phage-Display Technology and Its Applications. In *Antibody Phage Display*; Humana Press: New Jersey, 2002; Vol. 178, pp 1–37. https://doi.org/10.1385/1-59259-240-6:001.
(47) Vazquez-Lombardi, R.; Phan, T. G.; Zimmermann, C.; Lowe, D.; Jermutus, L.; Christ, D. Challenges and Opportunities for Non-Antibody Scaffold Drugs. *Drug Discov. Today* **2015**, *20* (10), 1271–1283. https://doi.org/10.1016/j.drudis.2015.09.004.
(48) Ackerman, M.; Levary, D.; Tobon, G.; Hackel, B.; Orcutt, K. D.; Wittrup, K. D. Highly Avid Magnetic Bead Capture: An Efficient Selection Method for de Novo Protein Engineering Utilizing Yeast Surface Display. *Biotechnol. Prog.* **2009**, *25* (3), 774–783. https://doi.org/10.1002/btpr.174.
(49) Georgiou, G.; Stathopoulos, C.; Daugherty, P. S.; Nayak, A. R.; Iverson, B. L.; III, R. C. Display of Heterologous Proteins on the Surface of Microorganisms: From the Screening of Combinatorial Libraries to Live Recombinant Vaccines. *Nat. Biotechnol.* **1997**, *15* (1), 29–34. https://doi.org/10.1038/nbt0197-29.
(50) Freudl, R.; MacIntyre, S.; Degen, M.; Henning, U. Cell Surface Exposure of the Outer Membrane Protein OmpA of Escherichia Coli K-12. *J. Mol. Biol.* **1986**, *188* (3), 491–494. https://doi.org/10.1016/0022-2836(86)90171-3.
(51) Samuelson, P.; Gunneriusson, E.; Nygren, P.-Å.; Ståhl, S. Display of Proteins on Bacteria. *J. Biotechnol.* **2002**, *96* (2), 129–154. https://doi.org/10.1016/S0168-1656(02)00043-3.

(52) Brown, S. Engineered Iron Oxide-Adhesion Mutants of the Escherichia Coli Phage λ Receptor. *Proc. Natl. Acad. Sci. U. S. A.* **1992**, *89* (18), 8651–8655. https://doi.org/10.1073/pnas.89.18.8651.
(53) Lu, Z.; Murray, K. S.; Van Cleave, V.; Lavallie, E. R.; Stahl, M. L.; McCoy, J. M. Expression of Thioredoxin Random Peptide Libraries on the Escherichia Coli Cell Surfeice as Functional Fusions to Flagellin: A System Designed for Exploring Protein-Protein Interactions. *Bio/Technology* **1995**, *13* (4), 366–372. https://doi.org/10.1038/nbt0495-366.
(54) Daugherty, P. S.; Chen, G.; Olsen, M. J.; Iverson, B. L.; Georgiou, G. Antibody Affinity Maturation Using Bacterial Surface Display. *Protein Eng. Des. Sel.* **1998**, *11* (9), 825–832. https://doi.org/10.1093/protein/11.9.825.
(55) Beerli, R. R.; Bauer, M.; Buser, R. B.; Gwerder, M.; Muntwiler, S.; Maurer, P.; Saudan, P.; Bachmann, M. F. Isolation of Human Monoclonal Antibodies by Mammalian Cell Display. *Proc. Natl. Acad. Sci.* **2008**, *105* (38), 14336–14341. https://doi.org/10.1073/pnas.0805942105.
(56) Ho, M.; Pastan, I. Mammalian Cell Display for Antibody Engineering. In *Methods in Molecular Biology*; 2009; Vol. 525, pp 337–352. https://doi.org/10.1007/978-1-59745-554-1_18.
(57) Ho, M.; Nagata, S.; Pastan, I. Isolation of Anti-CD22 Fv with High Affinity by Fv Display on Human Cells. *Proc. Natl. Acad. Sci.* **2006**, *103* (25), 9637–9642. https://doi.org/10.1073/pnas.0603653103.
(58) Zhang, J.; Zhang, X.; Liu, Q.; Li, M.; Gao, L.; Gao, X.; Xiang, S.; Wu, L.; Fu, J.; Song, H. Mammalian Cell Display for Rapid Screening ScFv Antibody Therapy. *Acta Biochim. Biophys. Sin. (Shanghai).* **2014**, *46* (10), 859–866. https://doi.org/10.1093/abbs/gmu079.
(59) Robertson, N.; Lopez-Anton, N.; Gurjar, S. A.; Khalique, H.; Khalaf, Z.; Clerkin, S.; Leydon, V. R.; Parker-Manuel, R.; Raeside, A.; Payne, T.; Jones, T. D.; Seymour, L.; Cawood, R. Development of a Novel Mammalian Display System for Selection of Antibodies against Membrane Proteins. *J. Biol. Chem.* **2020**, *295* (52), 18436–18448. https://doi.org/10.1074/jbc.RA120.015053.
(60) Boder, E. T.; Wittrup, K. D. Yeast Surface Display for Screening Combinatorial Polypeptide Libraries. *Nat. Biotechnol.* **1997**, *15* (6), 553–557. https://doi.org/10.1038/nbt0697-553.
(61) Hackel, B. J.; Wittrup, D. Yeast Surface Display in Protein Engineering and Analysis. In *Protein Engineering Handbook*; Wiley-VCH Verlag GmbH & Co. KGaA: Weinheim, Germany, 2011; pp 621–648. https://doi.org/10.1002/9783527634026.ch26.
(62) Stern, L. A.; Lown, P. S.; Hackel, B. J. Ligand Engineering via Yeast Surface Display and Adherent Cell Panning. In *Genotype Phenotype Coupling*; Zielonka, S., Krah, S., Eds.; UNP - Nebraska: New York, NY, 2020; Vol. 2070, pp 303–320. https://doi.org/10.1007/978-1-4939-9853-1_17.
(63) Kondo, A.; Ueda, M. Yeast Cell-Surface Display-Applications of Molecular Display. *Appl. Microbiol. Biotechnol.* **2004**, *64* (1), 28–40. https://doi.org/10.1007/s00253-003-1492-3.
(64) Huang, G.; Zhang, M.; Erdman, S. E. Posttranslational Modifications Required for

Cell Surface Localization and Function of the Fungal Adhesin Aga1p. *Eukaryot. Cell* **2003**, *2* (5), 1099–1114. https://doi.org/10.1128/EC.2.5.1099-1114.2003.
(65) Stern, L. A.; Schrack, I. A.; Johnson, S. M.; Deshpande, A.; Bennett, N. R.; Harasymiw, L. A.; Gardner, M. K.; Hackel, B. J. Geometry and Expression Enhance Enrichment of Functional Yeast-Displayed Ligands via Cell Panning. *Biotechnol. Bioeng.* **2016**, *113* (11), 2328–2341. https://doi.org/10.1002/bit.26001.
(66) Stern, L. A.; Csizmar, C. M.; Woldring, D. R.; Wagner, C. R.; Hackel, B. J. Titratable Avidity Reduction Enhances Affinity Discrimination in Mammalian Cellular Selections of Yeast-Displayed Ligands. *ACS Comb. Sci.* **2017**, *19* (5), 315–323. https://doi.org/10.1021/acscombsci.6b00191.
(67) Bowley, D. R.; Labrijn, A. F.; Zwick, M. B.; Burton, D. R. Antigen Selection from an HIV-1 Immune Antibody Library Displayed on Yeast Yields Many Novel Antibodies Compared to Selection from the Same Library Displayed on Phage. *Protein Eng. Des. Sel.* **2007**, *20* (2), 81–90. https://doi.org/10.1093/protein/gzl057.
(68) Woldring, D. R.; Holec, P. V; Stern, L. A.; Du, Y.; Hackel, B. J. A Gradient of Sitewise Diversity Promotes Evolutionary Fitness for Binder Discovery in a Three-Helix Bundle Protein Scaffold. *Biochemistry* **2017**, *56* (11), 1656–1671. https://doi.org/10.1021/acs.biochem.6b01142.
(69) Koide, A.; Bailey, C. W.; Huang, X.; Koide, S. The Fibronectin Type III Domain as a Scaffold for Novel Binding Proteins. *J. Mol. Biol.* **1998**, *284* (4), 1141–1151.
(70) Woldring, D. R.; Holec, P. V.; Zhou, H.; Hackel, B. J. High-Throughput Ligand Discovery Reveals a Sitewise Gradient of Diversity in Broadly Evolved Hydrophilic Fibronectin Domains. *PLoS One* **2015**, *10* (9), 1–29. https://doi.org/10.1371/journal.pone.0138956.
(71) Kruziki, M. A.; Bhatnagar, S.; Woldring, D. R.; Duong, V. T.; Hackel, B. J. A 45-Amino-Acid Scaffold Mined from the PDB for High-Affinity Ligand Engineering. *Chem. Biol.* **2015**, *22* (7), 946–956. https://doi.org/10.1016/j.chembiol.2015.06.012.
(72) Benatuil, L.; Perez, J. M.; Belk, J.; Hsieh, C.-M. An Improved Yeast Transformation Method for the Generation of Very Large Human Antibody Libraries. *Protein Eng. Des. Sel.* **2010**, *23* (4), 155–159. https://doi.org/10.1093/protein/gzq002.
(73) Denisov, I. G.; Sligar, S. G. Nanodiscs for Structural and Functional Studies of Membrane Proteins. *Nat. Struct. Mol. Biol.* **2016**, *23* (6), 481–486. https://doi.org/10.1038/nsmb.3195.
(74) Bayburt, T. H.; Grinkova, Y. V.; Sligar, S. G. Self-Assembly of Discoidal Phospholipid Bilayer Nanoparticles with Membrane Scaffold Proteins. *Nano Lett.* **2002**, *2* (8), 853–856. https://doi.org/10.1021/nl025623k.
(75) Zhang, X.; Gureasko, J.; Shen, K.; Cole, P. A.; Kuriyan, J. An Allosteric Mechanism for Activation of the Kinase Domain of Epidermal Growth Factor Receptor. *Cell* **2006**, *125* (6), 1137–1149. https://doi.org/10.1016/j.cell.2006.05.013.
(76) Ogiso, H.; Ishitani, R.; Nureki, O.; Fukai, S.; Yamanaka, M.; Kim, J.-H.; Saito, K.; Sakamoto, A.; Inoue, M.; Shirouzu, M.; Yokoyama, S. Crystal Structure of the Complex of Human Epidermal Growth Factor and Receptor Extracellular

Domains. *Cell* **2002**, *110* (6), 775–787. https://doi.org/10.1016/S0092-8674(02)00963-7.

(77) Bocharov, E. V.; Mineev, K. S.; Volynsky, P. E.; Ermolyuk, Y. S.; Tkach, E. N.; Sobol, A. G.; Chupin, V. V.; Kirpichnikov, M. P.; Efremov, R. G.; Arseniev, A. S. Spatial Structure of the Dimeric Transmembrane Domain of the Growth Factor Receptor ErbB2 Presumably Corresponding to the Receptor Active State. *J. Biol. Chem.* **2008**, *283* (11), 6950–6956. https://doi.org/10.1074/jbc.M709202200.

(78) Wikman, M.; Steffen, A.-C.; Gunneriusson, E.; Tolmachev, V.; Adams, G. P.; Carlsson, J.; Stahl, S. Selection and Characterization of HER2/Neu-Binding Affibody Ligands. *Protein Eng. Des. Sel.* **2004**, *17* (5), 455–462. https://doi.org/10.1093/protein/gzh053.

(79) Yeung, Y. A.; Wittrup, K. D. Quantitative Screening of Yeast Surface-Displayed Polypeptide Libraries by Magnetic Bead Capture. *Biotechnol. Prog.* **2002**, *18* (2), 212–220. https://doi.org/10.1021/bp010186l.

(80) VanAntwerp, J. J.; Wittrup, K. D. Fine Affinity Discrimination by Yeast Surface Display and Flow Cytometry. *Biotechnol. Prog.* **2000**, *16* (1), 31–37.

(81) Hackel, B. J.; Ackerman, M. E.; Howland, S. W.; Wittrup, K. D. Stability and CDR Composition Biases Enrich Binder Functionality Landscapes. *J. Mol. Biol.* **2010**, *401* (1), 84–96. https://doi.org/10.1016/j.jmb.2010.06.004.

(82) Friedman, M.; Nordberg, E.; Höidén-Guthenberg, I.; Brismar, H.; Adams, G. P.; Nilsson, F. Y.; Carlsson, J.; Ståhl, S. Phage Display Selection of Affibody Molecules with Specific Binding to the Extracellular Domain of the Epidermal Growth Factor R Eceptor. *Protein Eng. Des. Sel.* **2007**, *20* (4), 189–199. https://doi.org/10.1093/protein/gzm011.

(83) Horak, E.; Heitner, T.; Robinson, M. K.; Simmons, H. H.; Garrison, J.; Russeva, M.; Furmanova, P.; Lou, J.; Zhou, Y.; Yuan, Q.-A.; Weiner, L. M.; Adams, G. P.; Marks, J. D. Isolation of ScFvs to *In Vitro* Produced Extracellular Domains of EGFR Family Members. *Cancer Biother. Radiopharm.* **2005**, *20* (6), 603–613. https://doi.org/10.1089/cbr.2005.20.603.

(84) Kruziki, M. A.; Sarma, V.; Hackel, B. J. Constrained Combinatorial Libraries of Gp2 Proteins Enhance Discovery of PD-L1 Binders. *ACS Comb. Sci.* **2018**, *20* (7), 423–435. https://doi.org/10.1021/acscombsci.8b00010.

(85) Zellweger, F.; Gasser, P.; Brigger, D.; Buschor, P.; Vogel, M.; Eggel, A. A Novel Bispecific DARPin Targeting FcγRIIB and FcεRI-Bound IgE Inhibits Allergic Responses. *Allergy* **2017**, *72* (8), 1174–1183. https://doi.org/10.1111/all.13109.

(86) Xiao, L.; Hung, K.-C.; Takahashi, T. T.; Joo, K.-I.; Lim, M.; Roberts, R. W.; Wang, P. Antibody-Mimetic Ligand Selected by MRNA Display Targets DC-SIGN for Dendritic Cell-Directed Antigen Delivery. *ACS Chem. Biol.* **2013**, *8* (5), 967–977. https://doi.org/10.1021/cb300680c.

(87) Baneyx, F.; Mujacic, M. Recombinant Protein Folding and Misfolding in Escherichia Coli. *Nat. Biotechnol.* **2004**, *22* (11), 1399–1407. https://doi.org/10.1038/nbt1029.

(88) Demain, A. L.; Vaishnav, P. Production of Recombinant Proteins by Microbes and Higher Organisms. *Biotechnology Advances*. May 2009, pp 297–306. https://doi.org/10.1016/j.biotechadv.2009.01.008.

(89) Gasser, B.; Saloheimo, M.; Rinas, U.; Dragosits, M.; Rodríguez-Carmona, E.; Baumann, K.; Giuliani, M.; Parrilli, E.; Branduardi, P.; Lang, C.; Porro, D.; Ferrer, P.; Tutino, M.; Mattanovich, D.; Villaverde, A. Protein Folding and Conformational Stress in Microbial Cells Producing Recombinant Proteins: A Host Comparative Overview. *Microb. Cell Fact.* **2008**, *7*, 1–18. https://doi.org/10.1186/1475-2859-7-11.

(90) van Oers, M. M.; Pijlman, G. P.; Vlak, J. M. Thirty Years of Baculovirus–Insect Cell Protein Expression: From Dark Horse to Mainstream Technology. *J. Gen. Virol.* **2015**, *96* (1), 6–23. https://doi.org/10.1099/vir.0.067108-0.

(91) Gomord, V.; Faye, L. Posttranslational Modification of Therapeutic Proteins in Plants. *Curr. Opin. Plant Biol.* **2004**, *7* (2), 171–181. https://doi.org/10.1016/j.pbi.2004.01.015.

(92) Bábíčková, J.; Tóthová, Ľ.; Boor, P.; Celec, P. In Vivo Phage Display — A Discovery Tool in Molecular Biomedicine. *Biotechnol. Adv.* **2013**, *31* (8), 1247–1259. https://doi.org/10.1016/j.biotechadv.2013.04.004.

(93) Pasqualini, R.; Ruoslahti, E. Organ Targeting In Vivo Using Phage Display Peptide Libraries. *Nature* **1996**, *380* (6572), 364–366. https://doi.org/10.1038/380364a0.

(94) Teesalu, T.; Sugahara, K. N.; Ruoslahti, E. *Mapping of Vascular ZIP Codes by Phage Display*, 1st ed.; Elsevier Inc., 2012; Vol. 503. https://doi.org/10.1016/B978-0-12-396962-0.00002-1.

(95) Pleiko, K.; Põšnograjeva, K.; Haugas, M.; Paiste, P.; Tobi, A.; Kurm, K.; Riekstina, U.; Teesalu, T. In Vivo Phage Display: Identification of Organ-Specific Peptides Using Deep Sequencing and Differential Profiling across Tissues. *Nucleic Acids Res.* **2021**, *49* (7), e38–e38. https://doi.org/10.1093/nar/gkaa1279.

(96) Staquicini, F. I.; Cardo-Vila, M.; Kolonin, M. G.; Trepel, M.; Edwards, J. K.; Nunes, D. N.; Sergeeva, A.; Efstathiou, E.; Sun, J.; Almeida, N. F.; Tu, S.-M.; Botz, G. H.; Wallace, M. J.; O'Connell, D. J.; Krajewski, S.; Gershenwald, J. E.; Molldrem, J. J.; Flamm, A. L.; Koivunen, E.; Pentz, R. D.; Dias-Neto, E.; Setubal, J. C.; Cahill, D. J.; Troncoso, P.; Do, K.-A.; Logothetis, C. J.; Sidman, R. L.; Pasqualini, R.; Arap, W. Vascular Ligand-Receptor Mapping by Direct Combinatorial Selection in Cancer Patients. *Proc. Natl. Acad. Sci.* **2011**, *108* (46), 18637–18642. https://doi.org/10.1073/pnas.1114503108.

(97) Zou, J.; Dickerson, M. T.; Owen, N. K.; Landon, L. A.; Deutscher, S. L. Biodistribution of Filamentous Phage Peptide Libraries in Mice. *Mol. Biol. Rep.* **2004**, *31* (2), 121–129. https://doi.org/10.1023/B:MOLE.0000031459.14448.af.

(98) Wang, X. X.; Shusta, E. V. The Use of ScFv-Displaying Yeast in Mammalian Cell Surface Selections. *J. Immunol. Methods* **2005**, *304* (1–2), 30–42. https://doi.org/10.1016/j.jim.2005.05.006.

(99) Tillotson, B. J.; Cho, Y. K.; Shusta, E. V. Cells and Cell Lysates: A Direct Approach for Engineering Antibodies against Membrane Proteins Using Yeast Surface Display. *Methods* **2013**, *60* (1), 27–37. https://doi.org/10.1016/j.ymeth.2012.03.010.

(100) Cai, X.; Garen, A. Anti-Melanoma Antibodies from Melanoma Patients Immunized with Genetically Modified Autologous Tumor Cells: Selection of

Specific Antibodies from Single-Chain Fv Fusion Phage Libraries. *Proc. Natl. Acad. Sci.* **1995**, *92* (14), 6537–6541. https://doi.org/10.1073/pnas.92.14.6537.
(101) Alfaleh, M.; Jones, M.; Howard, C.; Mahler, S. Strategies for Selecting Membrane Protein-Specific Antibodies Using Phage Display with Cell-Based Panning. *Antibodies* **2017**, *6* (10), 1–19. https://doi.org/10.3390/antib6030010.
(102) Xu, M. Y.; Xu, X. H.; Chen, G. Z.; Deng, X. L.; Li, J.; Yu, X. J.; Chen, M. Z. Production of a Human Single-Chain Variable Fragment Antibody against Esophageal Carcinoma. *World J. Gastroenterol.* **2004**, *10* (18), 2619–2623. https://doi.org/10.3748/wjg.v10.i18.2619.
(103) Shen, Y.; Yang, X.; Dong, N.; Xie, X.; Bai, X.; Shi, Y. Generation and Selection of Immunized Fab Phage Display Library against Human B Cell Lymphoma. *Cell Res.* **2007**, *17* (7), 650–660. https://doi.org/10.1038/cr.2007.57.
(104) Dangaj, D.; Lanitis, E.; Zhao, A.; Joshi, S.; Cheng, Y.; Sandaltzopoulos, R.; Ra, H.-J.; Danet-Desnoyers, G.; Powell, D. J.; Scholler, N. Novel Recombinant Human B7-H4 Antibodies Overcome Tumoral Immune Escape to Potentiate T-Cell Antitumor Responses. *Cancer Res.* **2013**, *73* (15), 4820–4829. https://doi.org/10.1158/0008-5472.CAN-12-3457.
(105) Williams, R. M.; Hajiran, C. J.; Nayeem, S.; Sooter, L. J. Identification of an Antibody Fragment Specific for Androgen-Dependent Prostate Cancer Cells. *BMC Biotechnol.* **2014**, *14* (1), 1–11. https://doi.org/10.1186/1472-6750-14-81.
(106) Wang, X. X.; Cho, Y. K.; Shusta, E. V. Mining a Yeast Library for Brain Endothelial Cell-Binding Antibodies. *Nat. Methods* **2007**, *4* (2), 143–145. https://doi.org/10.1038/nmeth993.
(107) Jones, A. R.; Stutz, C. C.; Zhou, Y.; Marks, J. D.; Shusta, E. V. Identifying Blood-Brain-Barrier Selective Single-Chain Antibody Fragments. *Biotechnol. J.* **2014**, *9* (5), 664–674. https://doi.org/10.1002/biot.201300550.
(108) Umlauf, B. J.; Clark, P. A.; Lajoie, J. M.; Georgieva, J. V.; Bremner, S.; Herrin, B. R.; Kuo, J. S.; Shusta, E. V. Identification of Variable Lymphocyte Receptors That Can Target Therapeutics to Pathologically Exposed Brain Extracellular Matrix. *Sci. Adv.* **2019**, *5* (5), 1–12. https://doi.org/10.1126/sciadv.aau4245.
(109) Zorniak, M.; Clark, P. A.; Umlauf, B. J.; Cho, Y.; Shusta, E. V.; Kuo, J. S. Yeast Display Biopanning Identifies Human Antibodies Targeting Glioblastoma Stem-like Cells. *Sci. Rep.* **2017**, *7* (1), 1–12. https://doi.org/10.1038/s41598-017-16066-1.
(110) Cho, Y. K.; Shusta, E. V. Antibody Library Screens Using Detergent-Solubilized Mammalian Cell Lysates as Antigen Sources. *Protein Eng. Des. Sel.* **2010**, *23* (7), 567–577.
(111) Chan, J. Y.; Hackel, B. J.; Yee, D. Targeting Insulin Receptor in Breast Cancer Using Small Engineered Protein Scaffolds. *Mol. Cancer Ther.* **2017**, *16* (7), 1324–1334. https://doi.org/10.1158/1535-7163.MCT-16-0685.
(112) Jones, M. L.; Alfaleh, M. A.; Kumble, S.; Zhang, S.; Osborne, G. W.; Yeh, M.; Arora, N.; Hou, J. J. C.; Howard, C. B.; Chin, D. Y.; Mahler, S. M. Targeting Membrane Proteins for Antibody Discovery Using Phage Display. *Sci. Rep.* **2016**, *6* (1), 26240. https://doi.org/10.1038/srep26240.
(113) Jones, M. L.; Mahler, S. M.; Kumble, S. Selection of Antibodies to Transiently

Expressed Membrane Proteins Using Phage Display. In *Antibody Engineering: Methods and Protocols*; Nevoltris, D., Chames, P., Eds.; Springer New York: New York, NY, 2018; pp 179–195. https://doi.org/10.1007/978-1-4939-8648-4_10.
(114) Alfaleh, M.; Arora, N.; Yeh, M.; de Bakker, C.; Howard, C.; Macpherson, P.; Allavena, R.; Chen, X.; Harkness, L.; Mahler, S.; Jones, M. Canine CD117-Specific Antibodies with Diverse Binding Properties Isolated from a Phage Display Library Using Cell-Based Biopanning. *Antibodies* **2019**, *8* (1), 15. https://doi.org/10.3390/antib8010015.
(115) Jeoung, M. H.; Kim, T.-K.; Kim, J. W.; Cho, Y. Bin; Na, H. J.; Yoo, B. C.; Shim, H.; Song, D.-K.; Heo, K.; Lee, S. Antibody-Based Targeting of Cell Surface GRP94 Specifically Inhibits Cetuximab-Resistant Colorectal Cancer Growth. *Biomolecules* **2019**, *9* (11), 681. https://doi.org/10.3390/biom9110681.
(116) Case, B. A.; Kruziki, M. A.; Johnson, S. M.; Hackel, B. J. Engineered Charge Redistribution of Gp2 Proteins through Guided Diversity for Improved PET Imaging of Epidermal Growth Factor Receptor. *Bioconjug. Chem.* **2018**, *29* (5), 1646–1658. https://doi.org/10.1021/acs.bioconjchem.8b00144.
(117) Keller, T.; Kalt, R.; Raab, I.; Schachner, H.; Mayrhofer, C.; Kerjaschki, D.; Hantusch, B. Selection of ScFv Antibody Fragments Binding to Human Blood versus Lymphatic Endothelial Surface Antigens by Direct Cell Phage Display. *PLoS One* **2015**, *10* (5), 1–29. https://doi.org/10.1371/journal.pone.0127169.
(118) Hoogenboom, H. R.; Lutgerink, J. T.; Pelsers, M. M. A. L.; Rousch, M. J. M. M.; Coote, J.; Van Neer, N.; De Bruïne, A.; Van Nieuwenhoven, F. A.; Glatz, J. F. C.; Arends, J. W. Selection-Dominant and Nonaccessible Epitopes on Cell-Surface Receptors Revealed by Cell-Panning with a Large Phage Antibody Library. *Eur. J. Biochem.* **1999**, *260* (3), 774–784. https://doi.org/10.1046/j.1432-1327.1999.00214.x.
(119) Richman, S. A.; Healan, S. J.; Weber, K. S.; Donermeyer, D. L.; Dossett, M. L.; Greenberg, P. D.; Allen, P. M.; Kranz, D. M. Development of a Novel Strategy for Engineering High-Affinity Proteins by Yeast Display. *Protein Eng. Des. Sel.* **2006**, *19* (6), 255–264. https://doi.org/10.1093/protein/gzl008.
(120) Siegel, D. L.; Chang, T. Y.; Russell, S. L.; Bunya, V. Y. Isolation of Cell Surface-Specific Human Monoclonal Antibodies Using Phage Display and Magnetically-Activated Cell Sorting: Applications in Immunohematology. *J. Immunol. Methods* **1997**, *206* (1–2), 73–85. https://doi.org/10.1016/S0022-1759(97)00087-2.
(121) Takahashi, S.; Mok, H.; Parrott, M. B.; Marini, F. C.; Andreeff, M.; Brenner, M. K.; Barry, M. A. Selection of Chronic Lymphocytic Leukemia Binding Peptides. *Cancer Res.* **2003**, *63* (17), 5213–5217.
(122) Even-Desrumeaux, K.; Chames, P. Phage Display and Selections on Cells. In *Antibody Engineering: Methods and Protocols, Second Edition*; Chames, P., Ed.; Humana Press: Totowa, NJ, 2012; Vol. 907, pp 225–235. https://doi.org/10.1007/978-1-61779-974-7_12.
(123) Eisenhardt, S. U.; Schwarz, M.; Bassler, N.; Peter, K. Subtractive Single-Chain Antibody (ScFv) Phage-Display: Tailoring Phage-Display for High Specificity against Function-Specific Conformations of Cell Membrane Molecules. *Nat. Protoc.* **2007**, *2* (12), 3063–3073. https://doi.org/10.1038/nprot.2007.455.

(124) Weber, T.; Pscherer, S.; Gamerdinger, U.; Teigler-Schlegel, A.; Rutz, N.; Blau, W.; Rummel, M.; Gattenlöhner, S.; Tur, M. K. Parallel Evaluation of Cell-based Phage Display Panning Strategies: Optimized Selection and Depletion Steps Result in AML Blast-binding Consensus Antibodies. *Mol. Med. Rep.* **2021**, *24* (5), 1–13. https://doi.org/10.3892/mmr.2021.12407.
(125) Even-Desrumeaux, K.; Nevoltris, D.; Lavaut, M. N.; Alim, K.; Borg, J.-P.; Audebert, S.; Kerfelec, B.; Baty, D.; Chames, P. Masked Selection: A Straightforward and Flexible Approach for the Selection of Binders Against Specific Epitopes and Differentially Expressed Proteins by Phage Display. *Mol. Cell. Proteomics* **2014**, *13* (2), 653–665. https://doi.org/10.1074/mcp.O112.025486.
(126) Mäbert, K.; Cojoc, M.; Peitzsch, C.; Kurth, I.; Souchelnytskyi, S.; Dubrovska, A. Cancer Biomarker Discovery: Current Status and Future Perspectives. *Int. J. Radiat. Biol.* **2014**, *90* (8), 659–677. https://doi.org/10.3109/09553002.2014.892229.
(127) Banta, S.; Dooley, K.; Shur, O. Replacing Antibodies: Engineering New Binding Proteins. *Annu. Rev. Biomed. Eng.* **2013**, *15*, 93–113.
(128) James, M. L.; Gambhir, S. S. A Molecular Imaging Primer: Modalities, Imaging Agents, and Applications. *Physiol. Rev.* **2012**, *92* (2), 897–965. https://doi.org/10.1152/physrev.00049.2010.
(129) McCafferty, J.; Griffiths, a D.; Winter, G.; Chiswell, D. J. Phage Antibodies: Filamentous Phage Displaying Antibody Variable Domains. *Nature* **1990**, *348* (6301), 552–554. https://doi.org/10.1038/348552a0.
(130) Durandy, A.; Gauchat, J.-F.; Mazzei, G. J.; Edgerton, M. D.; Losberger, C.; Lecoanet-Henchoz, S.; Graber, P.; Bernard, A.; Allet, B.; Bonnefoy, J.-Y. Recombinant Soluble Trimeric CD40 Ligand Is Biologically Active. *J. Biol. Chem.* **1995**, *270* (13), 7025–7028. https://doi.org/10.1074/jbc.270.13.7025.
(131) Singer, E.; Landgraf, R.; Horan, T.; Slamon, D.; Eisenberg, D. Identification of a Heregulin Binding Site in HER3 Extracellular Domain. *J. Biol. Chem.* **2001**, *276* (47), 44266–44274. https://doi.org/10.1074/jbc.M105428200.
(132) Chen, T. F.; de Picciotto, S.; Hackel, B. J.; Wittrup, K. D. Engineering Fibronectin-Based Binding Proteins by Yeast Surface Display. In *Methods in Enzymology*; Elsevier Inc., 2013; Vol. 523, pp 303–326. https://doi.org/10.1016/B978-0-12-394292-0.00014-X.
(133) Hofmeyer, K. A.; Ray, A.; Zang, X. The Contrasting Role of B7-H3. *Proc. Natl. Acad. Sci.* **2008**, *105* (30), 10277–10278. https://doi.org/10.1073/pnas.0805458105.
(134) Crispen, P. L.; Sheinin, Y.; Roth, T. J.; Lohse, C. M.; Kuntz, S. M.; Frigola, X.; Houston Thompson, R.; Boorjian, S. A.; Dong, H.; Leibovich, B. C.; Blute, M. L.; Kwon, E. D. Tumor Cell and Tumor Vasculature Expression of B7-H3 Predict Survival in Clear Cell Renal Cell Carcinoma. *Clin. Cancer Res.* **2008**, *14* (16), 5150–5157. https://doi.org/10.1158/1078-0432.CCR-08-0536.
(135) Wang, J.; Chong, K. K.; Nakamura, Y.; Nguyen, L.; Huang, S. K.; Kuo, C.; Zhang, W.; Yu, H.; Morton, D. L.; Hoon, D. S. B. B7-H3 Associated with Tumor Progression and Epigenetic Regulatory Activity in Cutaneous Melanoma. *J. Invest.*

Dermatol. **2013**, *133* (8), 2050–2058. https://doi.org/10.1038/jid.2013.114.
(136) Zhou, Z.; Luther, N.; Ibrahim, G. M.; Hawkins, C.; Vibhakar, R.; Handler, M. H.; Souweidane, M. M. B7-H3, a Potential Therapeutic Target, Is Expressed in Diffuse Intrinsic Pontine Glioma. *J. Neurooncol.* **2013**, *111* (3), 257–264. https://doi.org/10.1007/s11060-012-1021-2.
(137) Katayama, A.; Takahara, M.; Kishibe, K.; Nagato, T.; Kunibe, I.; Katada, A.; Hayashi, T.; Harabuchi, Y. Expression of B7-H3 in Hypopharyngeal Squamous Cell Carcinoma as a Predictive Indicator for Tumor Metastasis and Prognosis. *Int. J. Oncol.* **2011**, *38* (5), 1219–1226. https://doi.org/10.3892/ijo.2011.949.
(138) Yuan, H.; Wei, X.; Zhang, G.; Li, C.; Zhang, X.; Hou, J. B7-H3 over Expression in Prostate Cancer Promotes Tumor Cell Progression. *J. Urol.* **2011**, *186* (3), 1093–1099. https://doi.org/10.1016/j.juro.2011.04.103.
(139) Lutz, A. M.; Bachawal, S. V.; Drescher, C. W.; Pysz, M. A.; Willmann, J. K.; Gambhir, S. S. Ultrasound Molecular Imaging in a Human CD276 Expression-Modulated Murine Ovarian Cancer Model. *Clin. Cancer Res.* **2014**, *20* (5), 1313–1322. https://doi.org/10.1158/1078-0432.CCR-13-1642.
(140) Yamato, I.; Sho, M.; Nomi, T.; Akahori, T.; Shimada, K.; Hotta, K.; Kanehiro, H.; Konishi, N.; Yagita, H.; Nakajima, Y. Clinical Importance of B7-H3 Expression in Human Pancreatic Cancer. *Br. J. Cancer* **2009**, *101* (10), 1709–1716. https://doi.org/10.1038/sj.bjc.6605375.
(141) Zhao, X.; Li, D. C.; Zhu, X. G.; Gan, W. J.; Li, Z.; Xiong, F.; Zhang, Z. X.; Zhang, G. B.; Zhang, X. G.; Zhao, H. B7-H3 Overexpression in Pancreatic Cancer Promotes Tumor Progression. *Int. J. Mol. Med.* **2013**, *31* (2), 283–291. https://doi.org/10.3892/ijmm.2012.1212.
(142) Foygel, K.; Wang, H.; Machtaler, S.; Lutz, A. M.; Chen, R.; Pysz, M.; Lowe, A. W.; Tian, L.; Carrigan, T.; Brentnall, T. A.; Willmann, J. K. Detection of Pancreatic Ductal Adenocarcinoma in Mice by Ultrasound Imaging of Thymocyte Differentiation Antigen 1. *Gastroenterology* **2013**, *145* (4), 885-894.e3.
(143) Lipovšek, D. Adnectins: Engineered Target-Binding Protein Therapeutics. *Protein Eng. Des. Sel.* **2011**, *24* (1–2), 3–9. https://doi.org/10.1093/protein/gzq097.
(144) Nord, K.; Nilsson, J.; Nilsson, B. A Combinatorial Library of an α-Helical Bacterial Receptor Domain. *Protein Eng.* **1995**, *8* (6), 601–608. https://doi.org/10.1093/protein/8.6.601.
(145) Lofblom, J.; Feldwisch, J.; Tolmachev, V.; Carlsson, J.; Stahl, S.; Frejd, F. Y. Affibody Molecules: Engineered Proteins for Therapeutic, Diagnostic and Biotechnological Applications. *FEBS Lett.* **2010**, *584* (12), 2670–2680. https://doi.org/10.1016/j.febslet.2010.04.014.
(146) Baum, R. P.; Prasad, V.; Müller, D.; Schuchardt, C.; Orlova, A.; Wennborg, A.; Tolmachev, V.; Feldwisch, J. Molecular Imaging of HER2-Expressing Malignant Tumors in Breast Cancer Patients Using Synthetic 111In- or 68Ga-Labeled Affibody Molecules. *J. Nucl. Med.* **2010**, *51* (6), 892–897.
(147) Hackel, B. J.; Kimura, R. H.; Gambhir, S. S. Use of 64Cu-Labeled Fibronectin Domain with EGFR- Overexpressing Tumor Xenograft: Molecular Imaging. *Radiology* **2012**, *263* (1), 179–188. https://doi.org/10.1148/radiol.12111504/-/DC1.
(148) Case, B. A.; Kruziki, M. A.; Stern, L. A.; Hackel, B. J. Evaluation of Affibody

Charge Modification Identified by Synthetic Consensus Design in Molecular PET Imaging of Epidermal Growth Factor Receptor. *Mol. Syst. Des. Eng.* **2018**, *3* (1), 171–182. https://doi.org/10.1039/c7me00095b.

(149) Barbas, C. F.; Hu, D.; Dunlop, N.; Sawyer, L.; Cababa, D.; Hendry, R. M.; Nara, P. L.; Burton, D. R. In Vitro Evolution of a Neutralizing Human Antibody to Human Immunodeficiency Virus Type 1 to Enhance Affinity and Broaden Strain Cross-Reactivity. *Proc. Natl. Acad. Sci.* **1994**, *91* (9), 3809–3813. https://doi.org/10.1073/pnas.91.9.3809.

(150) Lipovšek, D.; Lippow, S. M.; Hackel, B. J.; Gregson, M. W.; Cheng, P.; Kapila, A.; Wittrup, K. D. Evolution of an Interloop Disulfide Bond in High-Affinity Antibody Mimics Based on Fibronectin Type III Domain and Selected by Yeast Surface Display: Molecular Convergence with Single-Domain Camelid and Shark Antibodies. *J. Mol. Biol.* **2007**, *368* (4), 1024–1041. https://doi.org/10.1016/j.jmb.2007.02.029.

(151) Hackel, B. J.; Kapila, A.; Wittrup, K. D. Picomolar Affinity Fibronectin Domains Engineered Utilizing Loop Length Diversity, Recursive Mutagenesis, and Loop Shuffling. *J. Mol. Biol.* **2008**, *381* (5), 1238–1252.

(152) Zaccolo, M.; Williams, D. M.; Brown, D. M.; Gherardi, E. An Approach to Random Mutagenesis of DNA Using Mixtures of Triphosphate Derivatives of Nucleoside Analogues. *J. Mol. Biol.* **1996**, *255* (4), 589–603.

(153) Gill, S. C.; von Hippel, P. H. Calculation of Protein Extinction Coefficients from Amino Acid Sequence Data. *Anal. Biochem.* **1989**, *182* (2), 319–326. https://doi.org/10.1016/0003-2697(89)90602-7.

(154) Kamta, J.; Chaar, M.; Ande, A.; Altomare, D. A.; Ait-Oudhia, S. Advancing Cancer Therapy with Present and Emerging Immuno-Oncology Approaches. *Front. Oncol.* **2017**, *7*, 1–15. https://doi.org/10.3389/fonc.2017.00064.

(155) Dijkstra, S.; Mulders, P. F. A.; Schalken, J. A. Clinical Use of Novel Urine and Blood Based Prostate Cancer Biomarkers: A Review. *Clin. Biochem.* **2014**, *47* (10–11), 889–896. https://doi.org/10.1016/j.clinbiochem.2013.10.023.

(156) Husseinzadeh, N. Status of Tumor Markers in Epithelial Ovarian Cancer Has There Been Any Progress? A Review. *Gynecol. Oncol.* **2011**, *120* (1), 152–157. https://doi.org/10.1016/j.ygyno.2010.09.002.

(157) Yotsukura, S.; Mamitsuka, H. Evaluation of Serum-Based Cancer Biomarkers: A Brief Review from a Clinical and Computational Viewpoint. *Crit. Rev. Oncol. Hematol.* **2015**, *93* (2), 103–115. https://doi.org/10.1016/j.critrevonc.2014.10.002.

(158) Lin, K. Y.; Kwong, G. A.; Warren, A. D.; Wood, D. K.; Bhatia, S. N. Nanoparticles That Sense Thrombin Activity as Synthetic Urinary Biomarkers of Thrombosis. *ACS Nano* **2013**, *7* (10), 9001–9009. https://doi.org/10.1021/nn403550c.

(159) Desai, A. N.; Jere, A. Next-Generation Sequencing for Cancer Biomarker Discovery. *Next Gener. Seq. Cancer Res.* **2015**, *2*, 103–125. https://doi.org/10.1007/978-3-319-15811-2.

(160) Surinova, S.; Schiess, R.; Hüttenhain, R.; Cerciello, F.; Wollscheid, B.; Aebersold, R. On the Development of Plasma Protein Biomarkers. *J. Proteome Res.* **2011**, *10* (1), 5–16. https://doi.org/10.1021/pr1008515.

(161) Crutchfield, C. A.; Thomas, S. N.; Sokoll, L. J.; Chan, D. W. Advances in Mass Spectrometry-Based Clinical Biomarker Discovery. *Clin. Proteomics* **2016**, *13* (1), 1–12. https://doi.org/10.1186/s12014-015-9102-9.
(162) Tillotson, B. J.; Lajoie, J. M.; Shusta, E. V. Yeast Display-Based Antibody Affinity Maturation Using Detergent-Solubilized Cell Lysates. In *Methods in Molecular Biology*; 2015; Vol. 1319, pp 65–78. https://doi.org/10.1007/978-1-4939-2748-7_4.
(163) Orlova, A.; Magnusson, M.; Eriksson, T. L. J.; Nilsson, M.; Larsson, B.; Höidén-Guthenberg, I.; Widström, C.; Carlsson, J.; Tolmachev, V.; Ståhl, S.; Nilsson, F. Y. Tumor Imaging Using a Picomolar Affinity HER2 Binding Affibody Molecule. *Cancer Res.* **2006**, *66* (8), 4339–4348. https://doi.org/10.1158/0008-5472.CAN-05-3521.
(164) Horiya, S.; Bailey, J. K.; Krauss, I. J. Directed Evolution of Glycopeptides Using MRNA Display. In *Methods in Enzymology*; Imperiali, B., Ed.; Elsevier Inc., 2017; Vol. 597, pp 83–141. https://doi.org/10.1016/bs.mie.2017.06.029.
(165) Doerner, A.; Rhiel, L.; Zielonka, S.; Kolmar, H. Therapeutic Antibody Engineering by High Efficiency Cell Screening. *FEBS Lett.* **2014**, *588* (2), 278–287. https://doi.org/10.1016/j.febslet.2013.11.025.
(166) Stern, L. A.; Lown, P. S.; Kobe, A. C.; Abou-Elkacem, L.; Willmann, J. K.; Hackel, B. J. Cellular-Based Selections Aid Yeast-Display Discovery of Genuine Cell-Binding Ligands: Targeting Oncology Vascular Biomarker CD276. *ACS Comb. Sci.* **2019**, *21* (3), 207–222. https://doi.org/10.1021/acscombsci.8b00156.
(167) Suñé, P.; Suñé, J. M.; Montoro, J. B. Positive Outcomes Influence the Rate and Time to Publication, but Not the Impact Factor of Publications of Clinical Trial Results. *PLoS One* **2013**, *8* (1), 1–8. https://doi.org/10.1371/journal.pone.0054583.
(168) Yang, Z.; Wan, Y.; Tao, P.; Qiang, M.; Dong, X.; Lin, C.-W.; Yang, G.; Zheng, T.; Lerner, R. A. A Cell–Cell Interaction Format for Selection of High-Affinity Antibodies to Membrane Proteins. *Proc. Natl. Acad. Sci.* **2019**, *116* (30), 14971–14978. https://doi.org/10.1073/pnas.1908571116.
(169) Watters, J. M.; Telleman, P.; Junghans, R. P. An Optimized Method for Cell-Based Phage Display Panning. *Immunotechnology* **1997**, *3* (1), 21–29. https://doi.org/10.1016/S1380-2933(96)00056-5.
(170) Giordano, R. J.; Cardó-Vila, M.; Lahdenranta, J.; Pasqualini, R.; Arap, W. Biopanning and Rapid Analysis of Selective Interactive Ligands. *Nat. Med.* **2001**, *7* (11), 1249–1253. https://doi.org/10.1038/nm1101-1249.
(171) Yoon, H.; Song, J. M.; Ryu, C. J.; Kim, Y. G.; Lee, E. K.; Kang, S.; Kim, S. J. An Efficient Strategy for Cell-Based Antibody Library Selection Using an Integrated Vector System. *BMC Biotechnol.* **2012**, *12* (62), 1–10. https://doi.org/10.1186/1472-6750-12-62.
(172) Ridgway, J. B. B.; Ng, E.; Kern, J. A.; Lee, J.; Brush, J.; Goddard, A.; Carter, P. Identification of a Human Anti-CD55 Single-Chain Fv by Subtractive Panning of a Phage Library Using Tumor and Nontumor Cell Lines. *Cancer Res.* **1999**, *59* (11), 2718–2723.
(173) Neurauter, A. A.; Bonyhadi, M.; Lien, E.; Nøkleby, L.; Ruud, E.; Camacho, S.; Aarvak, T. Cell Isolation and Expansion Using Dynabeads. *Adv. Biochem. Eng.*

Biotechnol. **2007**, *106*, 41–73. https://doi.org/10.1007/10_2007_072.
(174) Schlapschy, M.; Binder, U.; Borger, C.; Theobald, I.; Wachinger, K.; Kisling, S.; Haller, D.; Skerra, A. PASylation: A Biological Alternative to PEGylation for Extending the Plasma Half-Life of Pharmaceutically Active Proteins. *Protein Eng. Des. Sel.* **2013**, *26* (8), 489–501. https://doi.org/10.1093/protein/gzt023.
(175) Gera, N.; Hussain, M.; Wright, R. C.; Rao, B. M. Highly Stable Binding Proteins Derived from the Hyperthermophilic Sso7d Scaffold. *J. Mol. Biol.* **2011**, *409* (4), 601–616. https://doi.org/10.1016/j.jmb.2011.04.020.
(176) Plückthun, A. Designed Ankyrin Repeat Proteins (DARPins): Binding Proteins for Research, Diagnostics, and Therapy. *Annu. Rev. Pharmacol. Toxicol.* **2015**, *55* (1), 489–511. https://doi.org/10.1146/annurev-pharmtox-010611-134654.
(177) Bozovičar, K.; Bratkovič, T. Evolving a Peptide: Library Platforms and Diversification Strategies. *Int. J. Mol. Sci.* **2019**, *21* (1), 215. https://doi.org/10.3390/ijms21010215.
(178) Krohl, P. J.; Kim, K. B.; Lew, L.; VanDyke, D.; Ludwig, S. D.; Spangler, J. B. A Suspension Cell-based Interaction Platform for Interrogation of Membrane Proteins. *AIChE J.* **2020**, *66* (12), 1–13. https://doi.org/10.1002/aic.16995.
(179) Lown, P. S.; Hackel, B. J. Magnetic Bead-Immobilized Mammalian Cells Are Effective Targets to Enrich Ligand-Displaying Yeast. *ACS Comb. Sci.* **2020**, *22* (5), 274–284. https://doi.org/10.1021/acscombsci.0c00036.
(180) Dupres, V.; Dufrêne, Y. F.; Heinisch, J. J. Measuring Cell Wall Thickness in Living Yeast Cells Using Single Molecular Rulers. *ACS Nano* **2010**, *4* (9), 5498–5504. https://doi.org/10.1021/nn101598v.
(181) Klis, F. Dynamics of Cell Wall Structure in Saccharomyces Cerevisiae. *FEMS Microbiol. Rev.* **2002**, *26* (3), 239–256. https://doi.org/10.1016/S0168-6445(02)00087-6.
(182) McMahon, C.; Baier, A. S.; Pascolutti, R.; Wegrecki, M.; Zheng, S.; Ong, J. X.; Erlandson, S. C.; Hilger, D.; Rasmussen, S. G. F.; Ring, A. M.; Manglik, A.; Kruse, A. C. Yeast Surface Display Platform for Rapid Discovery of Conformationally Selective Nanobodies. *Nat. Struct. Mol. Biol.* **2018**, *25* (3), 289–296. https://doi.org/10.1038/s41594-018-0028-6.
(183) Wang, L.; Rivera, E. V.; Benavides-Garcia, M. G.; Nall, B. T. Loop Entropy and Cytochrome c Stability. *J. Mol. Biol.* **2005**, *353* (3), 719–729. https://doi.org/10.1016/j.jmb.2005.08.038.
(184) Flory, P. J. *Statistical Mechanics of Chain Molecules*; Interscience Publishers: New York, 1969.
(185) Zhou, H.-X. Polymer Models of Protein Stability, Folding, and Interactions †. *Biochemistry* **2004**, *43* (8), 2141–2154. https://doi.org/10.1021/bi036269n.
(186) Berges, S. M. *Engineering a Fluorescent Barcoding System for Highly Multiplexed, Single-Cell Analysis of Biomolecular and Cellular Libraries*; University of Delaware: Newark, 2017.
(187) Evers, T. H.; van Dongen, E. M. W. M.; Faesen, A. C.; Meijer, E. W.; Merkx, M. Quantitative Understanding of the Energy Transfer between Fluorescent Proteins Connected via Flexible Peptide Linkers. *Biochemistry* **2006**, *45* (44), 13183–13192. https://doi.org/10.1021/bi061288t.

(188) Breibeck, J.; Skerra, A. The Polypeptide Biophysics of Proline/Alanine-Rich Sequences (PAS): Recombinant Biopolymers with PEG-like Properties. *Biopolymers* **2018**, *109* (1), 1–12. https://doi.org/10.1002/bip.23069.
(189) Schimmel, P. R.; Flory, P. J. Conformational Energy and Configurational Statistics of Poly-L-Proline. *Proc. Natl. Acad. Sci.* **1967**, *58* (1), 52–59. https://doi.org/10.1073/pnas.58.1.52.
(190) Brant, D. A.; Miller, W. G.; Flory, P. J. Conformational Energy Estimates for Statistically Coiling Polypeptide Chains. *J. Mol. Biol.* **1967**, *23* (1), 47–65. https://doi.org/10.1016/S0022-2836(67)80066-4.
(191) Vunnam, N.; Szymonski, S.; Hirsova, P.; Gores, G. J.; Sachs, J. N.; Hackel, B. J. Noncompetitive Allosteric Antagonism of Death Receptor 5 by a Synthetic Affibody Ligand. *Biochemistry* **2020**, *59* (40), 3856–3868. https://doi.org/10.1021/acs.biochem.0c00529.
(192) Fowler, D. M.; Araya, C. L.; Fleishman, S. J.; Kellogg, E. H.; Stephany, J. J.; Baker, D.; Fields, S. High-Resolution Mapping of Protein Sequence-Function Relationships. *Nat. Methods* **2010**, *7* (9), 741–746. https://doi.org/10.1038/nmeth.1492.
(193) Hietpas, R. T.; Jensen, J. D.; Bolon, D. N. A. Experimental Illumination of a Fitness Landscape. *Proc. Natl. Acad. Sci.* **2011**, *108* (19), 7896–7901. https://doi.org/10.1073/pnas.1016024108.
(194) Wrenbeck, E. E.; Faber, M. S.; Whitehead, T. A. Deep Sequencing Methods for Protein Engineering and Design. *Curr. Opin. Struct. Biol.* **2017**, *45*, 36–44. https://doi.org/10.1016/j.sbi.2016.11.001.
(195) Strauch, E.-M.; Fleishman, S. J.; Baker, D. Computational Design of a PH-Sensitive IgG Binding Protein. *Proc. Natl. Acad. Sci.* **2014**, *111* (2), 675–680. https://doi.org/10.1073/pnas.1313605111.
(196) Dou, J.; Goreshnik, I.; Bryan, C.; Baker, D.; Strauch, E.-M. Parallelized Identification of On- and off-Target Protein Interactions. *Mol. Syst. Des. Eng.* **2020**, *5* (1), 349–357. https://doi.org/10.1039/C9ME00118B.
(197) Whitehead, T. A.; Chevalier, A.; Song, Y.; Dreyfus, C.; Fleishman, S. J.; De Mattos, C.; Myers, C. A.; Kamisetty, H.; Blair, P.; Wilson, I. A.; Baker, D. Optimization of Affinity, Specificity and Function of Designed Influenza Inhibitors Using Deep Sequencing. *Nat. Biotechnol.* **2012**, *30* (6), 543–548. https://doi.org/10.1038/nbt.2214.
(198) Hua, H.; Kong, Q.; Yin, J.; Zhang, J.; Jiang, Y. Insulin-like Growth Factor Receptor Signaling in Tumorigenesis and Drug Resistance: A Challenge for Cancer Therapy. *J. Hematol. Oncol.* **2020**, *13* (1), 64. https://doi.org/10.1186/s13045-020-00904-3.
(199) Belfiore, A.; Frasca, F.; Pandini, G.; Sciacca, L.; Vigneri, R. Insulin Receptor Isoforms and Insulin Receptor/Insulin-Like Growth Factor Receptor Hybrids in Physiology and Disease. *Endocr. Rev.* **2009**, *30* (6), 586–623. https://doi.org/10.1210/er.2008-0047.
(200) Sachdev, D.; Singh, R.; Fujita-Yamaguchi, Y.; Yee, D. Down-Regulation of Insulin Receptor by Antibodies against the Type I Insulin-Like Growth Factor Receptor: Implications for Anti–Insulin-Like Growth Factor Therapy in Breast

Cancer. *Cancer Res.* **2006**, *66* (4), 2391–2402. https://doi.org/10.1158/0008-5472.CAN-05-3126.
(201) Ulanet, D. B.; Ludwig, D. L.; Kahn, C. R.; Hanahan, D. Insulin Receptor Functionally Enhances Multistage Tumor Progression and Conveys Intrinsic Resistance to IGF-1R Targeted Therapy. *Proc. Natl. Acad. Sci.* **2010**, *107* (24), 10791–10798. https://doi.org/10.1073/pnas.0914076107.
(202) Puzanov, I.; Lindsay, C. R.; Goff, L.; Sosman, J.; Gilbert, J.; Berlin, J.; Poondru, S.; Simantov, R.; Gedrich, R.; Stephens, A.; Chan, E.; Evans, T. R. J. A Phase I Study of Continuous Oral Dosing of OSI-906, a Dual Inhibitor of Insulin-Like Growth Factor-1 and Insulin Receptors, in Patients with Advanced Solid Tumors. *Clin. Cancer Res.* **2015**, *21* (4), 701–711. https://doi.org/10.1158/1078-0432.CCR-14-0303.
(203) Lown, P. S.; Cai, J. J.; Ritter, S. C.; Otolski, J. J.; Wong, R.; Hackel, B. J. Extended Yeast Surface Display Linkers Enhance the Enrichment of Ligands in Direct Mammalian Cell Selections. *Protein Eng. Des. Sel.* **2021**, *34*, 1–9. https://doi.org/10.1093/protein/gzab004.
(204) Sell, C.; Rubini, M.; Rubin, R.; Liu, J. P.; Efstratiadis, A.; Baserga, R. Simian Virus 40 Large Tumor Antigen Is Unable to Transform Mouse Embryonic Fibroblasts Lacking Type 1 Insulin-like Growth Factor Receptor. *Proc. Natl. Acad. Sci.* **1993**, *90* (23), 11217–11221. https://doi.org/10.1073/pnas.90.23.11217.
(205) Edgar, R. C. Search and Clustering Orders of Magnitude Faster than BLAST. *Bioinformatics* **2010**, *26* (19), 2460–2461. https://doi.org/10.1093/bioinformatics/btq461.
(206) Ren, H.; Li, J.; Zhang, N.; Hu, L. A.; Ma, Y.; Tagari, P.; Xu, J.; Zhang, M.-Y. Function-Based High-Throughput Screening for Antibody Antagonists and Agonists against G Protein-Coupled Receptors. *Commun. Biol.* **2020**, *3* (1), 146. https://doi.org/10.1038/s42003-020-0867-7.
(207) Kajiwara, K.; Aoki, W.; Ueda, M. Evaluation of the Yeast Surface Display System for Screening of Functional Nanobodies. *AMB Express* **2020**, *10* (1), 51. https://doi.org/10.1186/s13568-020-00983-y.
(208) Wentz, A. E.; Shusta, E. V. A Novel High-Throughput Screen Reveals Yeast Genes That Increase Secretion of Heterologous Proteins. *Appl. Environ. Microbiol.* **2007**, *73* (4), 1189–1198. https://doi.org/10.1128/AEM.02427-06.